University of Alberta

2-D Pore and Core Scale Visualization and Modeling of Immiscible and Miscible CO_2 Injection in Fractured Systems

by

Vahapcan Er

A thesis submitted to the Faculty of Graduate Studies and Research
in partial fulfillment of the requirements for the degree of

Master of Science
in
Petroleum Engineering

Department of Civil and Environmental Engineering

Fall 2009
Edmonton, Alberta

Examining Committee

Dr. Tayfun Babadagli, Civil and Environmental Engineering

Dr. Ergun Kuru, Civil and Environmental Engineering

Dr. Sushanta Mitra, Mechanical Engineering

Abstract

Pore scale interaction between matrix and fracture during miscible and immiscible CO_2 injection was studied experimentally using visual models. Initially, visualization experiments were conducted on 2-D glass bead packed models by injecting n-heptane (solvent) displacing different kinds of processed oil. The focus was on the displacement patterns and solvent breakthrough controlled by matrix-fracture interaction and the pore scale behaviour of solvent-oil interaction for different fracture and injection conditions (rate, vertical vs. horizontal injection) as well as oil viscosity. Besides the visual investigation, effluent was also analyzed to calculate the solvent cut and oil recovery.

Next, the process was modeled numerically using a commercial compositional simulator and the saturation distribution in the matrix was matched to the experimental data. The key parameters in the matching process were the effective diffusion coefficients and the longitudinal and transverse dispersivities. The diffusion coefficients were specified for each fluid and dispersivities were assigned into grid blocks separately for the fracture and the matrix.

Finally, glass etched microfluidic models were used to investigate pore scale interaction between the matrix and the fracture. The models were prepared by etching homogeneous and heterogeneous micro scale pore patterns on glass

sheets bonded together and then saturated with colored n-decane as the oleic phase. CO_2 was injected at miscible and immiscible conditions. The focus was on visual pore scale analysis of miscibility, breakthrough of CO_2 and oil/CO_2 transfer between the matrix and the fracture under different miscibility, injection rate and wettability conditions.

Acknowledgements

This research was funded by NSERC (Strategic Grant No: G121990070). The funds for the equipment used in the experiments were obtained from the Canadian Foundation for Innovation (CFI, Project #7566) and the University of Alberta. I also thank the National Institute for Nanotechnology at the University of Alberta for allowing us to use their Nanofab facilities and its staff for their support during the micromodel fabrication process.

I am grateful to my supervisor Dr. Tayfun Babadagli who not only support but also encouraged and challenged me throughout my academic program.

I would like to express my profound gratitude to my close friend Serdar Atmaca for his encouragement and support before and during my study. I am as ever, especially indebted to my parents for their love and support throughout my life.

My sincere thanks to fellow students Barkim Demirdal, Mert Ozdemirtas, Dmitry Bogatkov, Khosrow Naderi and Al Muatasim Al Bahlani for their help and friendship. I also thank to all the members of EOGRRC for their helpful advices.

Finally, I would like to extend my deepest thanks to Sinem for her invaluable support.

Table of Contents

List of Tables

List of Figures

Nomenclature

b =	*Fracture width m,*
D_M =	*Diffusion coefficient (oil and solvent) m^2/s,*
EOR=	*Enhanced Oil Recovery*
FDI =	*Fracture diffusion index, dimensionless,*
MMP=	*Minimum Miscibility Pressure*
NFR=	*Naturally Fractured Reservoirs*
LMO=	*Light Mineral Oil*
HMO=	*Heavy Mineral Oil*
KER=	*Kerosene*
$f(\theta)$=	*Wettability index, dimensionless*
g =	*Gravity force m/s^2,*
k_f =	*Fracture permeability m^2,*
k_m =	*Matrix permeability m^2,*
L =	*Length of Fracture m,*
L =	*Length of matrix m,*
r =	*Flow velocity m/s,*
μ_w =	*Viscosity of water, cp,*

ρ_s = *Density of injected (solvent) phase, kg/m^3,*

ρ_o = *Density of displaced (oil) phase, kg/m^3,*

$\emptyset_F$ = *Porosity (Fracture)*

$\emptyset_M$ = *Porosity (matrix)*

μ_s = *Solvent viscosity, kg/m.s,*

μ_o = *Solute viscosity, kg/m.s,*

$\Delta\mu$ = *Viscosity difference, kg/m.s,*

$\Delta\rho$ = *Density difference, kg/m^3.*

Chapter 1

Introduction

1.1 Overview

After primary and secondary production periods, considerable amount of oil remains trapped in the reservoirs. Complexities and high costs of production of unconventional sources urged industry to search for new methods to produce as much as possible from conventional reservoirs. Chemical injection, miscible and immiscible gas injection and thermal techniques, and even unconventional techniques such as seismic stimulation and microbial injection are becoming more popular due to increasing demand for oil and a significantly reduced number of new discoveries of giant fields.

Among them, CO_2 injection and sequestration gained special respect from environmentalists and petroleum engineers as an economically and environmentally convenient operation. CO_2 sequestration into geologic formations such as oil reservoirs, coal beds and aquifers is a possible way to reduce the emissions of this anthropogenic gas into the atmosphere. Among these, sequestration into oil reservoirs while enhancing oil recovery is one of the most feasible ways as the additional oil recovery would offset the cost of CO_2 sequestration operation. Besides, the matrix, the main source of oil, could be a good CO_2 storage medium.

Proper design of this operation is essential to maximize both the amount of CO_2 sequestered and the oil recovered. Matrix, fracture, injected and reservoir fluid properties have great effect on the efficiency of the process. Clear understanding of the contributions of each on the dynamics

of the matrix-fracture interaction is required in designing EOR and CO_2 sequestration applications.

1.2 Statement of the Problem

Naturally fractured reservoirs constitute a great portion of current and potential CO_2 flooding and sequestration operations. In those reservoirs, injected CO_2 breaks through in very a short time generally and the fate of the operation mostly depends on fluid transfers between the matrix and the fracture. It is invaluable to understand the physics of matrix-fracture interaction in this type of applications to maximize the efficiency of the process; maximizing the incremental oil production with maximum CO_2 storage. In this co-optimization process, miscibility, oil viscosity, matrix properties (permeability, porosity, pore characteristics, wettability, etc.), fracture properties (permeability, orientation, and connectivity), injection rate, gravity, and the physical state of CO_2 play a critical role.

Although numerous studies focused on the different aspects of this problem, the physics of the matrix-fracture interaction is not well understood. Available studies are mostly carried out on core samples using "dummy solvents" to represent CO_2. Experiments with core samples can provide data to some extent. Production and injection performance can help to construct analytical models and handle the problem on a larger scale. Information about the phase distributions in the dual-porosity medium and saturation profiles within the matrix are important data for more realistic modelling of the process. Limited studies have been reported on visual analysis of the CO_2 displacements and these studies mostly focused on the effect of the fracture in immiscible displacements. Surprisingly, there is no any visual study purely focusing on matrix-fracture interaction during miscible injection of CO_2 (high pressure experiments) at pore scale, at least to our knowledge.

Visual investigation is required to observe the saturation distributions and front progress within the matrix and with respect to viscous flow in the fracture and also to reveal the physics of matrix-fracture interaction at the pore scale. Modelling studies matching the visual observations are also required to represent the physics of the process more inclusively in the numerical models of this complex process.

1.3 Solution Methodology

In order to investigate the matrix-fracture interaction during CO_2 injection 2-D core scale and pore scale laboratory experiments were conducted. To obtain critical parameters in miscible displacements, core scale experiments were simulated using a commercial reservoir simulator.

First, matrix fracture interaction during miscible CO_2 displacement was studied visually with 2-D glass bead packed models. To mimic the first contact miscibility, hydrocarbon solvent pentane was employed as an injecting fluid. Various parameters- injection rate, oil viscosity and fracture orientation- were changed and the effect of each on the displacement pattern and production profile was analyzed.

Next, first contact miscible displacement experiments were modeled and the visual results were matched to clarify the parameters controlling the matrix-fracture interaction and the phase distribution in the system. Rather than the production data, visual data was used in matching process as the phase distribution in a such system was believed to be more representative of the physics involved in matrix-fracture interaction.

Finally, glass etched micromodels were utilized to reveal the pore scale interactions during miscible and immiscible CO_2 displacements. Injection pressure and rate were changed to investigate CO_2 breakthrough and fluid transfers between matrix and fracture under different miscibility conditions.

Chapter 2

Literature Review

2.1 Displacement Mechanisms and Efficiency of Diffusion Controlled Miscible Displacements

CO_2 injection and sequestration into fractured oil reservoirs deserves a detailed investigation regarding the mechanisms involved and the optimum conditions to get the maximum benefit out of it.

Huang and Tracht (1974) studied oil recovery mechanisms during CO_2 injection and reported that the dominant controlling mechanisms are CO_2 swelling and the CO_2 extraction of oil. Bahralolom and Orr (1988-a) supported that through their micro model visualization study. They also suggested that extraction is more effective than solubility. In general, the most common mechanisms controlling oil recovery by CO_2 injection are (1) oil displacement by the generation of miscibility, (2) oil swelling and (3) reduction in oil viscosity (Schramm *et al.*, 2000). The presence of water can decrease the efficiency of miscible CO_2 displacements in water wet systems as the higher saturation of wetting phase decreases the flow fraction of the nonwetting phase and consequently decreases the recovery of oil in water wet systems (Campbell and Orr, 1985). The interaction of phase behaviour with heterogeneities leads to residual oil saturations due to preferential flow paths (Bahralolom *et al*., 1988-b).

One of the main issues is the miscibility. Injecting CO_2 at immiscible conditions into fractured reservoirs may not be efficient due to early breakthrough of the gas; achieving miscibility can be costly in terms

of operation. In their experimental study, Asghari and Torabi (2008) investigated the effect of miscibility on gravity drainage of oil in CO_2 flooding. Their results showed that increasing the pressure helped increase production up to the minimum miscibility pressure (MMP); beyond this point higher pressures reduced the ultimate recovery. After the miscibility is achieved, diffusion and dispersion in the fracture, and more importantly in the matrix where the oil is stored, take the control of displacement and the efficiency of the displacement depends on the injected and saturated fluids as well as matrix and fracture conditions. To reveal the extent of the influence of each, and to understand the physics involved, investigators have also carried out different types of experimental studies. Darvish *et al*. (2006) conducted CO_2 flooding experiments at reservoir conditions using outcrop samples of the reservoir rock using a high pressure core holder where fracture surrounds the core. What they observed was that CO_2 extracted the lighter components which had the higher diffusion coefficient in the early stages of production while heavier components were produced at later stages. They concluded that the diffusion was the main recovery mechanism. Similarly, Trivedi and Babadagli (2008-a) studied the effect of continuous CO_2 injection as well as blow-down considering the sequestration aspect of the operation under immiscible, near-miscible and miscible conditions. According to their study, during the continuous miscible injection, lighter components were extracted in the matrix adjacent to fracture and produced while leaving heavier components behind and making it harder for CO_2 to diffuse further into the matrix. Heavier components could be produced by vaporizing but they needed a significant amount of time and CO_2 injection. They figured out that soaking after the continuous injection helped to extract heavier components under miscible conditions, where the same could not be said under immiscible conditions.

What is critical for petroleum engineers is the efficiency of miscible displacements during enhanced oil recovery applications where the efficiency is defined as the optimal injection conditions that maximize oil

recovery while minimizing the amount of injectant. Over the last four decades, scientists have investigated the factors and mechanisms controlling miscible displacement. Due to high influence on the process, the primary interest was on diffusion and dispersion in the oil industry (Perkins and Johnston, 1963). Many investigators developed experimental and numerical methods to calculate diffusion and dispersion coefficients for the displacing and displaced fluids (Leahy-Dios and Firoozabadi, 2007; Goss, 1971; Islaz-Juarez et al., 2004 and Garder et al., 1963). The reason behind those studies was that the complex nature of multicomponent reservoir fluids limits the usage of available analytical methods.

The efficiency problem is more crucial in a fractured medium as a highly fractured system creates complexities causing irregular distribution of the injected phase. Factors affecting the efficiency of miscible displacements and mechanisms in the presence of fractures were also studied (Silvia and Belery, 1989; Thompson and Mungan, 1969; Er and Babadagli, 2007; Trivedi and Babadagli, 2006, and Firoozabadi and Markset, 1994). Mass transfer and convective dispersion between matrix and fracture lead to the higher ultimate recoveries compared to immiscible displacements. Early breakthrough, however, is the major issue for miscible displacement in fractured reservoirs. Geometrical properties of fracture are important as well as matrix and fluid properties in controlling the breakthrough of the injected fluid. Thompson and Mungan (1969) analyzed the effect of fracture length, orientation and density in their experimental study with core samples. Their study revealed the effect of displacement velocity on recovery efficiency. Similarly, Firoozabadi and Markset (1994) investigated the effects of fracture aperture on the process. Their study showed that the miscible displacement is still efficient even in the case of high fracture apertures.

Several other studies aimed to introduce matrix-fracture transfer functions (Lenormand et al, 1998 and Perez et al, 1990). Perez et al. (1990)

proposed that the only way to model the transfer between matrix and fracture is to define an "effective diffusion coefficient" which is the functions of fracture geometry, fluid velocity and fluid compositions. Although matrix, fracture and fluid properties are important in the efficiency of the process, the most effective and the only controllable one is the displacement rate (Trivedi and Babadagli, 2006).

2.2 Visualization Studies

Besides the experiments conducted with core samples which handles the dynamics in macro scale, some researchers also focused on 2-D experiments to visualize the micro scale interactions. Visualization experiments provided substantial information and enabled us to monitor the process at the pore scale especially with the technological developments in fabrication of microfluidic devices and visualization techniques.

Glass bead packed models were used for 2-D visualization in several studies as the glass beads were transparent and allowed light to be transmitted through the model when packed in transparent sheets (Sohrabi *et al.* 2001; Al-Wahaibi *et al.*, 2006 and 2007; Hatiboglu and Babadagli, 2005). In his unique study, Paidin (2006) prepared glass bead pack model with fracture to study the effect of fracture on gas assisted gravity drainage. His 2-D model consisted of two separate transparent plastic plates held together between two aluminum frames and a mesh box covered with a sieve placed in the model simulating the fracture. Wang (1982) tested the effect of miscibility in CO_2 displacements with a high pressure set-up and glass bead packed model and showed that all three types of displacements - miscible, near-miscible and immiscible- could exist at the same time. Pictures clearly showed residual oil rings around the glass beads, CO_2 front in miscible and immiscible displacements, and depositions of different types of oil after CO_2 and water flooding

Researchers also used thin sections from cores to analyze fluid distributions in pores after the experiments (Sincock and Black, 1988). To analyze the dynamics in real pores, Sun and Tang (2006) placed thin sections between two glass sheets with a special cementing method and visualized water injection in low permeability sandstone.

Etching technology enabled investigators to produce a variety of pore patterns and visualize immiscible displacement processes (Chatzis and Lim, 1983; Bahrololom and Orr, 1988; Feng *et al*., 2004; Smith *et al.*, 2002; Wan *et al.,* 1996; Romero-Zeron and Kantzas, 2006; Dijke *et al.*, 2004). As important as the matrix part itself, fractures also got the attention of researchers due to their effect on fluid distributions in the matrix. Investigators used available the etching technique as in the previous models but included a fracture in the model as a uniform channel that is much wider than the pore network. Matrix-fracture interaction was studied with gravity drainage, imbibition, and gas and/or water injection experiments by several authors (Rangel-German and Kovscek*,* 2004a and2004-b; Dastayari *et al.*, 2005; Shariatpanahi *et al*., 2005;Haghighi *et al.*, 1994).

Unlike the immiscible displacement experiments, studying miscible displacement in micromodels requires quite complicated equipment and effort due to difficulties arising from high pressure conditions. In one of the earliest study of its kind, Campbell and Orr (1985) conducted high pressure CO_2/Crude-oil displacement experiments with glass etched micromodels having a homogeneous or heterogeneous pore network. They visualized the development of fingers and the diffusion of CO_2 through the water into trapped oil in dead-end pores. Bahralolom *et al.*(1988-a and 1988-b) also used micro-models similar to the one used previously[4]. The main difference in Bahralolom's model was that pore networks on the models were etched by tracing pore patterns from an enlarged photo of thin-sections. The aim was to reflect the complexity of the reservoir rock on the efficiency of CO_2 displacement.

Sohrabi *et al.*, (2000, 2001, 2007-a and 2007-b) were able to conduct experiments up to 5100 psi investigating near miscible hydrocarbon gas, water alternating gas and simultaneous water and gas injections. In previous studies, fluids have been colored to observe patterns, interfaces and saturation changes within the matrix and fracture. In a recent study, Javadpour and Fisher (2008) provided information about fabrication of new generation micromodels and a new technique to monitor saturation changes without coloring the fluids.

It is interesting that most of the CO_2 injection applications are performed in naturally fractured oil reservoirs and it is very critical to represent the effect of fracture on the models. However, there is a lack of visual investigations with fractured models in the literature except some immiscible displacement studies (Dastayari *et al*., 2005; Haghighi *et al*., 1994 and Shariatpanahi *et al*., 2005).

Chapter 3

First Contact Miscible Displacement Experiments in Fractured Systems

In this paper, we investigated the effect of several factors (displaced fluid viscosity, rate, gravity and wettability) on miscible oil displacements in the presence of fracture. This is the very first step towards the understanding of matrix-fracture interaction during CO_2 injection in oil reservoirs to eventually assess the oil recovery and CO_2 sequestration potentials. We used a first contact miscible solvent to mimic fully miscible CO_2 injection. The focus was on the displacement patterns and solvent breakthrough controlled by matrix fracture interaction and pore scale behaviour of solvent-oil interaction for different fracture and injection conditions (rate, vertical vs. horizontal injection) as well as oil viscosityWe analyzed the visual observations obtained through the experiments qualitatively. We also provided quantitative analysis of the recovery and sequestration potential using the production data monitored during experimental runs.

3.1 Experimental

A series of experiments were conducted by injecting colored pentane into the glass bead models saturated 100% with oil. Effects of the following factors on displacement efficiency were investigated;

- Injection rate
- Viscosity ratio
- Gravity

A version of this chapter has been published

Er V. and Babadagli T., 2007, CIPC-2007-033, Canadian Int. Pet. Conf., Calgary, 12-14 June

3.1.1 Models

Transparent 2-D models were prepared using acrylic sheets and glass beads (**Figure 3.1**). Before gluing the sheets, two parallel channels were cut in the middle of one of the acrylic sheets and large (2.0-2.3mm) glass beads were placed in these grooves representing the fracture walls. Then, a layer of filter paper was placed between two lines of large glass beads to minimize the passing of small glass beads into the fracture. Production and injection ports were placed right over the fracture and acrylic sheets were glued around three sides with epoxy. Glued sheets were filled with small (0.3-0.6 mm) glass beads representing the matrix and model was closed by gluing the fourth side with epoxy (**Figure 3.2**). Before this process, a shaker was used to pack the beads tightly and uniformly.

3.1.2 Fluids

Three types of oil: kerosene, light and heavy mineral oil, were used as the displaced fluid. Pentane colored in red was used as the displacing fluid in all experiments. The properties of the fluids are given in **Table 3.1.**

3.1.3 Measurement techniques

Recovery and injection profiles were recorded during the experiments. The refractive index method (Trivedi and Babadagli, 2006) was used to distinguish the produced oil and solvent amounts.

3.1.4 Procedure

Models were saturated with oil under vacuum without any initial water saturation. The -red- colored pentane was continuously injected at constant rates using a pump and oil produced at atmospheric pressure. During the

Er V. and Babadagli T., 2007, CIPC-2007-033, Canadian Int. Pet. Conf., Calgary, 12-14 June

experiments, time lapse images were recorded to a computer via camera (**Figure 3.3** and **Figure 3.4**). Produced mixtures of oil and solvent were collected and analyzed using the refractometer. All experiments were conducted at room temperature and atmospheric pressure. A list of the experiments is given in **Table 3.2**. Seven experiments were conducted and visualized. The snapshots taken during the experiments are displayed in **Figures 3.5** through **Figure 3.11**. In these images, white and red colors represent the oil phase and solvent, respectively. The recovery plots comparing different cases are given in **Figure 3.12** through **Figure 3.16**

3.2 Analysis of the results

3.2.1 Effect of injection rate

One of the most critical parameters in any injection application in naturally fractured reservoirs is the injection (flow) rate. The injected fluid will flow in the fracture network due to its high permeability compared to the matrix. It is the only controllable parameter and the efficiency of the process could be improved by adjusting it depending on reservoir and fluid properties (Trivedi and Babadagl, 2006).

In order to analyze the effect of rate, solvent was injected at 15 ml/hr, 25 ml/hr and 45 ml/hr in light mineral oil saturated models and at 15 ml/hr and 45 ml/hr rates in heavy mineral oil saturated models. **Figure 3.12** shows that recovery rate per injected solvent is much lower at high rates especially in the heavy mineral oil case. In order to produce the same amount of oil, less solvent is required at low rates. On the other hand, higher rates yield faster oil recovery (**Figure 3.13)**. For the heavy mineral oil case, 3.8 PV of solvent and 180 min. are required to achieve the ultimate recovery at 15 ml/hr, but at 45 ml/hr, 6 PV of solvent and 80 min. are required to produce

A version of this chapter has been published
Er V. and Babadagli T., 2007, CIPC-2007-033, Canadian Int. Pet. Conf., Calgary, 12-14 June

0.9 PV of oil. Slower rates are more suitable for storage aimed processes, whereas higher rates should be preferred if oil recovery is the main target. For co-optimization, i.e., maximum oil recovery and maximum storage, a critical rate should be defined as a function of oil viscosity.

The ultimate recoveries in all cases except one (45 ml/hr, heavy mineral oil) reached 100% eventually. The recovery rate and the residual oil saturation are controlled by the viscosity ratio and the rate. As the oil viscosity is increased (compare **Figure 3.5**, **Figure 3.6** and **Figure 3.10** for the same rate but different oil viscosity cases), fracture effect becomes more critical. This is due to slower diffusion into matrix oil caused by increasing diffusion coefficient. For the lightest oil case (**Figure 3.5**), the matrix effect is felt in much earlier stages and the oil sweep is more efficient due to faster diffusion interaction between the solvent in the fracture and oil in matrix.

As the rate is increased, the transfer into matrix becomes less effective and more fingering is observed (compare **Figure 3.8** and **Figure3.9**).In the heavier oil cases, the sweep in the matrix becomes less efficient as the rate is increased. **Figure 3.11** shows that there were still some portions that had not contacted with solvent even though 5 PV of solvent had already been injected.

3.2.2 Effect of viscosity ratio

Models were saturated with different types of oils, namely, kerosene, light mineral oil and heavy mineral oil to analyze the effect of the viscosity difference between displacing and displaced fluids. **Figure 3.14** shows that as the viscosity difference between solvent and oil increases, the efficiency of the process decreases. That means it takes more time to reach ultimate recovery for more viscous oil. At 2.0 PV of solvent injected, 94% of kerosene, 86% of light mineral oil and 79% of heavy mineral oil is produced. Comparing **Figure 3.5**, **Figure 3.6** and **Figure 3.10** one can observe that although the fracture controls the progress of the front, diffusion of solvent into the matrix is much faster for lighter oils. Increasing

Er V. and Babadagli T., 2007, CIPC-2007-033, Canadian Int. Pet. Conf., Calgary, 12-14 June

viscosity difference also leads to unstable fronts and viscous fingers developed through the matrix from the fracture (**Figure 3.17).**

3.2.3 Effect of gravity

The horizontal light mineral oil experiment at 15ml/hr was repeated for vertical orientation to analyze the effect of gravity. Solvent was injected from the top, and oil and solvent mixture was produced at the bottom (**Figure 3.7**). Results show that the vertical injection condition is more efficient in terms of injected solvent amount and time (**Figure 3.15** and **Figure 3.16**). At 1.0 PV of injected solvent, 60% and 74% of light mineral oil were produced in horizontal and vertical cases, respectively. **Figure 3.7** shows clearly that although solvent breaks through early, a stable front is developed with maximum sweep efficiency.

3.3 Discussion

Experiments were conducted under different conditions to investigate the effect of (1) rate, (2) viscosity ratio between displaced and displacing fluids, and (3) gravity conditions. Experiments showed that in all cases fracture dominates the displacement pattern. The solvent injected filled the fracture immediately and broke through, and diffusion into the matrix took place while there was flow in fracture. Due to significant contrast between fracture and matrix permeabilities and injection of solvent directly through the fracture, we did not expect to have viscous flow in the matrix. Therefore, the matrix oil recovery was preferentially due to molecular diffusion. This diffusion process is controlled by the injection rate and the oil viscosity (or diffusion coefficient).

It was observed that rate is an important factor affecting the process as well as matrix, fracture and fluid properties. Lower injection rates created more

Er V. and Babadagli T., 2007, CIPC-2007-033, Canadian Int. Pet. Conf., Calgary, 12-14 June

stable fronts and gave sufficient time for solvent to diffuse into oil in the matrix. However, high rates resulted in more fingering while sweeping the matrix oil and earlier break through than lower rates. This decreased the sweep efficiency.

Viscosity differences between displacing and displaced fluids changed the displacement efficiency considerably. In a homogeneous porous medium, when the viscosity of displacing fluid is lower than that of displaced fluid, the process results in viscous fingers yielding an unfavorable displacement (Salama and Kantzas, 2005). The effect of unfavorable conditions was observed mostly in heavy mineral oil experiments of fractured model experiments. While the solvent was interacting with the matrix, fingers were established due to a high viscosity difference between the displaced and displacing fluids (**Figure 3.17)**. The fingers developed through the matrix caused reduction in the efficiency of the process due to poorer sweep of the matrix oil compared to the lighter oil cases.

The effect of gravity on the efficiency of displacement was observed in the vertical experiment. Initially, the solvent quickly moved down through the fracture and broke through. At the same time, it diffused into the matrix and had a tendency to accumulate at the top of the matrix, and a segregated fluid pattern was observed due to the density difference. Low injection rate and low mobility ratio prevented the fingering of solvent. The gravity overcame the viscous forces and formed a stable solvent front with a better sweep efficiency in the matrix. Solvent flowing in the fracture diffused in the matrix and produced the oil partially. However, most of the oil production was due to convection which made the process more efficient than in the horizontal case.

For comparison we plotted all cases in **Figure 3.18** and **Figure 3.19**. Despite high matrix permeability, the cases reflect significant differences in the oil cut for a given solvent injection, especially at early times. It is

Er V. and Babadagli T., 2007, CIPC-2007-033, Canadian Int. Pet. Conf., Calgary, 12-14 June

obvious that an optimum rate depends on the purpose of the project (EOR or sequestration). Trivedi and Babadagli (2006) quantified the critical rate for an efficient sweep of the matrix for a wide variety of matrix permeabilities, matrix wettabilities and injection rates using experimental data from consolidated -fractured- core samples. Our purpose in this paper was to emphasize the importance of the injection rate (as the only controllable parameter) and oil viscosity on the matrix-fracture interaction during miscible displacement.

Er V. and Babadagli T., 2007, CIPC-2007-033, Canadian Int. Pet. Conf., Calgary, 12-14 June

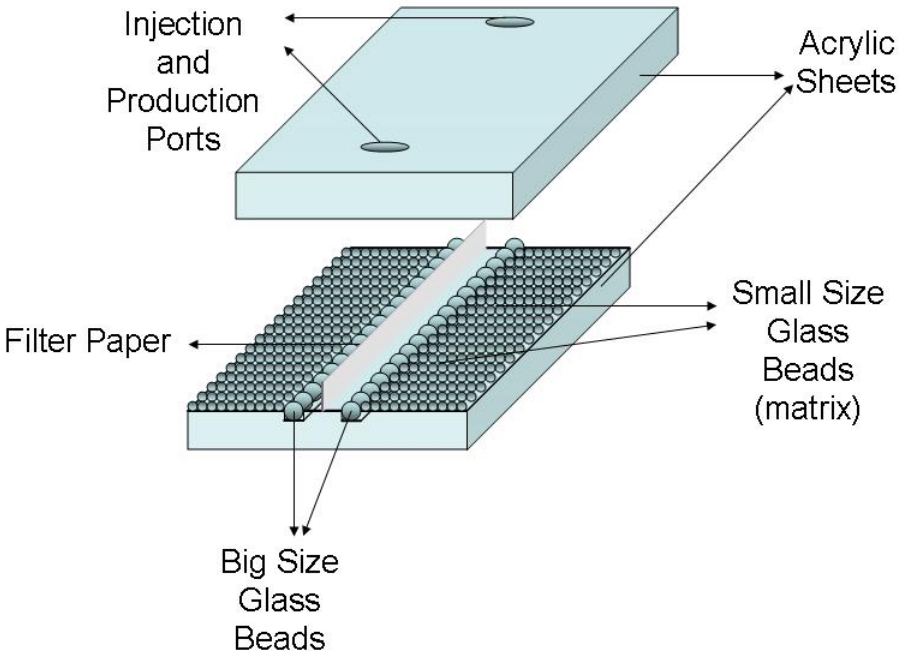

Figure 3.1 Glass bead model.

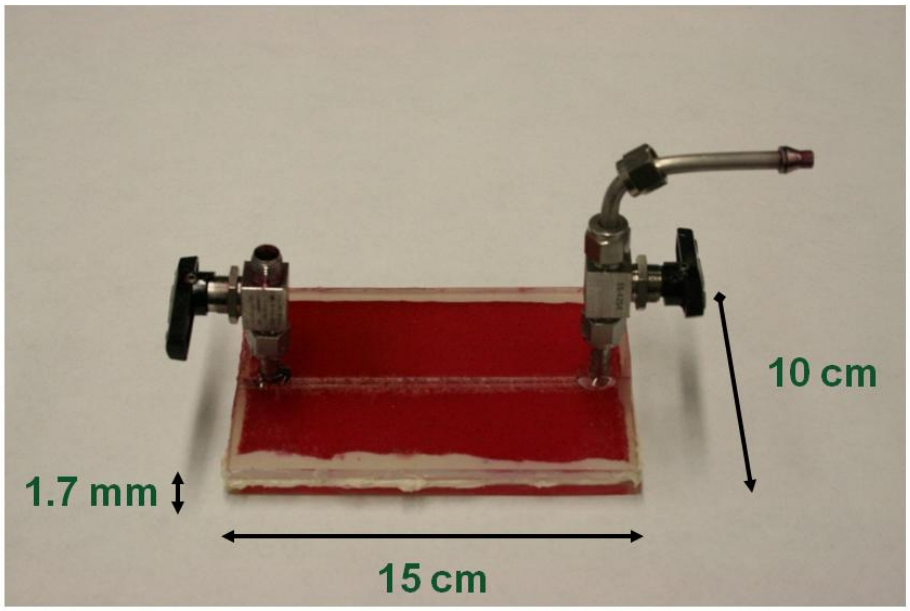

Figure 3.2 Model dimensions.

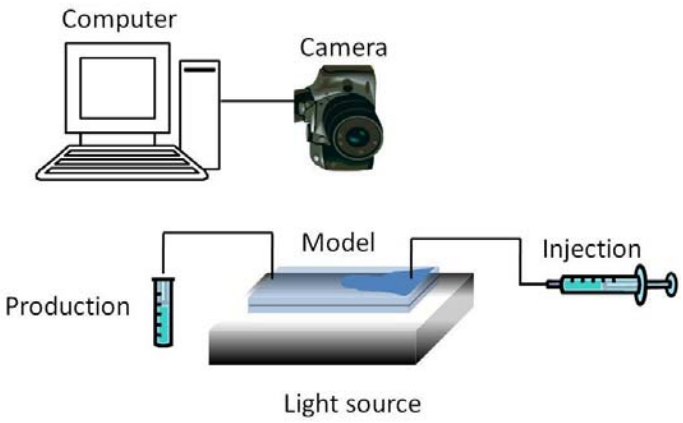

Figure 3.3 Experimental set-up

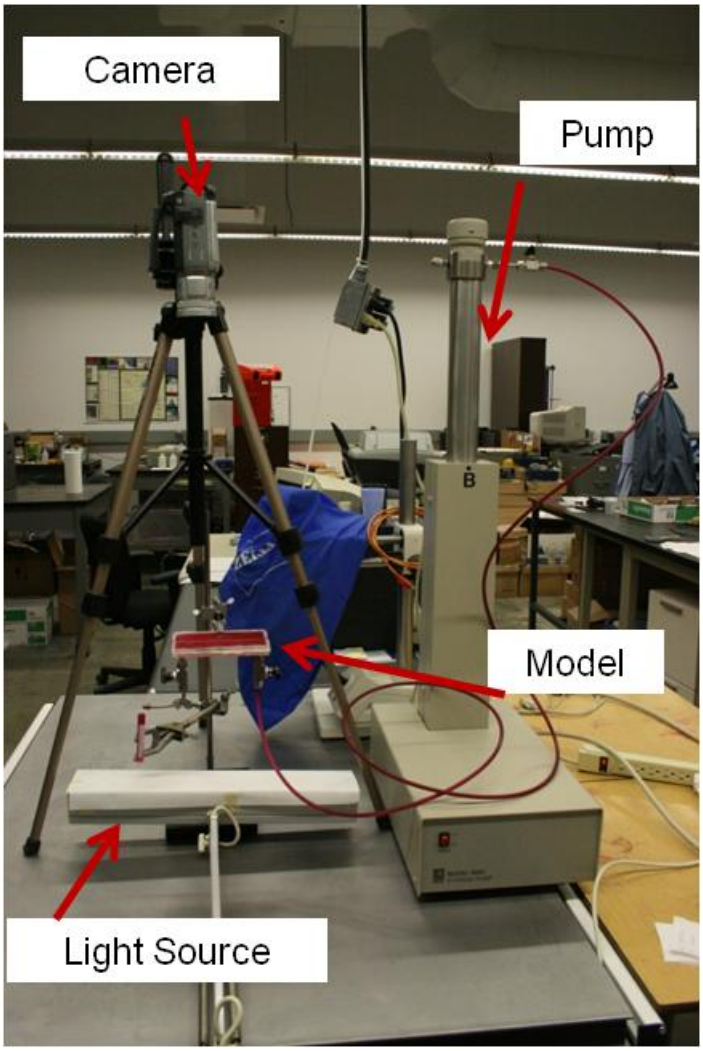

Figure 3.4 Picture of experimental set-up.

Er V. and Babadagli T., 2007, CIPC-2007-033, Canadian Int. Pet. Conf., Calgary, 12-14 June

Table 3.1 Fluid properties.

Fluid	density (g/cc)	viscosity (cp)	refraction index
pentane	0.63	0.38	1.3555
kerosene	0.79	2.9	1.4330
light mineral oil	0.81	33.5	1.4670
heavy mineral oil	0.89	500	1.4865

Table 3.2 Experiments conducted.

Experiment #	displaced fluid	rate (ml/hr)	orientation	wettability
1	kerosene	15	horizontal	water wet
2	light mineral oil	15	vertical	water wet
3	light mineral oil	15	horizontal	water wet
4	light mineral oil	25	horizontal	water wet
5	light mineral oil	45	horizontal	water wet
6	heavy mineral oil	15	horizontal	water wet
7	heavy mineral oil	45	horizontal	water wet

Er V. and Babadagli T., 2007, CIPC-2007-033, Canadian Int. Pet. Conf., Calgary, 12-14 June

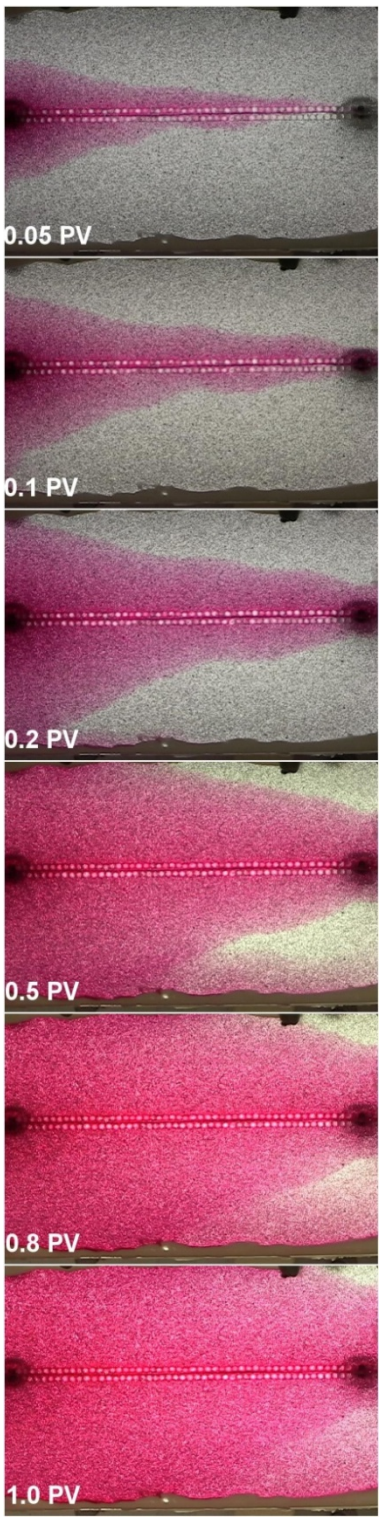

Figure 3.5 Horizontal kerosene (white) displacement at 15 ml/hr with water wet sample.

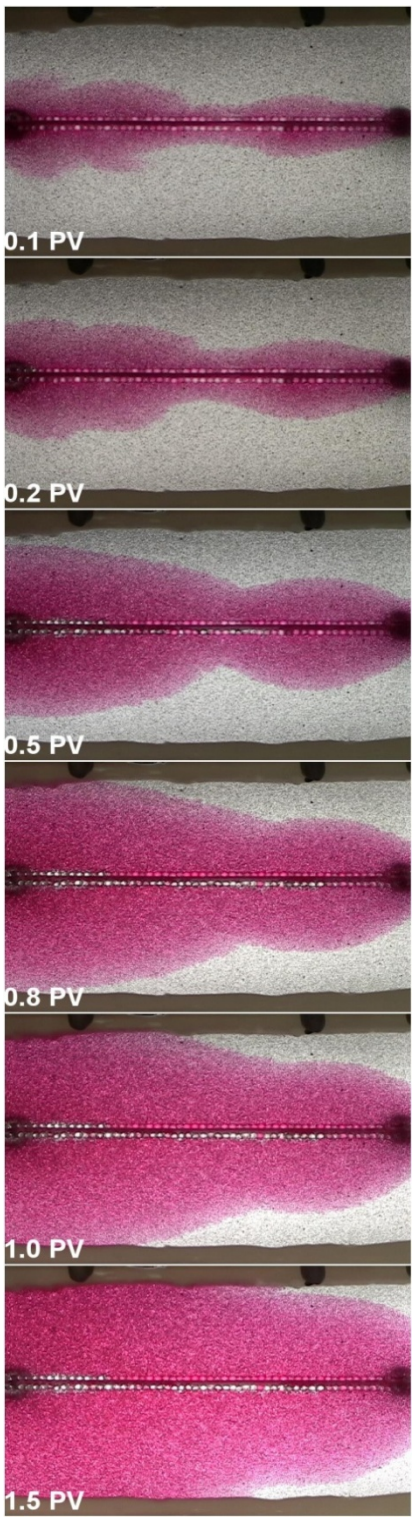

Figure 3.6 Horizontal light mineral oil (white) displacement at 15 ml/hr with water wet sample.

Er V. and Babadagli T., 2007, CIPC-2007-033, Canadian Int. Pet. Conf., Calgary, 12-14 June

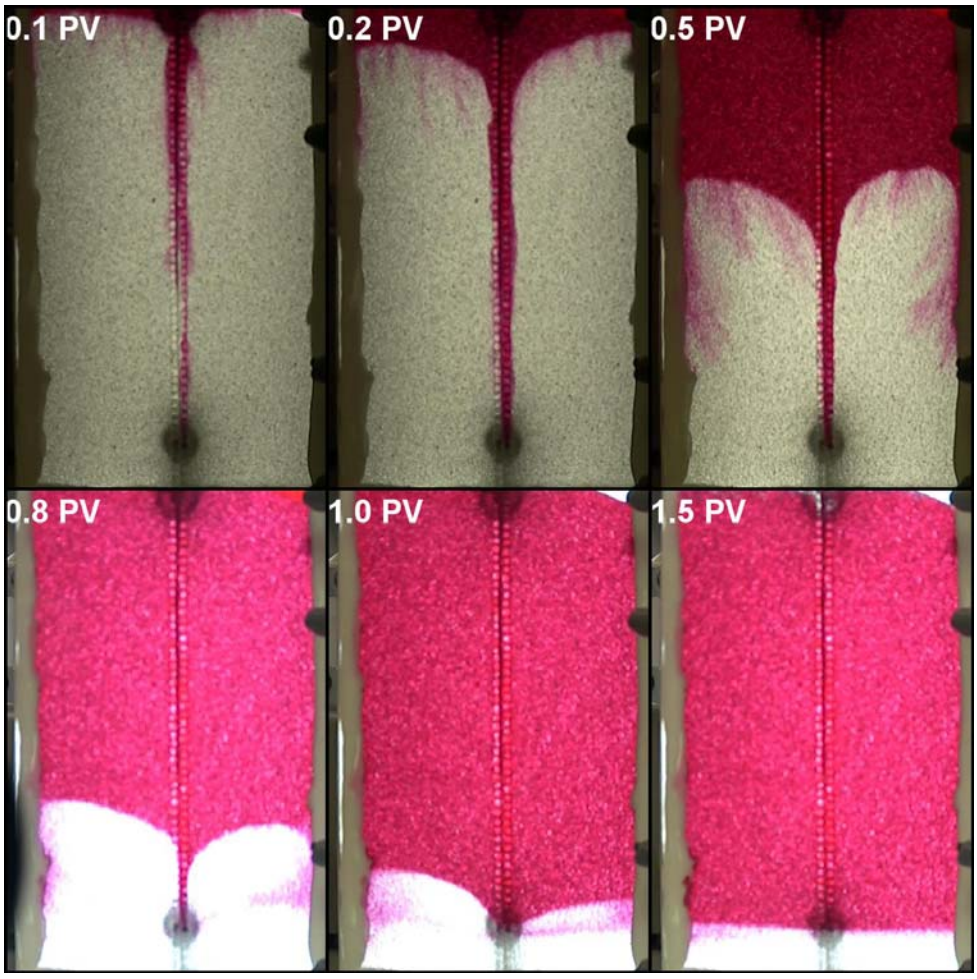

Figure 3.7 Vertical light mineral oil (white) displacement at 15 ml/hr with water wet sample (red: solvent).

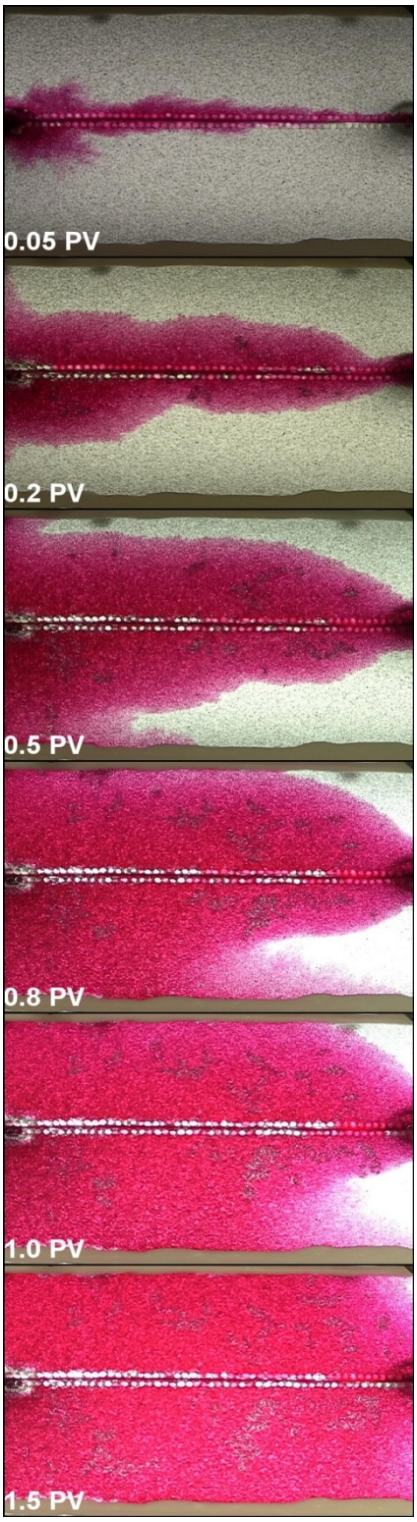

Figure 3.8 Horizontal light mineral oil (white) displacement at 25 ml/hr with water wet sample (red: solvent).

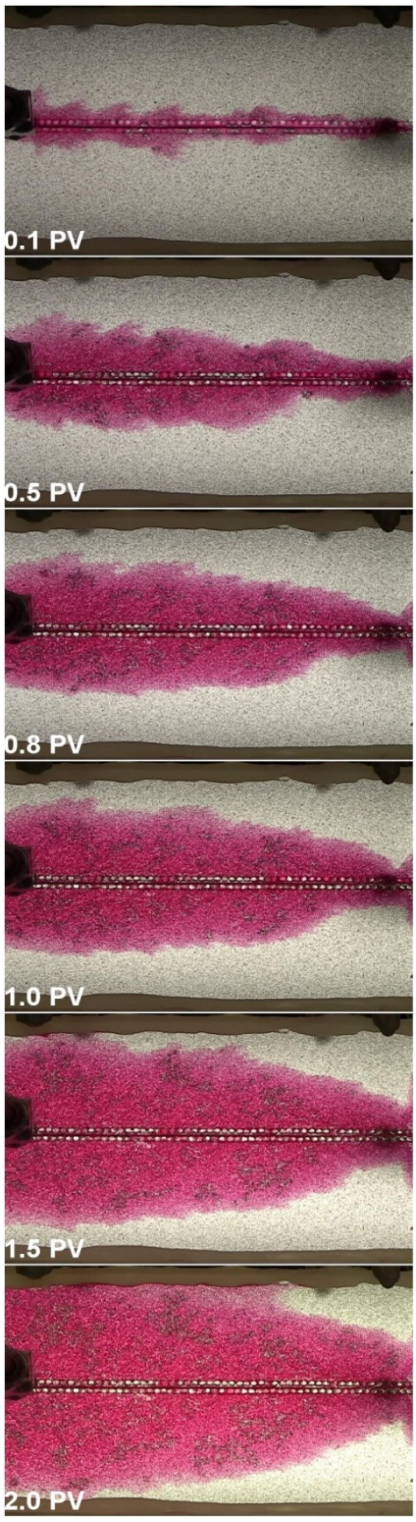

Figure 3.9 Horizontal light mineral oil (white) displacement at 45 ml/hr with water wet sample (red: solvent).

Er V. and Babadagli T., 2007, CIPC-2007-033, Canadian Int. Pet. Conf., Calgary, 12-14 June

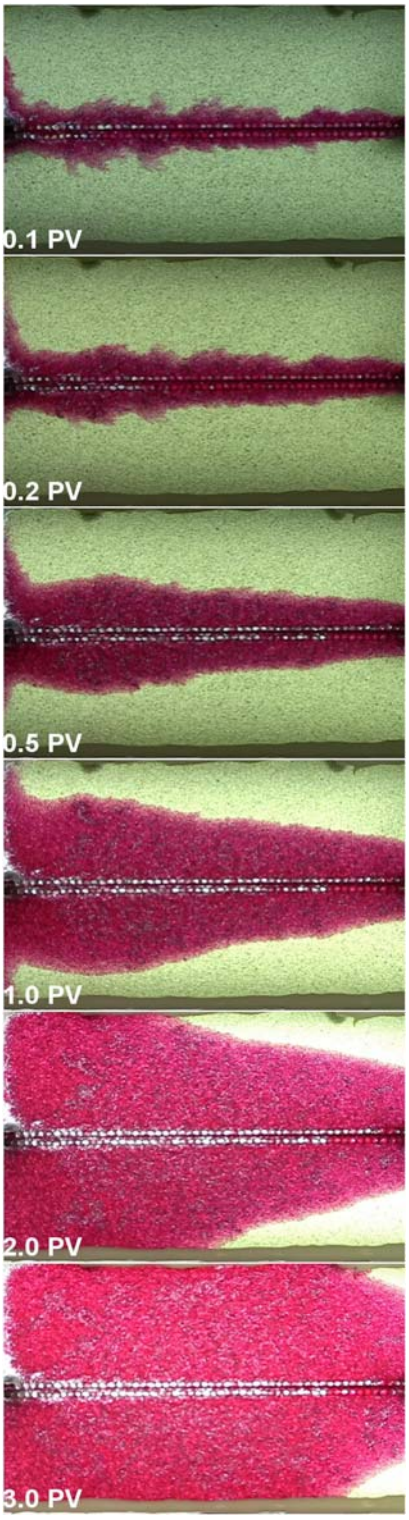

Figure 3.10 Horizontal heavy mineral oil (white) displacement at 15 ml/hr with water wet sample.

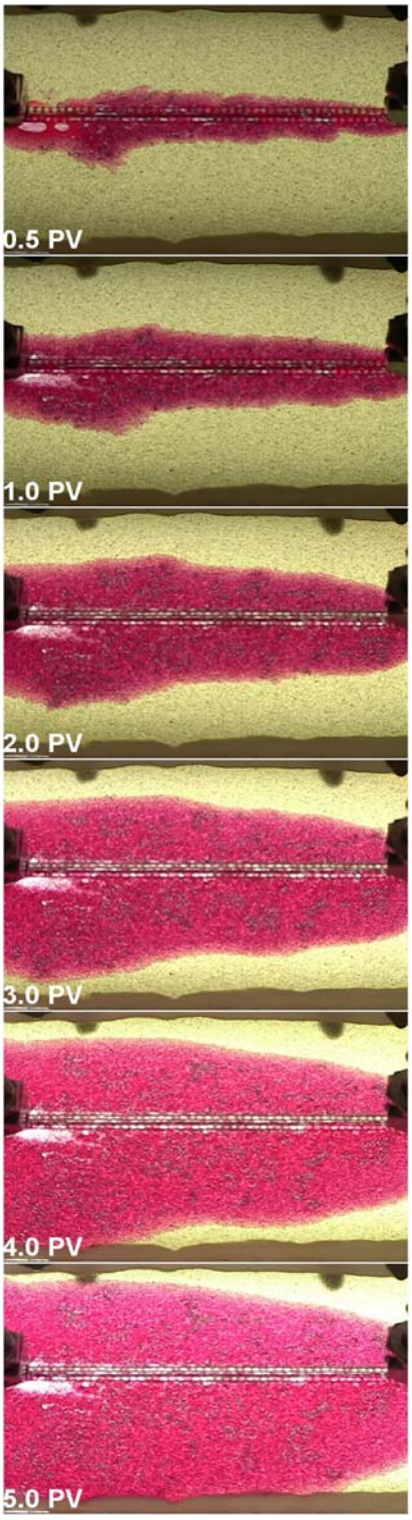

Figure 3.11 Horizontal heavy mineral oil (white) displacement at 45 ml/hr with water wet sample.

Er V. and Babadagli T., 2007, CIPC-2007-033, Canadian Int. Pet. Conf., Calgary, 12-14 June

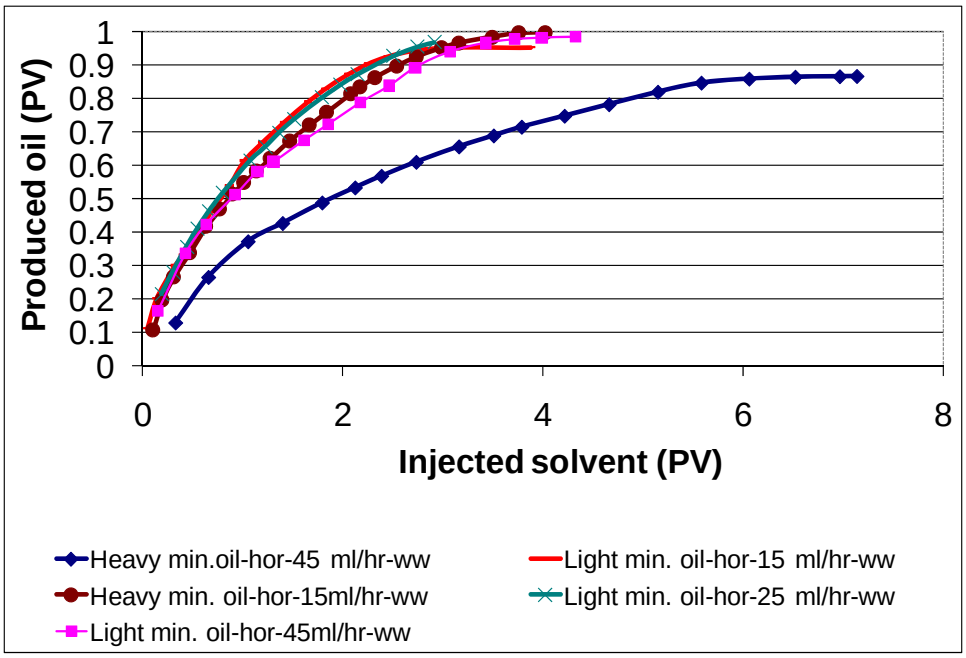

Figure 3.12 Pore volume of oil produced versus pore volume of injected solvent at different rates for different oil types.

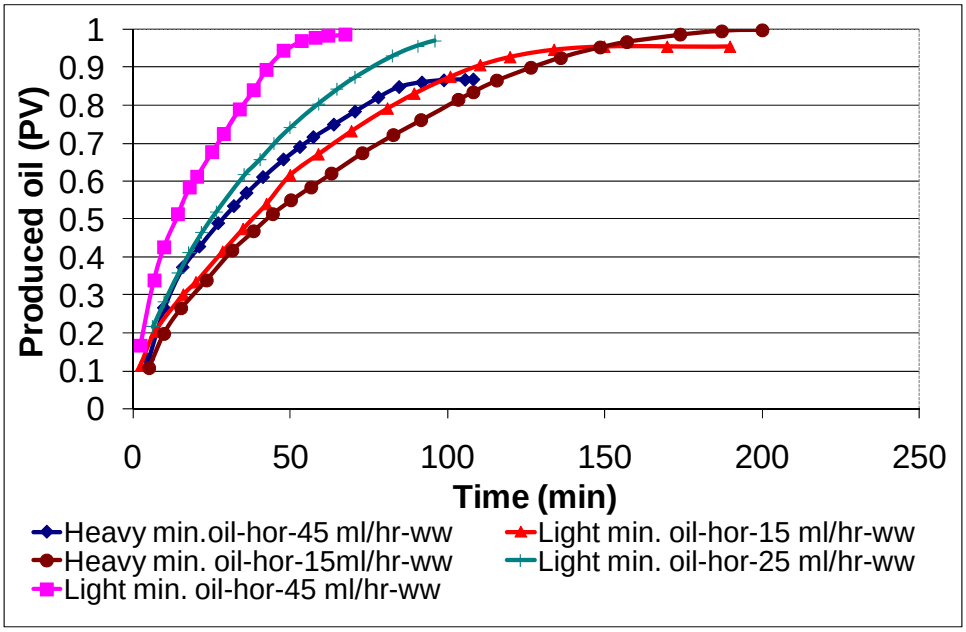

Figure 3.13 Pore volume of oil produced versus time at different rates for different oil types.

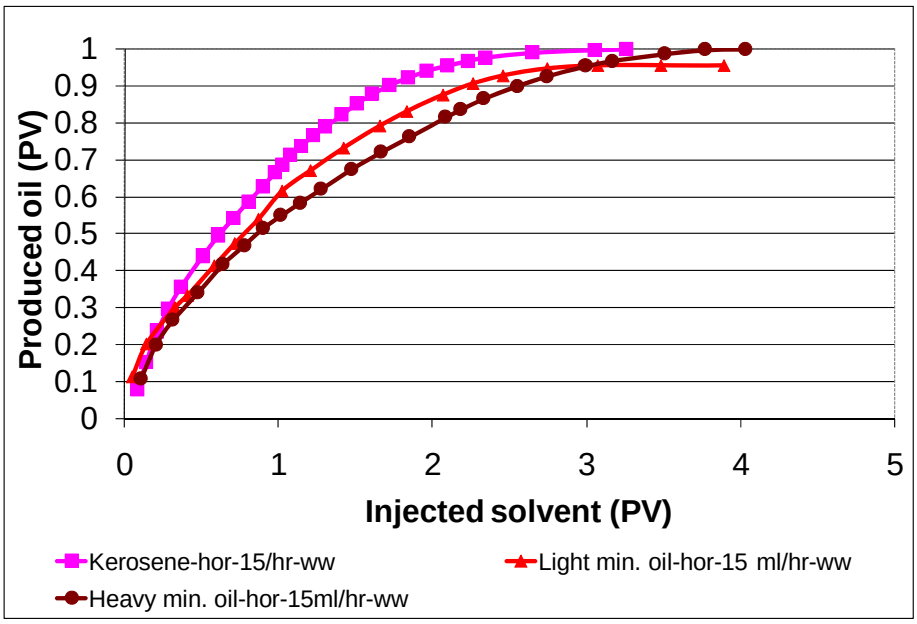

Figure 3.14 Pore volume of oil produced versus pore volume of injected solvent for different oil types.

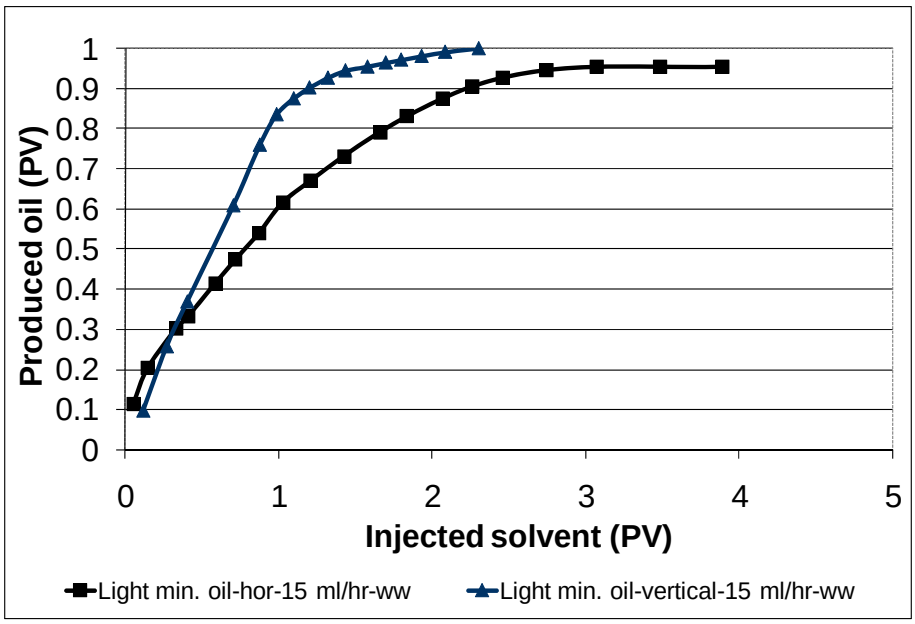

Figure 3.15 Pore volume of oil produced versus pore volume of injected solvent in horizontal and vertical flood at 15 ml/hr.

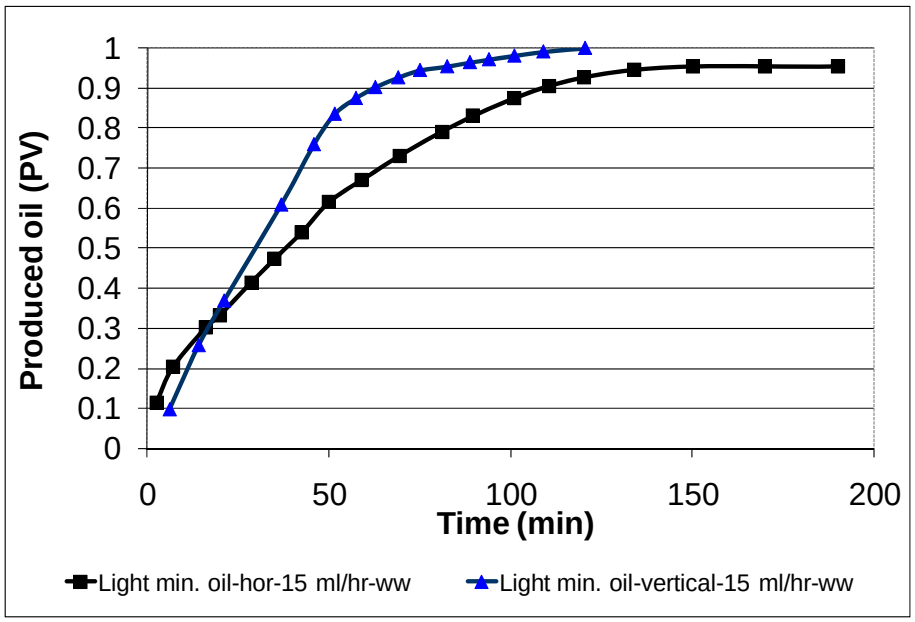

Figure 3.16 Pore volume of oil produced versus time in horizontal and vertical flood at 15 ml/hr.

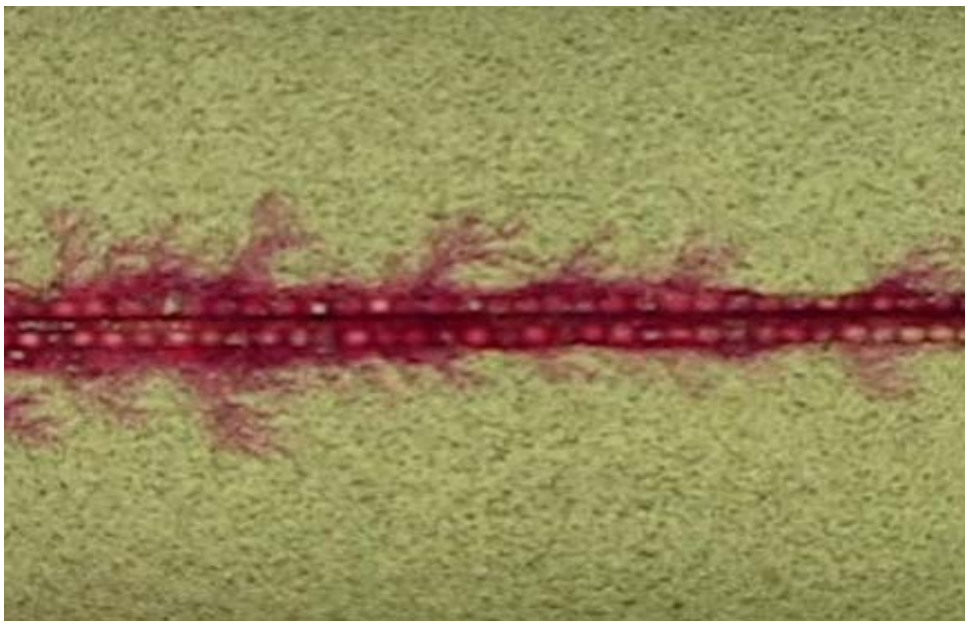

Figure 3.17 Viscous fingers observed during heavy mineral oil experiments.

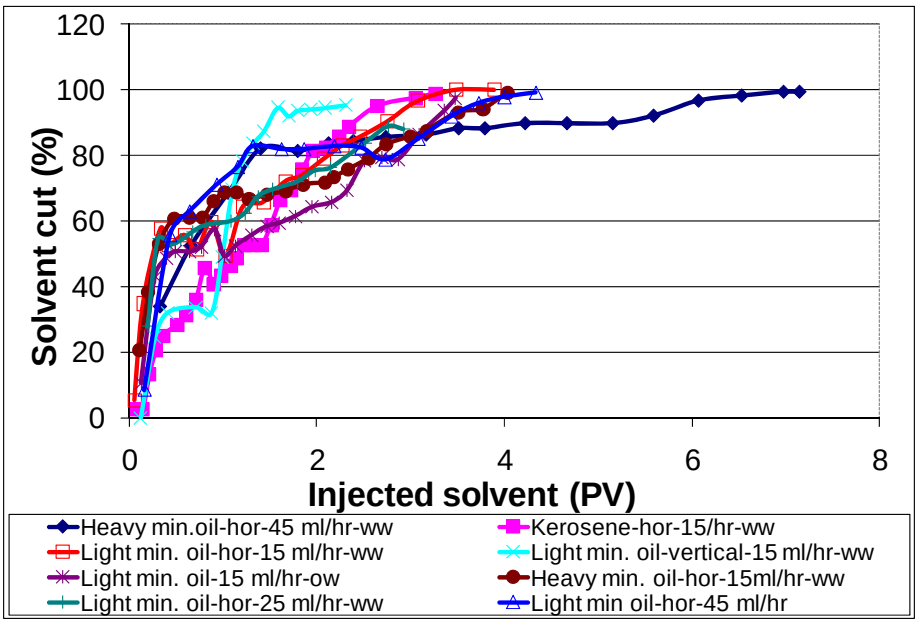

Figure 3.18 Solvent cuts versus pore volume of injected solvent at different conditions.

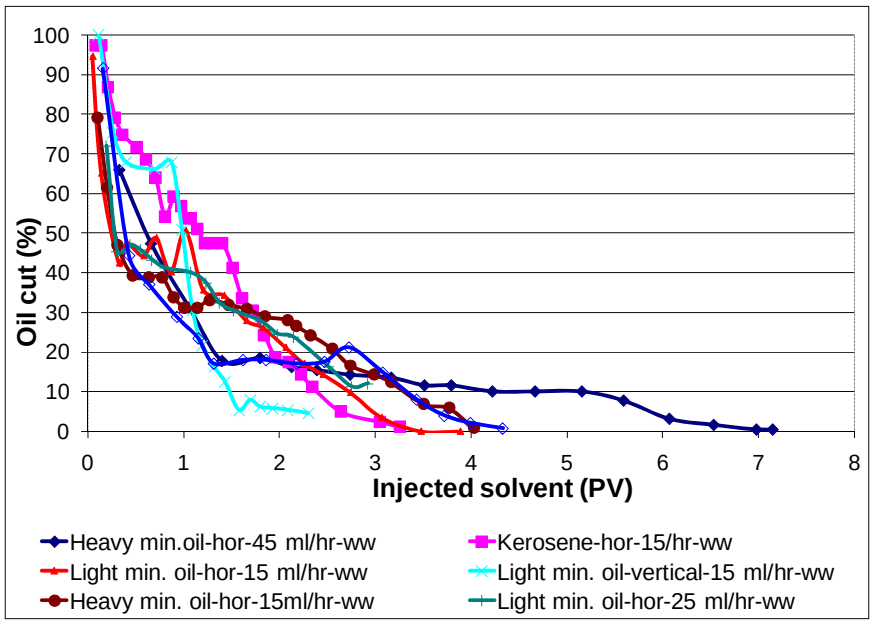

Figure 3.19 Oil cuts versus pore volume of injected solvent at different conditions..

Chapter 4

Modelling of First Contact Miscible Displacements in Fractured Systems

In a previous chapter, effect of fluid and fracture properties and the injection rate on the efficiency of miscible displacement in fractured reservoirs was studied using visual experiments. As a continuation of that study we conducted additional vertical miscible displacement experiments and modeled all of the experiments using a commercial compositional simulator to clarify the key parameters controlling the matrix-fracture interaction and phase distribution in the system.

4.1 Experimental Design

Models were created by packing 0.05 cm diameter glass beads between two acrylic sheets. The transparent nature of the glass beads and the acrylic provided high quality images of the flow movement. Model dimensions were 15cm×10cm×0.17cm (**Figure 3.2)**. The most difficult part was to place a fracture while preventing the glass beads representing the matrix to fill it. It was achieved by etching two parallel channels on inner side of one of the acrylic sheets and placing larger glass beads (~0.22 cm) in the channels (**Figure 3.1**). Permeability and porosity of the matrix portion of the model were measured as 150 Darcy and 0.40, respectively.

Inlet and outlet ports were drilled at both ends of the model (**Figure 3.3**). Models were saturated with either kerosene, light mineral oil or heavy mineral oil

(**Table 3.1**) under the vacuum with no initial water saturation. Dyed pentane (solvent) was injected and the oleic phase was displaced at ambient conditions. During the experiments, time lapse pictures of the displacement front were taken by a digital SLR camera connected to a PC. Besides the visual data, production data was also obtained using the Refractive index method (Trivedi and Babadagli, 2006). The experiments were conducted at atmospheric conditions and the outlet was open to the atmosphere yielding very small pressure drop due to low injection rate and very high permeability of unconsolidated porous medium. A total of nine experiments, as given in **Table 4.1**, were conducted to analyze the effects of the (1) injection rate, (2) viscosity ratio, and (3) gravity effects on the efficiency of the process and to provide data for further numerical modeling study.

4.1.1 Simulation Model

A commercial compositional numerical model (CMG) was utilized to model the experiments and compare the results with experimental images. The exact size of the experimental models was used in the numerical representation. The grid system was cartesian consisting of 50×30×1 blocks (**Figure 4.1**). The number of grids used in the modeling was obtained after a trial-and-error exercise and determined to be an optimal value. Fracture was represented by a layer of high permeability and a high porosity layer in the middle of the model. Fracture permeability and porosity were assumed to be 15000 D and 1.0, respectively. Other properties were the same as the experimental equivalents. The main objective of this exercise was to clarify the parameters controlling the matrix-fracture interaction and their relative importance on the process for different fluid and model types. We used the visual results rather than the production data in the matching process as the phase (saturation) distribution in the matrix was believed to be more representative of the physics of matrix-fracture interaction.

4.2 Analysis of the Results

To match the experimental results, the diffusion coefficients for fluids and dispersivity for matrix and fracture were tuned. Those terms obtained through the best match are listed in **Table 4.2** for each experiment. Simulation and experimental images of the displacement process are displayed in **Figure 4.2** through **Figure 4.10**. Results are compared in terms of injection rate, viscosity ratio and fracture orientation. In these images, white and red colors represent the oil and solvent, respectively.

4.2.1 Injection Rate

The effect of injection rate on the adjusted parameters was analyzed by comparing the different injection rate cases keeping the oil type and fracture orientation the same.

For the horizontal light mineral oil case (LMO-15ml-H vs. LMO-45ml-H), while the fracture dispersivities remained constant at 8.8×10^{-4} m and 1.1×10^{-4} m for the longitudinal and transverse respectively, the diffusion coefficient for the oil increased from 4×10^{-5} cm^2/s to 6×10^{-5} cm^2/s. In the vertical case of the same oil (LMO-V), the diffusion coefficients increased from 2.5×10^{-5} cm^2/s to 8×10^{-5} cm^2/s and from 3×10^{-5} cm^2/s to 4×10^{-5} cm^2/s for solvent and oil, respectively.

For the horizontal heavy mineral oil case (HMO-H), the diffusion coefficient of solvent was slightly reduced from 1.2×10^{-4} to 1.0×10^{-4}. In the vertical case (HMO-V), an increasing rate decreased the diffusion coefficient for solvent and fracture dispersivity from 6×10^{-5} cm^2/s to 3×10^{-6} cm^2/s and 8.8×10^{-2} m to 4×10^{-2} m, respectively.

4.2.2 Viscosity Ratio

Viscosity ratio was analyzed comparing the same injection rate and fracture orientation simulation results for different oil viscosities. Simulation results for horizontal displacement at 15ml/hr showed that increasing viscosity reduced the solvent and especially the oil diffusion coefficients (KER-15ml-H, LMO-15ml-H and HMO-15-H). In the vertical case of 15 ml/hr (LMO-15ml-V and HMO-15ml-V), the diffusion coefficient for the solvent and the oil, decreased from 2.5×10^{-5} cm^2/s to 6×10^{-5} cm^2/s and 3×10^{-5} cm^2/s to 2×10^{-6} cm^2/s, respectively.

Results showed that at a 45 ml/hr injection rate, increasing viscosity decreased the diffusion coefficients for solvent and oil in horizontal cases. In the vertical case a reduction in all parameters was observed.

4.2.3 Fracture Orientation (gravity effect)

The effect of gravity was studied by changing the injection direction (or orientation of the models) to horizontal and vertical (downward). At a 15 ml/hr injection rate for heavy mineral oil (HMO-15ml-H and HMO-15ml-V) changing the injection direction from horizontal to vertical resulted in a decrease in solvent diffusion coefficient and an increase in fracture longitudinal dispersivity, from 1×10^{-4} cm^2/s to 6×10^{-5} cm^2/s and 8.8×10^{-4} m to 8.8×10^{-2} m, respectively. At a 45 ml/hr injection rate, while solvent diffusion coefficient and transverse dispersivity decreased, longitudinal dispersivity increased in the heavy mineral oil case (HMO-45ml-H and HMO-45ml-V).

According to simulation results, vertical injection reduced the diffusion coefficients and transverse dispersivity during the displacement of light mineral at 15 ml/hr (LMO-15ml-H and LMO-15ml-V). However, it also increased longitudinal fracture and matrix dispersivities. At 45 ml/hr vertical injection, a decrease in all other parameters was observed in the light mineral oil case (LMO-45ml-H and LMO-45ml-V), except the longitudinal dispersivities.

4.3 Discussion

Using the compositional numerical simulation software, experimental results were matched and the diffusion coefficients and dispersivities were obtained for each case. The diffusion coefficients were the main parameters used in matching the visual results. The dispersivities were adjusted to do fine tuning on the displacement patterns. Although small changes in the diffusion coefficient affected the displacement pattern significantly, it required high adjustments in the order of hundreds for dispersivities to see the same effect. Dispersion is expected to be the dominant mechanism in miscible displacements. In this study, injected solvent flows in the fracture and there is no direct viscous interaction with the matrix part. Therefore, oil is produced by being transferred from matrix to the fracture due to diffusion only. In such displacement, dispersion which depends on the flow velocity becomes effective in the fracture only and diffusion becomes the dominant mechanism in the matrix.

Changes in conditions (injection rate, for example) slightly affect the oil diffusion coefficients for the same type of oil. On the contrary, although the same solvent was used in all experiments, the diffusion coefficient of the solvent was affected remarkably with changing conditions. The diffusion coefficient of a fluid is constant and changes with temperature and pressure only under static conditions (no flow). However, many factors including tortuosity, mobility, rate and gravity become effective under dynamic conditions. Then, the diffusion of fluids into each other does not occur as in static conditions. Thus, the need for usage of "apparent" or "effective" diffusion coefficient arises in miscible displacements, especially in fractured systems in which several mechanisms play a role at the same time due to heterogeneous structure.

Injection rate hardly had an impact on the diffusion coefficients of oil. However, it was observed that higher rates reduced the diffusion coefficients of solvent in vertical cases. In a previous study (Er and Babadagli, 2007), production analysis showed that an increasing rate reduced the efficiency of the displacement. In other words, much more solvent was required to produce the same amount of oil at higher injection rates compared to lower injection rates. However, production took a shorter time due to high volumes of injection. That is why, determining the critical injection rate is essential for the economics of the process. In the next part, dimensionless number analysis is employed to scale the obtained results.

From the analysis of the experimental results, it was observed that the increasing oil viscosity had a negative effect on diffusion coefficients, which is clearly observed at higher rates. As the dominant mechanism is diffusion of solvent into the matrix and transfer of oil to the fracture, reduced diffusion coefficient affects the efficiency of displacement as well. In an earlier attempt, production profiles showed that much more solvent was needed to achieve the same ultimate production at high rates especially for the high viscosity oil (Er and Babadagli, 2007).

The most difficult experiments to match were the vertical ones. Although there is no flow in (or direct injection into) the matrix, introducing the matrix longitudinal dispersion for some cases was required to match the displacement pattern observed in the experiments. Yet, the shape of the solvent front could not be matched even though the trend of displacement was captured. It is believed that gravity has an impact in the concave shape of the front in the experiments, and the simulator may not handle that impact accordingly, at least for the given size of the model and numerical grids. According to the simulation results of the vertical experiments, the diffusion coefficients of solvent decreased in all cases unlike the horizontal cases. However, the production results (Er and Babadagli, 2007 and Trivedi and Babadagli, 2006) showed that the vertical displacements

were more efficient compared to the horizontal ones. One can easily observe that gravity improves the efficiency of the process when the injection is implemented in a downward direction. This appears as improved convective dispersion in the matrix caused by gravity driven flow.

4.4 Quantitative Analysis

In the above analysis, the relative importance of diffusion and dispersivity terms on the first contact miscible displacement in a fractured porous media was clarified qualitatively. For more quantitative analysis, different dimensionless numbers were tested using these coefficients.

The following three dimensionless groups were selected in this analysis:

1. The Peclet number:

$$Pe = \left(\frac{bu_T}{D_m} \right) \quad \text{.....(1)}$$

2. Matrix-fracture diffusion number (Trivedi and Babadagli, 2008

$$N_{M-FD} = \left(\frac{\mu_0 u_T^2 b}{k_F \Delta\rho g D_m} \right) \left(\frac{L}{\phi_m r} \right) = \frac{Pe^* Ar_M}{Ng} \quad \text{.....(2)}$$

Ar_m is the aspect ratio for matrix defined as:

$$Ar_m = \left(\frac{\phi_m r}{L} \right)$$

and N_g is the gravity number defined as:

$$N_g = \left(\frac{k_F \Delta \rho g}{\mu_0 u_T} \right)$$

3. Fracture diffusion index (Trivedi and Babadagli, 2006):

$$FDI = \frac{\sqrt{k_f} * v * f(\theta) * \rho_s}{k_m * D_m * \rho_o} \quad \text{.....(3)}$$

All the parameters in these three dimensionless groups are directly measurable except the term, D_m, that defines the diffusion/dispersion process. This process mainly occurs between matrix and fracture, and usually an "effective matrix-fracture interaction" term is used to account for this. The four terms given in **Table 4.2**, namely, the diffusion coefficient for solvent, diffusion coefficient for oil, longitudinal dispersivity for fracture, and transverse dispersivity for fracture, were used as D_m in the dimensionless terms. The diffusion coefficient for oil was observed to be the only one yielding a good correlation with the TOP/TSI (total oil produced / total solvent injected) term, verifying the observations in the qualitative analysis given in the section, "Analysis of the Results". Those plots are given in **Figure 4.11** through **Figure 4.13**. These plots can be used to analyze the conditions for an efficient process. Low TOP/TSI indicates an efficient process in terms of the amount of solvent injected. This, however, yields a slow process that may not be economical. After a certain value of the dimensionless groups, the TOP/TSI stabilizes and no matter how much solvent is injected, the oil produced does not change, indicating an inefficient process. This can be clearly seen in **Figure 4.11** and **Figure 4.13**. The selection of the region defining the optimal zone depends on the application type (EOR or sequestration) and the economics of the process.

Table 4.1 Experiments.

Experiment #	displaced fluid	rate (ml/hr)	orientation
1	kerosene	15	horizontal
2	light mineral oil	15	horizontal
3	light mineral oil	45	horizontal
4	light mineral oil	15	vertical
5	light mineral oil	45	vertical
6	heavy mineral oil	15	horizontal
7	heavy mineral oil	45	horizontal
8	heavy mineral oil	15	vertical
9	heavy mineral oil	45	vertical

Table 4.2 Simulation results.

Experiment	Diffusion coeff. (cm^2/s)		Longitudinal Dispersivity (m)		Transverse Dispersivity (m)	
	Solvent	Solute	Fracture	Matrix	Fracture	Matrix
1-KER-15ml-H	4×10^{-4}	4×10^{-4}	8.8×10^{-4}	-	1.1×10^{-4}	-
2-LMO-15ml-H	2.5×10^{-4}	4×10^{-5}	8.8×10^{-4}	-	1.1×10^{-4}	-
3-LMO-45ml-H	2.5×10^{-4}	6×10^{-5}	8.8×10^{-4}	-	1.1×10^{-4}	-
4-LMO-15ml-V	2.5×10^{-5}	3×10^{-5}	8.8×10^{-2}	8×10^{-4}	1.1×10^{-7}	-
5-LMO-45ml-V	8×10^{-5}	4×10^{-5}	4×10^{-2}	2×10^{-3}	1.1×10^{-6}	-
6-HMO-15ml-H	1.2×10^{-4}	1×10^{-6}	8.8×10^{-4}	-	1.1×10^{-4}	-
7-HMO-45ml-H	1×10^{-4}	2×10^{-6}	8.8×10^{-4}	-	1.1×10^{-4}	-
8-HMO-15ml-V	6×10^{-5}	2×10^{-6}	8.8×10^{-2}	-	1.1×10^{-6}	-
9-HMO-45ml-V	3×10^{-6}	2×10^{-6}	4×10^{-2}	1×10^{-4}	1.1×10^{-7}	-

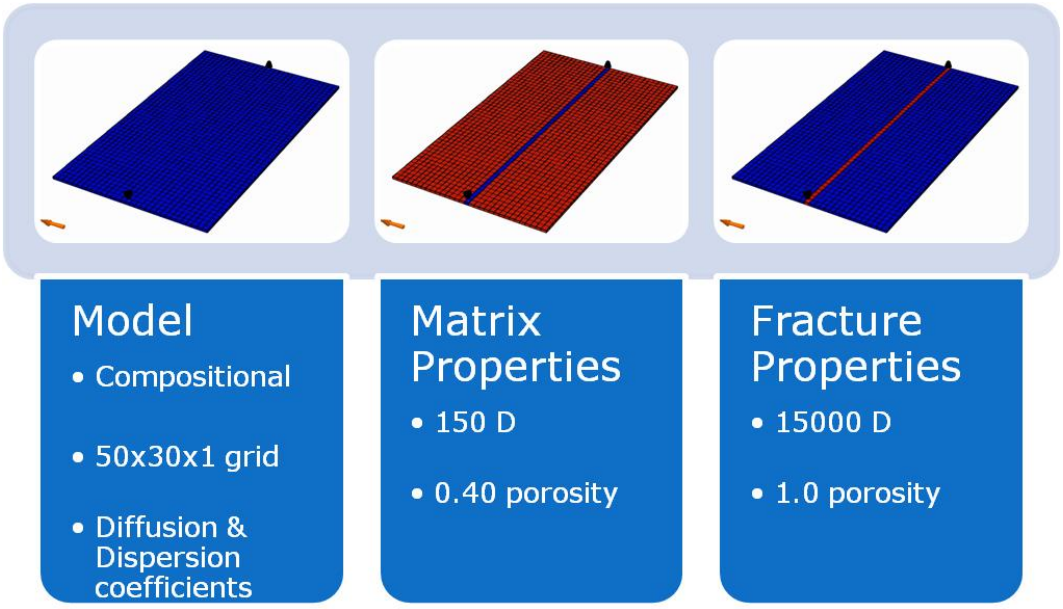

Figure 4.1 Simulation model.

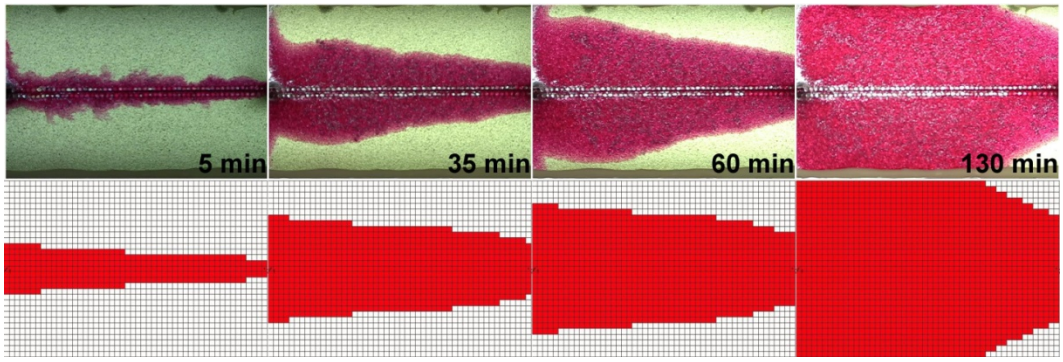

Figure 4.2 Comparison of experimental (upper images) and simulation (lower images) results for horizontal heavy mineral oil displacement at 15 ml/h.

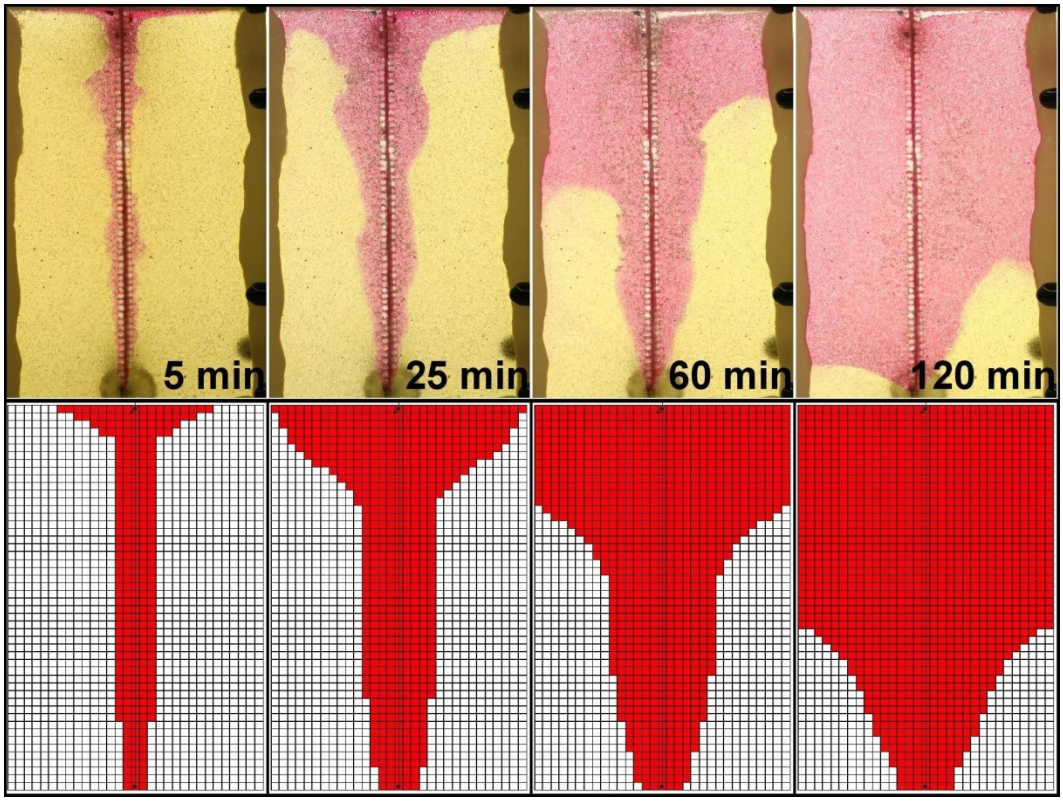

Figure 4.3 Comparison of experimental (upper images) and simulation (lower images) results for vertical heavy mineral oil displacement at 15 ml/h.

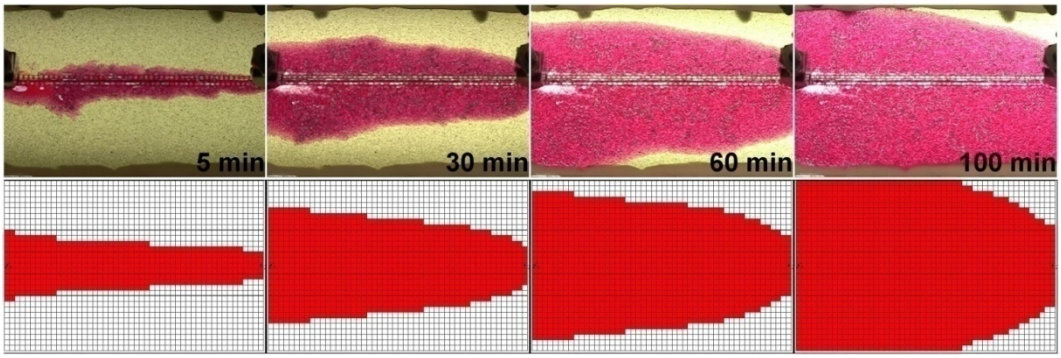

Figure 4.4 Comparison of experimental (upper images) and simulation (lower images) results for horizontal heavy mineral oil displacement at 45 ml/h.

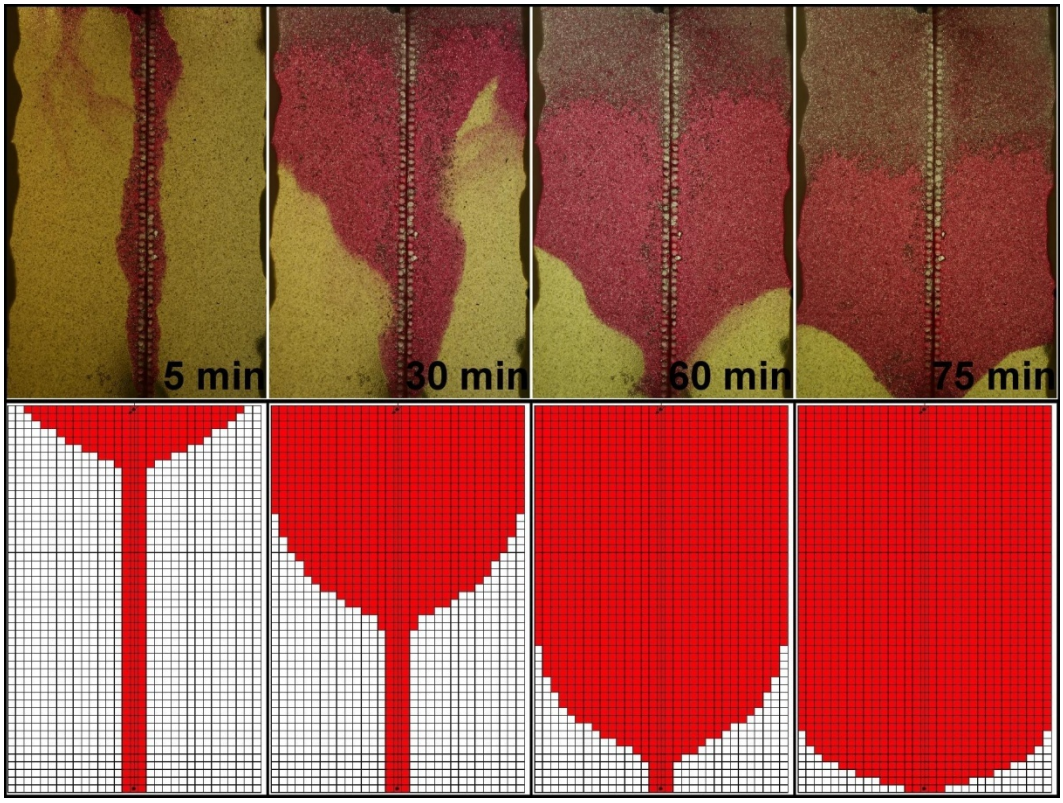

Figure 4.5 Comparison of experimental (upper images) and simulation (lower images) results for vertical heavy mineral oil displacement at 45 ml/h.

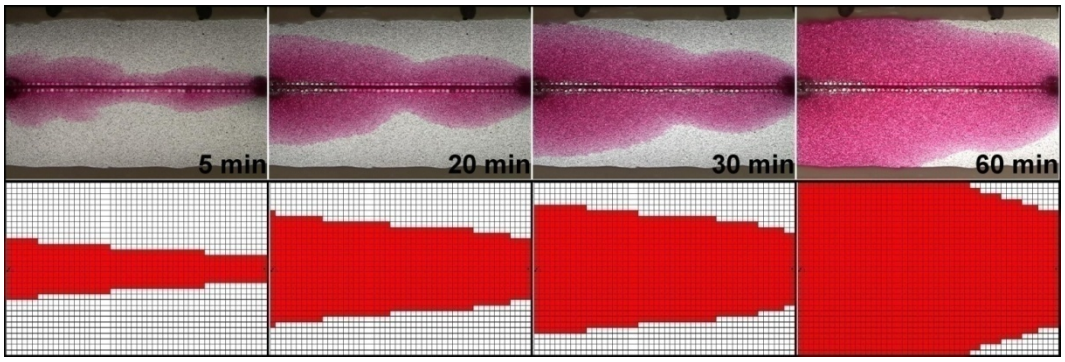

Figure 4.6 Comparison of experimental (upper images) and simulation (lower images) results for horizontal light mineral oil displacement at 15 ml/h.

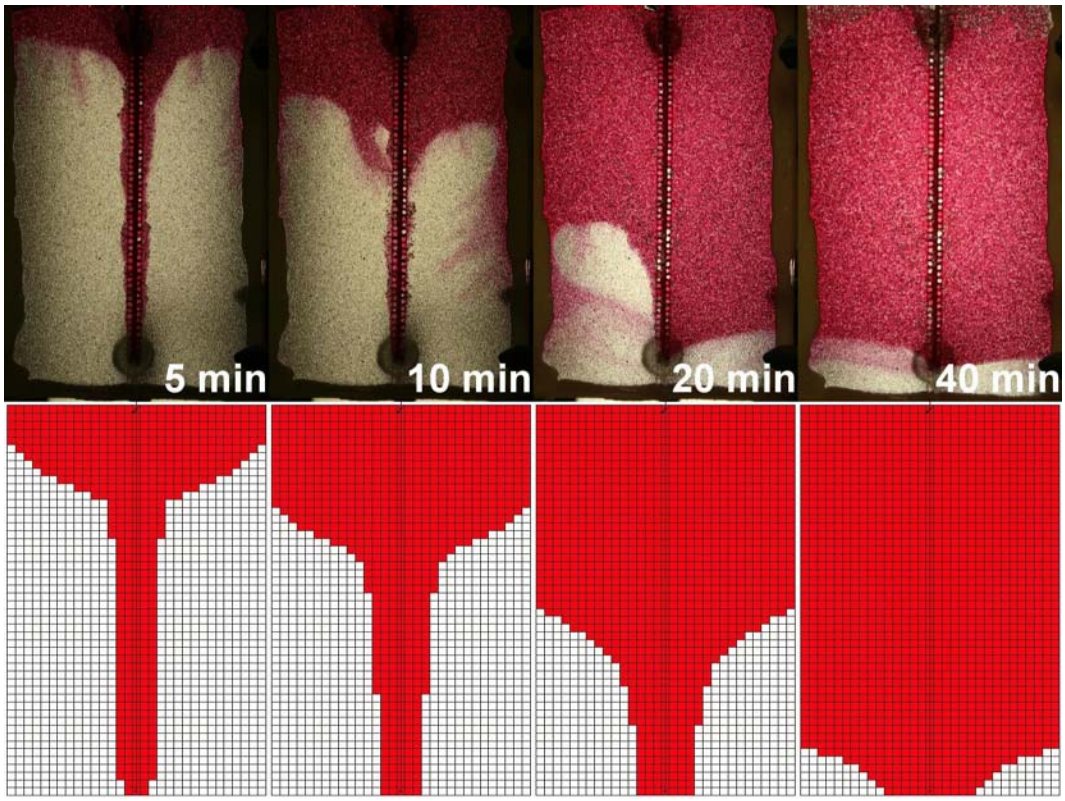

Figure 4.7 Comparison of experimental (upper images) and simulation (lower images) results for vertical light mineral oil displacement at 15 ml/h.

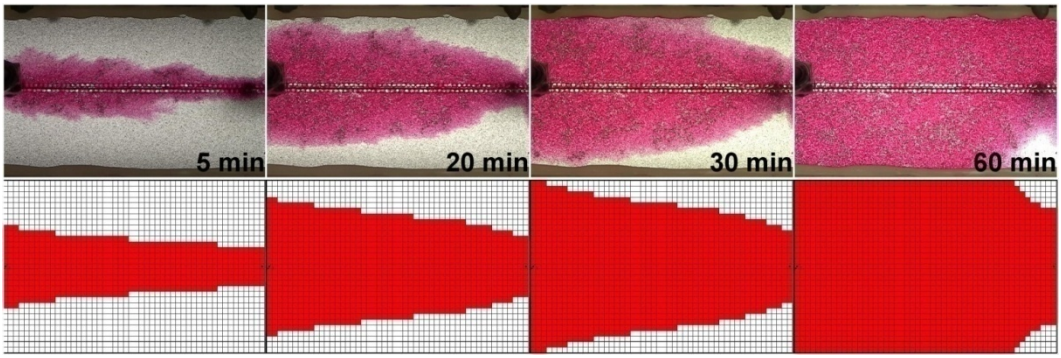

Figure 4.8 Comparison of experimental (upper images) and simulation (lower images) results for horizontal light mineral oil displacement at 45 ml/h.

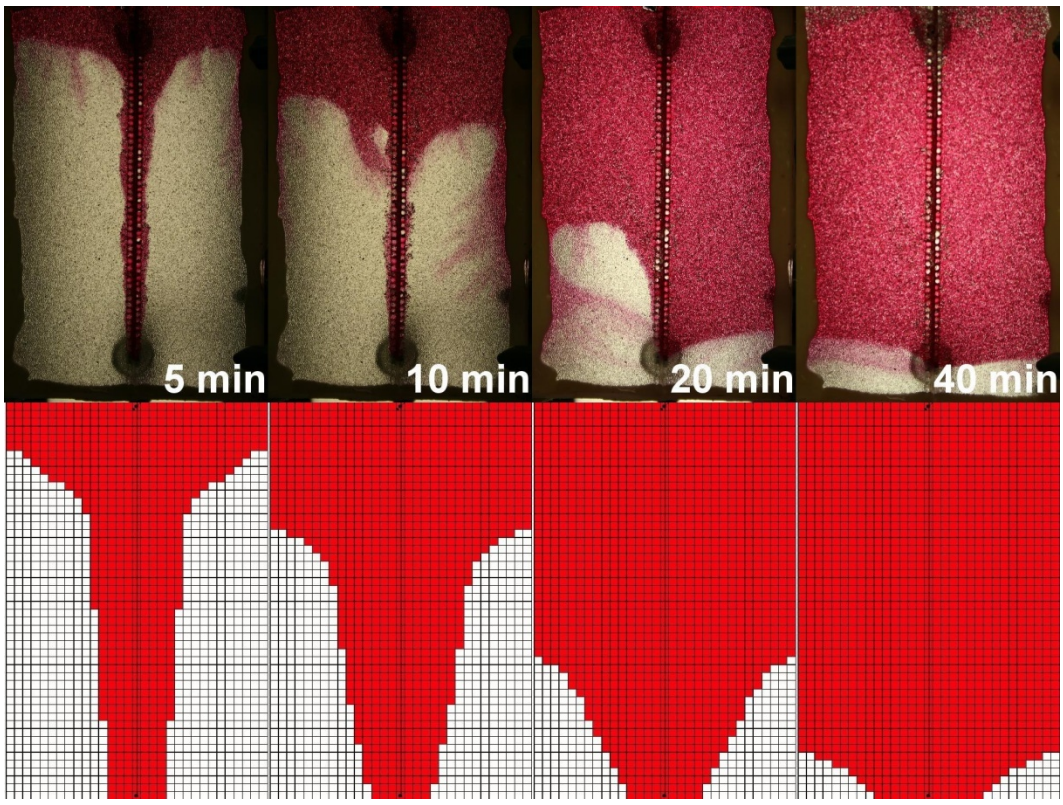

Figure 4.9 Comparison of experimental (upper images) and simulation (lower images) results for vertical light mineral oil displacement at 45 ml/h.

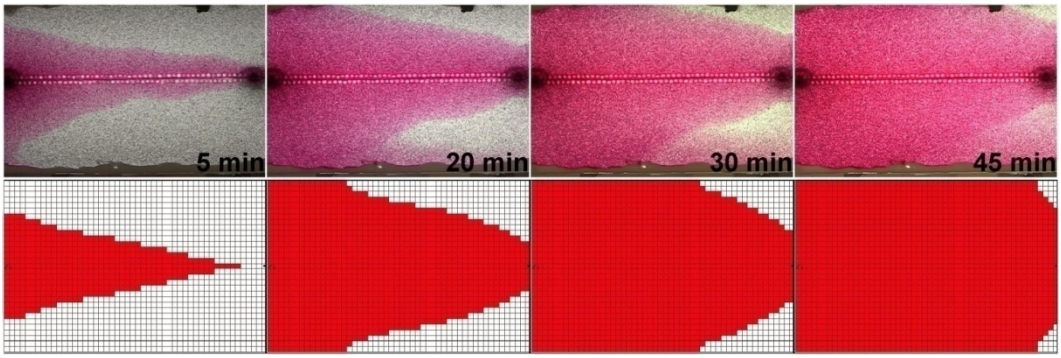

Figure 4.10 Comparison of experimental (upper images) and simulation (lower images) results for horizontal kerosene displacement at 15 ml/h.

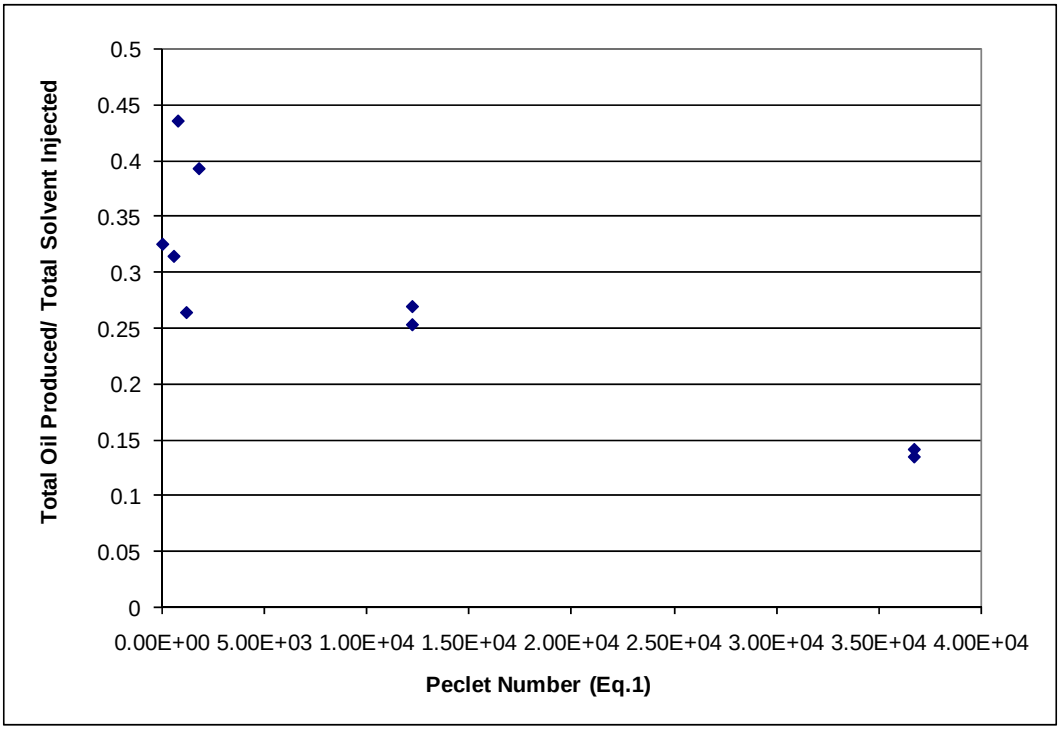

Figure 4.11 Normalized oil production with respect to the amount of solvent injected against the Peclet number (using oil diffusion coefficient).

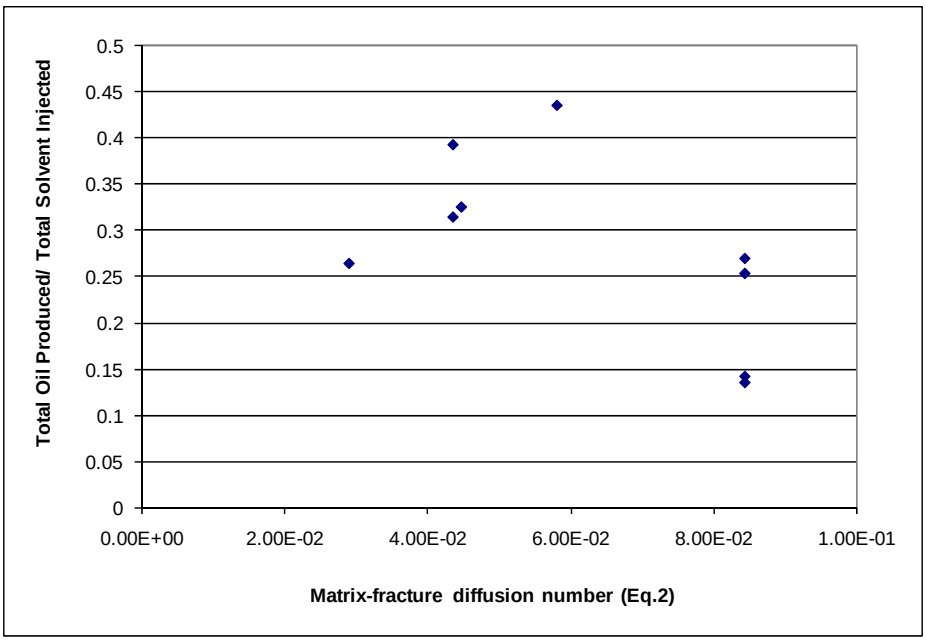

Figure 4.12 Normalized oil production with respect to the amount of solvent injected against the NM-FD (using oil diffusion coefficient).

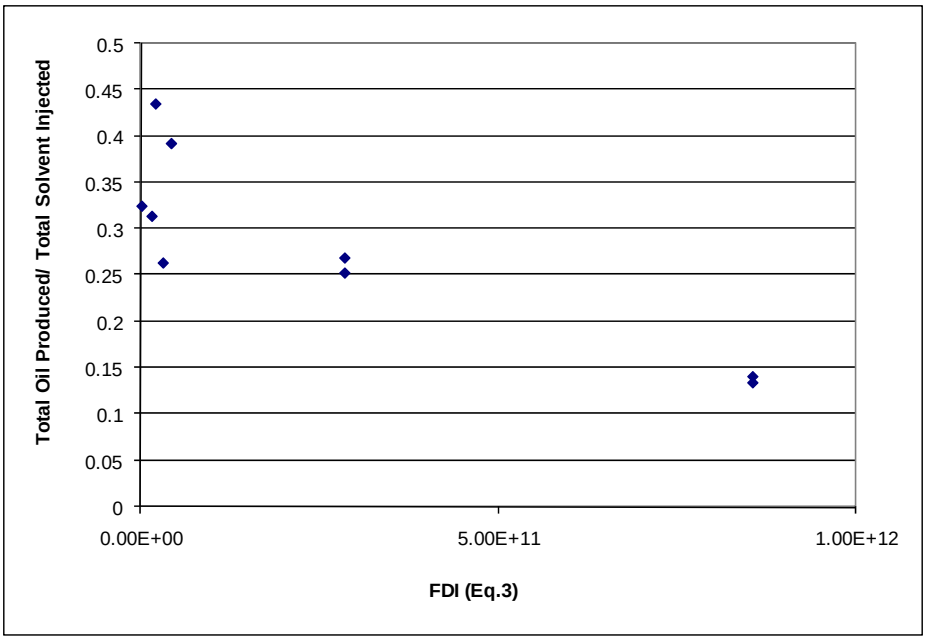

Figure 4.13 Normalized oil production with respect to the amount of solvent injected against the FDI (using oil diffusion coefficient).

Chapter 5

Pore Scale Investigation of Matrix-Fracture Interaction during CO_2 Injection

Glass etched microfluidic models were employed to investigate the pore scale interaction between matrix and fracture. Models were prepared by etching homogeneous and heterogeneous micro scale pore patterns with a fracture in the middle of the model on glass sheets bonded together and then saturated with colored n-decane as the oleic phase. CO_2 was injected at miscible and immiscible conditions. The focus of the study was on visual pore scale analysis of miscibility, breakthrough of CO_2 and oil/CO_2 transfer between matrix and fracture under different miscibility conditions. More specifically, the CO_2-oil interaction near the fracture region inside the matrix was visualized and its impacts on the further transport of CO_2 inside the matrix by diffusion, transfer of oil from matrix to fracture and its flow in fracture, and CO_2 storage inside the matrix during these processes were analyzed visually.

5.1 Experimental Set-up and Procedure

For the experiments, a high pressure cell has been used. The cell is rated up to 4000 psi and consists of a steel base, two high pressure durable glass windows and two steel frames. A visual chamber is obtained by attaching steel frames to the base via bolts and placing glass windows in between with the proper sealing. The high pressure cell is connected to CO_2 and n-decane injection pumps and a back pressure valve system.

5.1.1 Micromodel Fabrication

Fabrication of microfluidic devices includes several steps which are detailed below and in **Figure 5.1**

a. Design and Manufacturing of Photomask: To etch any pattern on the glass substrates, a photomask that includes the desired pattern should be obtained first. The photomask is basically open and covered areas depending on the design. Open areas on the mask let UV light pass through on photoresist and enable us to transfer a pattern on the masking layer. Homogeneous and heterogeneous pore patterns consist of a single fracture and two matrix blocks are designed using the L-Edit software. Then, the design is printed on 5″x5″ soda lime glass by coating with chrome with the help of the DWL 200 pattern generator.

b. Substrate and Mask Cleaning: Borosilicate glass substrate on which the pore pattern is etched and the photomask have to be free of contaminants before the other steps. As the process is done at micro scale, any small particle on surfaces may lead to fail of total model. To prevent this, substrate and the mask is cleaned by immersing in piranha mixture, 3:1 solution of Sulphuric Acid (H_2SO_4) and Hydrogen Peroxide (H_2O_2) in which temperature exceeds 100 ºC for 30 minutes and then rinsed.

c. Masking Layer Deposition: To be able to etch the desired pattern on the substrate, the glass surface should be covered with a masking layer which is a deposition of Chrome (Cr) and Gold (Au). 20-40 nm of Cr and 150-200 nm of Au

are deposited on the glass surface via surface bombarding of either Cr or Au in a reaction chamber under vacuum.

d. Masking Layer Photolithography: The designed pore pattern is transferred onto a thin-film masking layer by a series of steps called photolithography (1) UV light sensitive material named photoresist is applied on masking layer by spinning. (2) The photomask and substrate are aligned and exposed to UV light. Radiation from UV light changes the solubility of photoresist. Finally, the substrate is placed in the developer solution in which exposed areas are removed and the pattern is transferred on the photoresist.

e. Masking Layer Etching: After the pattern has transferred onto photoresist, the Au and Cr layers are removed by immersion in etchant liquids respectively and the pattern is transferred on the masking layer.

f. Glass Etching: As the masking layer is etched, the glass surface is accessible through the pore pattern printed on the photomask. The substrate is immersed in Hydrofluoric Acid (HF) and the finally pore pattern is etched on the glass surface through the openings on the masking layer and the photoresist. The back side of the substrate is covered with plastic tape to prevent any damage.

g. Device Substrate Stripping: In the reverse order of deposition, (1) the photoresist and (2) the masking layer are removed and (3) the remaining traces of metals are cleaned in the piranha solution.

h. Fusion Bonding: Once the substrate is etched it is ready to be bonded with another sheet of glass. To have better contact between two pieces of glass, smooth surfaces are required in the bonding process. Therefore, substrates are cleaned

well and initial bonding is done at room temperature by attaching the two surfaces together. Attraction forces are enough to keep two well cleaned glass pieces together. To make it stronger, a thermal fusion process is carried out. Thermal fusion is performed at temperatures above the annealing point but below the softening point. To bond our substrates, the glass pieces are kept in the box furnace for 120 minutes at 600 ºC.

i. Device Dicing: As the last step, devices (micromodels) fabricated on the same substrates are separated from each other with the help of the Diamond Touch Dicing Saw.

Models used in the current study were etched to 20 μm and 40 μm depths. The image used to produce heterogeneous pattern was obtained from Hatiboglu (2007). Details of the patterns are given in **Figure 5.2**.

5.1.2 Procedure

Once the micromodel was obtained, it was placed in to the high pressure cell (**Figure 5.4**). To seal the micromodel from the inner walls of the chamber, additional glass sheets and clear epoxy were utilized and the model was tested for any leaks. First, CO_2 was injected at a very low pressure. Then, a few pore volumes of n-decane was injected and pressurized to the desired experimental conditions to saturate the model.

CO_2 was injected at a constant rate continuously and time lapse pictures were taken and recorded during the displacements. To be able to visualize fluid distribution within the model, n-decane was colored with the fluorescent dye and experiments were conducted in the dark room under black light (**Figure 5.3** and **Figure 5.5**). Experiments were conducted at 50ml/hr and 150 ml/hr for the

pressures of 600 psi, 1200 psi and 1500 psi, representing immiscible, near-miscible, and miscible displacement for the n-decane-CO_2 pair, respectively. A secondary set of experiments were conducted at 50 ml/hr for the pressures of 600 psi, 1200 psi and 1500 psi on wettability altered. To change the wettability, dichlorooctamethyltetrasiloxane (SurfaSil^{TM}, a siliconizing fluid) was applied. SurfaSil^{TM} was mixed with pentane and injected through the model for a few pore volumes. Then, pentane was evaporated under vacuum while siliconizing fluid covered the surface of the pores. Finally, the model was saturated with the oleic phase and kept saturated for 24 hours.

5.2 Analysis and Discussion

Images are analyzed and compared to observe the effects of (a) pressure controlling the miscibility condition, (b) injection rate, and (c) wettability on the matrix-fracture transfer of oil and CO_2 during the process. In both immiscible and miscible displacements, CO_2 displaced the fluid within the fracture first, and then interacted with the fluid stored in the matrix although injection was throughout the whole cross section. Obviously, CO_2 will not be able to fully displace the matrix oil if it was injected only through the fracture in immiscible displacements.

A few snapshots are provided to highlight a few points with regard to the progress of the CO_2 front in the fracture and matrix. Under immiscible conditions, front displacement was piston-like and the interface between the oil and the CO_2 was clearly visible (**Figure 5.6**). A high amount of oil was trapped in the pores after immiscible displacements both in the homogeneous (**Figure 5.7**) and heterogeneous model (**Figure 5.8**).

One of the focuses was on the injection rate. CO_2 was injected at two different injection rates continuously: (a) 50 ml/hr, and (b) 150 ml/hr. At 50 ml/hr,

CO_2 displaced the fracture fluid first and started to penetrate into the matrix. However, gaseous CO_2 displaced the oil following the preferential paths due to heterogeneity in the pattern, leaving trapped oil in the pores. Although all of the oil stored in the fracture was displaced, the majority of oil was trapped within the matrix (**Figure 5.10**). The increased rate showed a similar behavior displacing the fracture fluid and invading into the matrix. Higher rates allowed CO_2 to penetrate more through the matrix leaving less amount of trapped oil overcoming the capillary forces and increased the production of oil (**Figure 5.9**). As seen, the amount of trapped oil at the higher rate case in much less (indicated by arrowed areas).

In the near-miscible (1200 psi) and miscible (1500 psi) displacement cases, all of the oil was displaced regardless of the rate, as can be seen through the color change over time in **Figure 5.11** through **Figure 5.14**. It took less time to reach the ultimate recovery for the higher rate (**Figure 5.12**). This, however, requires more CO_2 injection at higher rates compared to lower rates as also shown in our earlier fully –first contact- miscible experiment (Er and Babadagli, 2007 and 2008). At 1200 psi and 1500 psi, injected CO_2 at 50 ml/hr mixed with the fracture fluid first. Figs. 9 and 11 show the development of the miscible front in the fracture and the interaction with the oil in the matrix. At 150 ml/hr, displacements were similar to the lower rate in both 1200 psi and 1500 psi, however it was faster compared to lower rate cases (**Figure.12** and **Figure 14**).

Besides the injection rate, the effect of miscibility was also investigated. CO_2 is known to be miscible with n-decane around 1100 psi (Trivedi and Babadagli, 2008) at atmospheric pressure. To visualize the interaction of the CO_2 under different miscibility conditions, it is injected continuously at 600 psi, 1200 psi and 1500 psi representing immiscible, near-miscible and miscible conditions. While immiscible displacement left a considerable amount of oil trapped in the matrix even in the homogeneous pattern case, near-miscible and miscible

injections displaced n-decane totally. In the heterogeneous pore pattern, some of the oil was trapped in the dead end pores during miscible and near-miscible displacements; however, giving enough time, CO_2 was able to displace trapped oil by diffusion. That gave us a chance to compare diffusion coefficients of CO_2 at near-miscible and miscible conditions. Time lapse pictures given in **Figure 5.15** through **Figure 5.18** show that CO_2 displaces the trapped oil faster at higher pressures, which indicates higher diffusion coefficient at higher pressures. This may contradict some of the earlier studies (Asghari and Torabi, 2008 and Trivedi and Babadagli, 2008). As it is a single component system (n-decane), increasing pressure resulted in a faster recovery of oil. However, in a multi-component system at pressures well above the minimum miscibility pressure (MMP), the recovery factor decreases (Asghari and Torabi, 2008 and Trivedi and Babadagli, 2008). Considering the field applications, compression of the CO_2 further than the minimum miscibility pressure (MMP) does not help to produce more oil, however increases the operation costs.

Finally, the effect of wettability was tested with dry film treated models. Glass micromodels are naturally water wet and by processing the models with siliconizing fluid, wettability can be altered. This is critical as a great portion of CO_2 injection applications in the world are in the carbonates, which are relatively less water wet.General displacement patterns did not differ in treated and non treated models (**Figure 5.20** through **Figure 5.22**). In the case of immiscible displacement, residual oil in the treated model was slightly more than the non-treated model (**Figure 5.19**). Besides, in the treated model, the diffusion of CO_2 into trapped oil slightly delayed compared to the non-treated model (**Figure 5.16** and **Figure 5.18**). It is believed that the effect of the wettability alteration would be felt more with the multi-component oil system and with initial water saturation. This part of the research is ongoing.

5.3 Blow-down experiments

The blow-down is gradual depletion of the pressure to produce some extra oil after any injection or tertiary recovery method that pressurizes the reservoir. It is of particular importance in case of CO_2 injection as some amount of CO_2back diffuses from matrix to fracture during this process to eventually be re-produced. If the purpose is not only extra oil recovery but also the storage of CO_2in the reservoir matrix, one should be careful in the application of the blow-down process as it might cause excessive CO_2re-production. This eventually might yield to define the abandonment pressure for optimized oil production and CO_2storage.

To mimic this common practice in the oil fields, a blow-down experiment was carried out after each injection experiment. Injection was stopped and CO_2pumps were isolated from the system. Then, system pressure was dropped to atmospheric pressure step by step. Images were taken at 800 psi, 600 psi, 400 psi and 200 psi after the near-miscible and miscible experiments and at 400 psi and 200 psi after the immiscible experiments.

First, we look at the water-wet case. Initially the system is filled with $CO_2$and some amount of oil fully mixed with it as indicated by dark (blue) and fuzzy color (**Figure 5.23**) for the miscible and near-miscible cases. Obviously, the higher the pressure (like the miscible cases), the more oil from matrix was recovered and displaced before the blow-down. In the near-miscible and miscible cases, the reduced pressure below the critical pressure of CO_2caused oil to appear (and get trapped) again. In other words, as the miscibility is lost by reducing the pressure below the minimum miscibility pressure, some amount of oil came out of the solution. The amount of oil depends on the initial condition. When the miscible and immiscible cases are compared, one may observe that the amount of oil trapped is more in the case of near-miscible especially at lower pressures. The

immiscible case shows more oil trapped and this amount did not change significantly by reduced pressures. It is obvious that considering the cost of injection, the amount of CO_2stored and oil recovered, near-miscible case yield the optimal performance (technically and economically) with its almost the same amount of oil recovery and CO_2storage as the miscible case but with lower pressure requirement. This observation is in agreement with recent experimental observations on core samples by Trivedi and Babadagli (2008).

The same experiments were conducted for oil wet matrix. Images in **Figure 5.24** indicate that the amount of trapped oil in the miscible and near miscible cases by reduced pressure is more than the water wet case and this is more prominent for the near-miscible case. Some level of oil invasion from the dead volumes are expected during the blow-down experiments in all cases, which is inevitable due to nature of micro-model experiments (one cannot empty the dead volumes before starting the blow-down not to de-pressurize the system). The oil saturation increase in the matrix with decreasing pressure is remarkably higher in the oil-wet case and this amount is above the expected invasion of dead volume oil if there is any. Situation in the immiscible case is more complex when the wettability is also an issue as there are both capillary interaction and mass transfer processes are active since the beginning of the process. The oil entrapment is controlled by more parameters than the miscible and near-miscible cases. Obviously, oil trapped at 200 psi is less in the case of oil-wet matrix. This could be attributed to free non-wetting CO_2in the system (initially liquid or supercritical and then gas) which affects the fluid saturation distribution in the matrix. Note that this translates into more CO_2storage at the end of experiment. Hence, smaller process pressures from the beginning the CO_2injection application and lower abandonment pressures can be suggested for the carbonates case.

Note that Trivedi and Babadagli (2008) suggested abandonment pressures of 600 psi and 400 psi for sandstones (water wet) and carbonates (oil wet) for optimal results. Our visual observations are qualitatively in agreement with these results suggesting different abandonment pressures for water and oil-wet media for optimal oil recovery and CO_2storage.

It is obvious that, water wet matrix conditions are more desirable for sequestration projects as the amount of trapped oil is less compared to oil wet matrix conditions. In case of carbonates (oil-wet systems) one has to be careful in selecting the pressure as significant difference between miscible and near-miscible cases was observed.

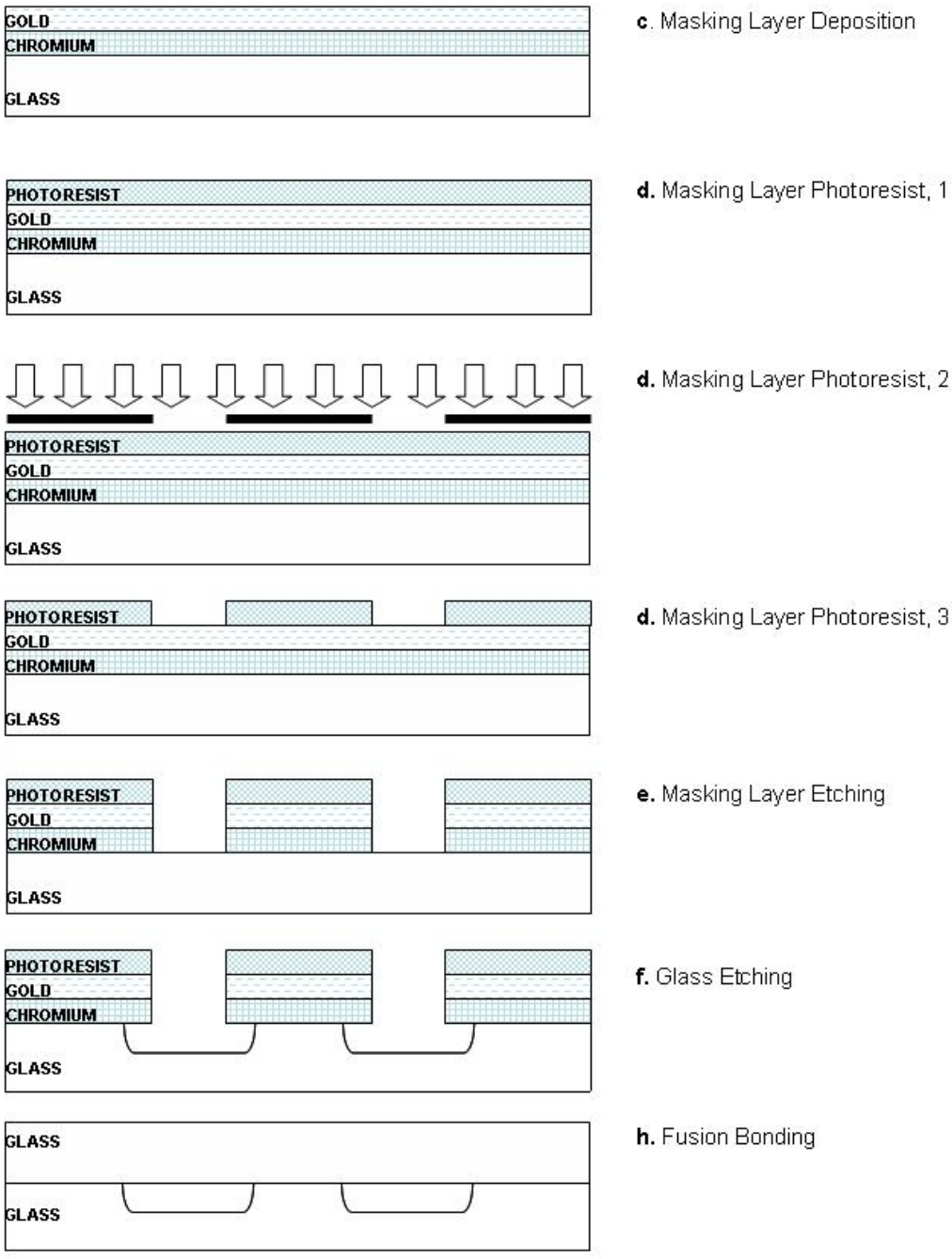

Figure 5.1 Micromodel fabrication steps.

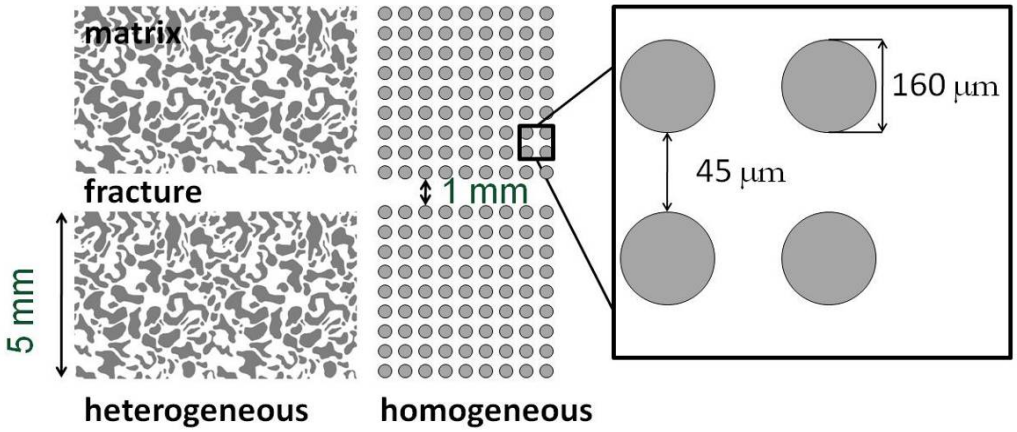

Figure 5.2 Pore pattern.

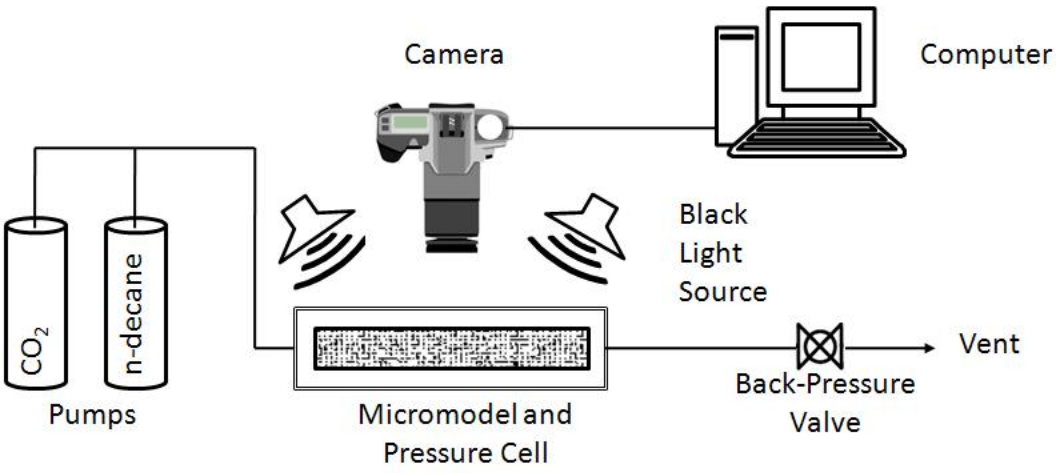

Figure 5.3 Experimental set-up.

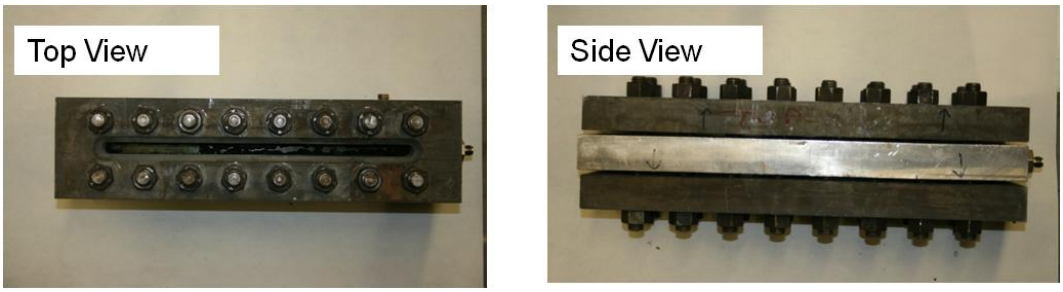

Figure 5.4 Pictures of pressure cell.

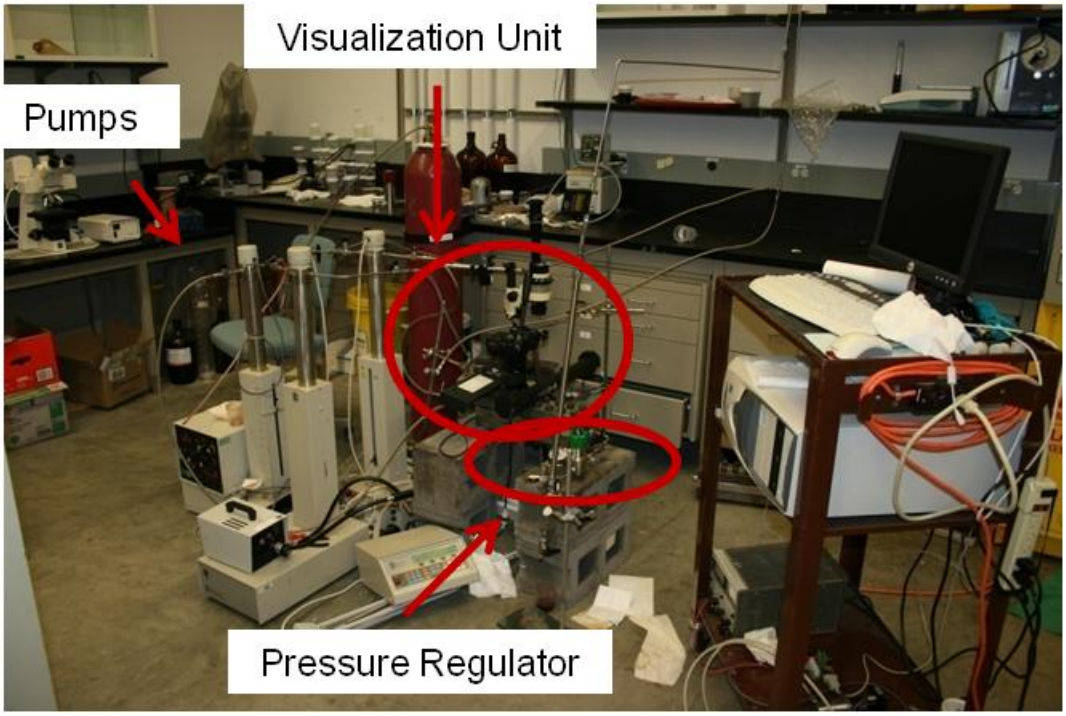

Figure 5.5 Picture of experimental set-up.

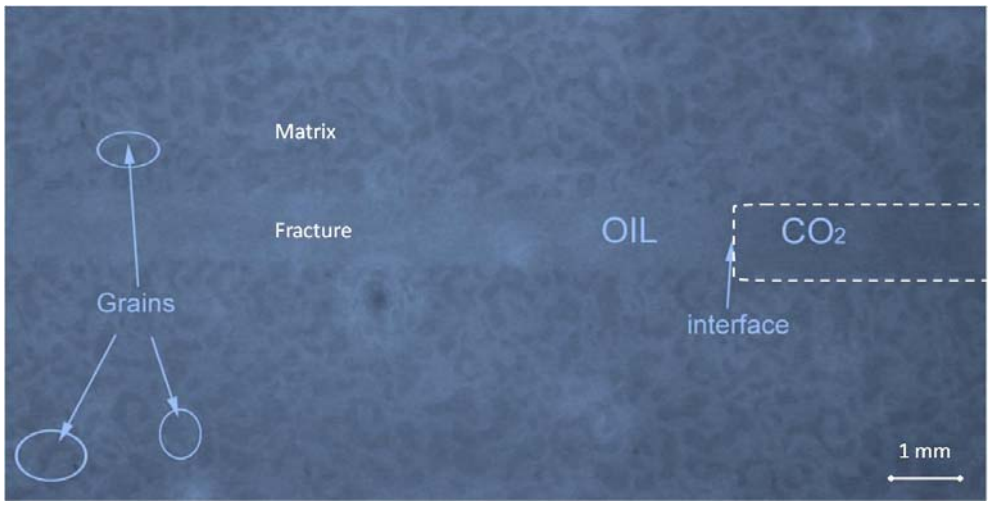

Figure 5.6 Immiscible oil-CO_2 interface during the displacement at 600 psi and 50 ml/hr after 1 second. Gaseous CO_2 displaces oil in the fracture initially. Heterogeneous matrix model (grains are indicated by arrows). See also image processed version in the Appendix.

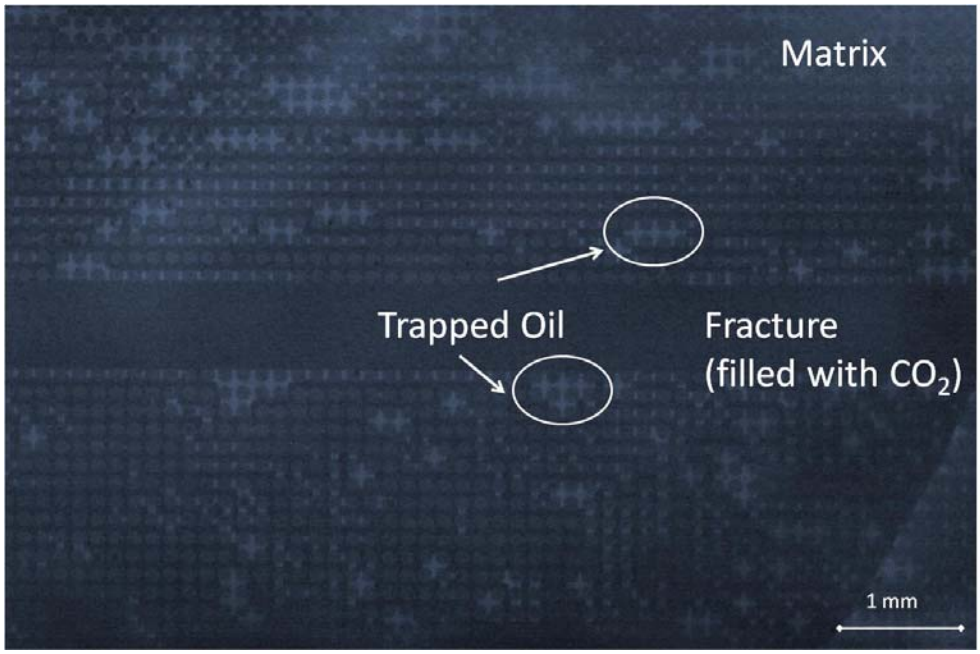

Figure 5.7 Trapped oil in the model with homogeneous matrix pattern after the completion of the displacement at 600 psi and 50ml/hr. Circles are the grains. Lighter color between circles shows trapped oil and dark color shows gaseous CO_2.

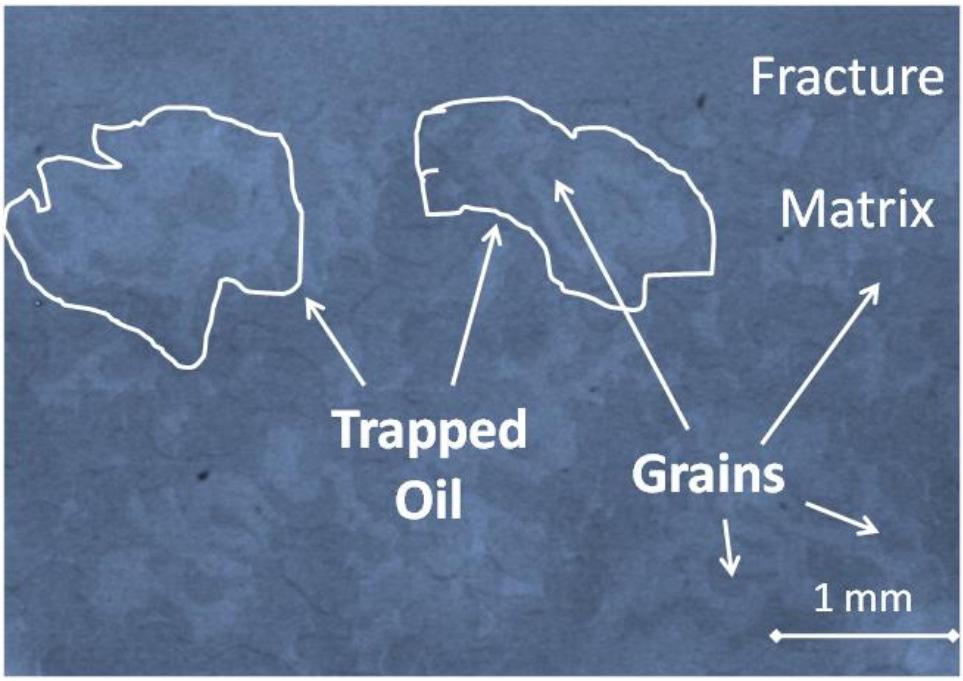

Figure 5.8 Trapped oil in the model with heterogeneous pattern after the displacement at 600 psi and 50 ml/hr. Dark color areas shows CO_2 phase and light color area shows oil phase. Some of the trapped oil is indicated by arrows. See also image processed version in the Appendix.

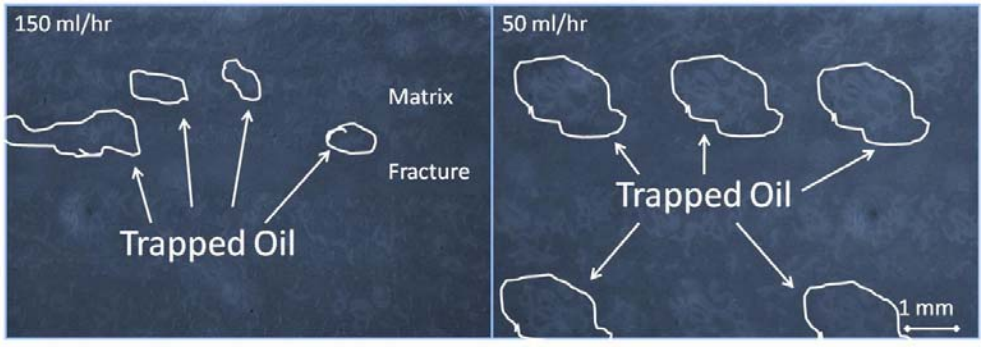

Figure 5.9 Comparison of residual oil patterns in the matrix after CO_2 injection at 150 ml/hr and 50 ml/hr in the model with heterogeneous pattern at 600 psi.The darker color represents CO_2 phase and the lighter color represents the oil phase. To differentiate it better, some of the trapped oil is indicated by arrows. See also image processed version in the Appendix.

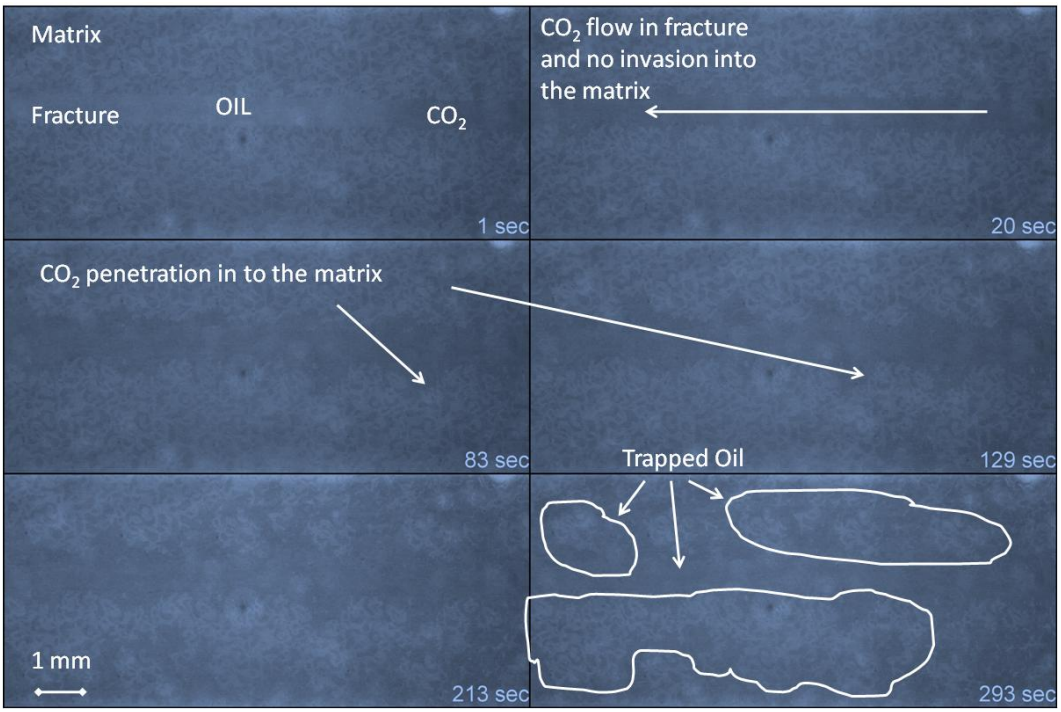

Figure 5.10 Displacement of n-decane by CO2 in the model with heterogeneous pattern at 600 psi and 50 ml/hr. Lighter color shows the oil phase and darker color shows CO_2 phase. Some of the trapped oil in the pores is indicated by arrows. See also image processed version in the Appendix.

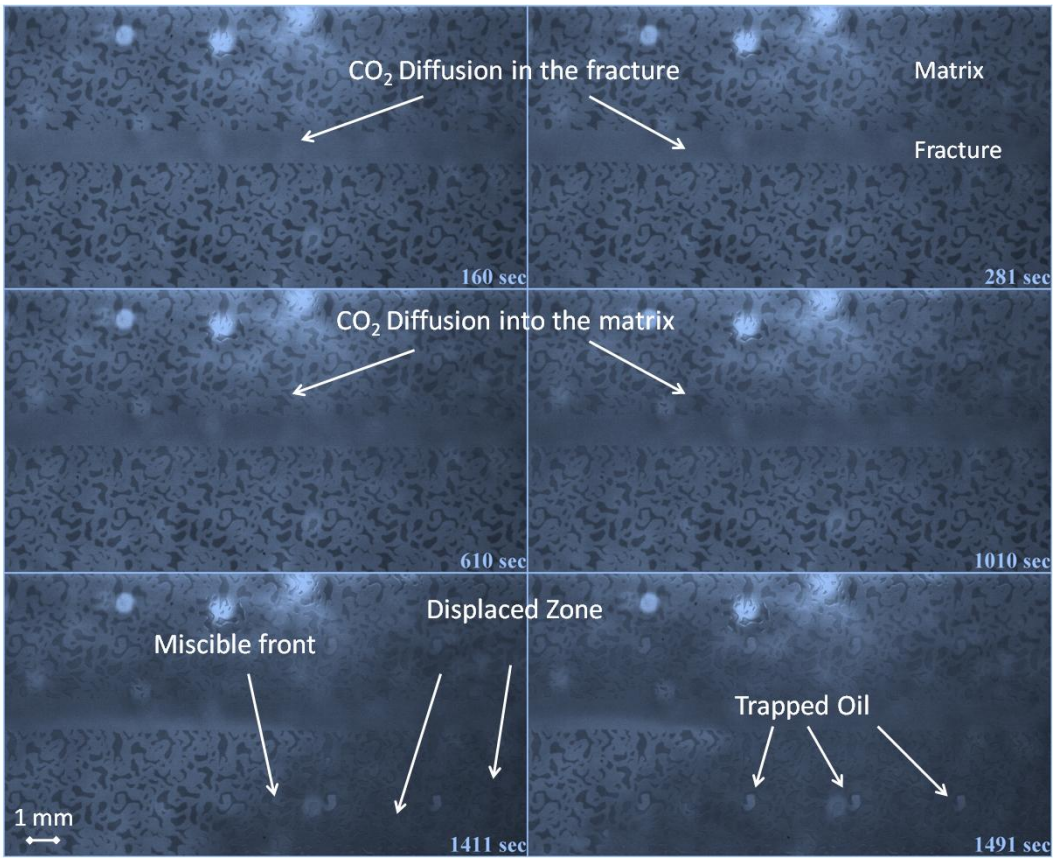

Figure 5.11 Displacement of n-decane by CO_2 in the model with heterogeneous pattern at 1200 psi and 50ml/hr. Lighter color shows oil phase and darker color shows CO_2 phase. Supercritical state CO_2 initially diffuses into the oil in the fracture then into the oil in the matrix. CO_2 diffusion into oil, miscible front and the trapped oil are indicated by arrows. See also image processed version in the Appendix.

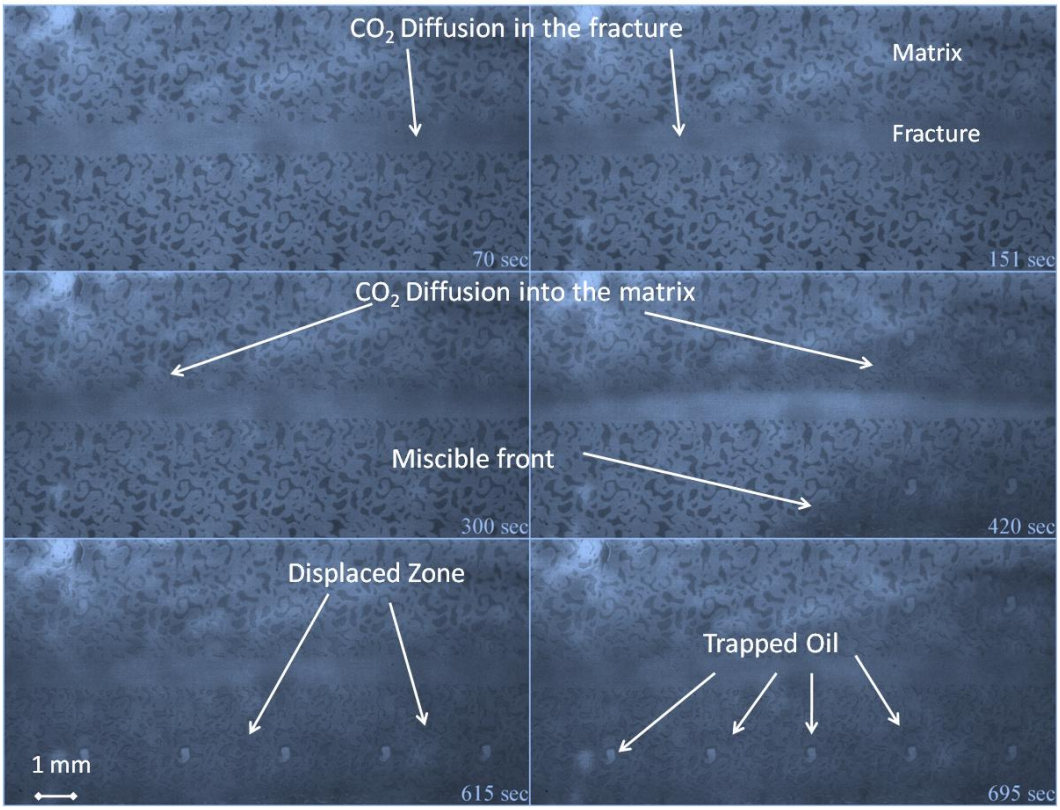

Figure 5.12 Displacement of n-decane by CO_2 in the model with heterogeneous pattern at 1200 psi and 150 ml/hr. Supercritical state CO_2 initially diffuses into the oil in the fracture then into the oil in the matrix. CO_2 diffusion into oil, miscible front and the trapped oil are indicated by arrows. See also image processed version in the Appendix.

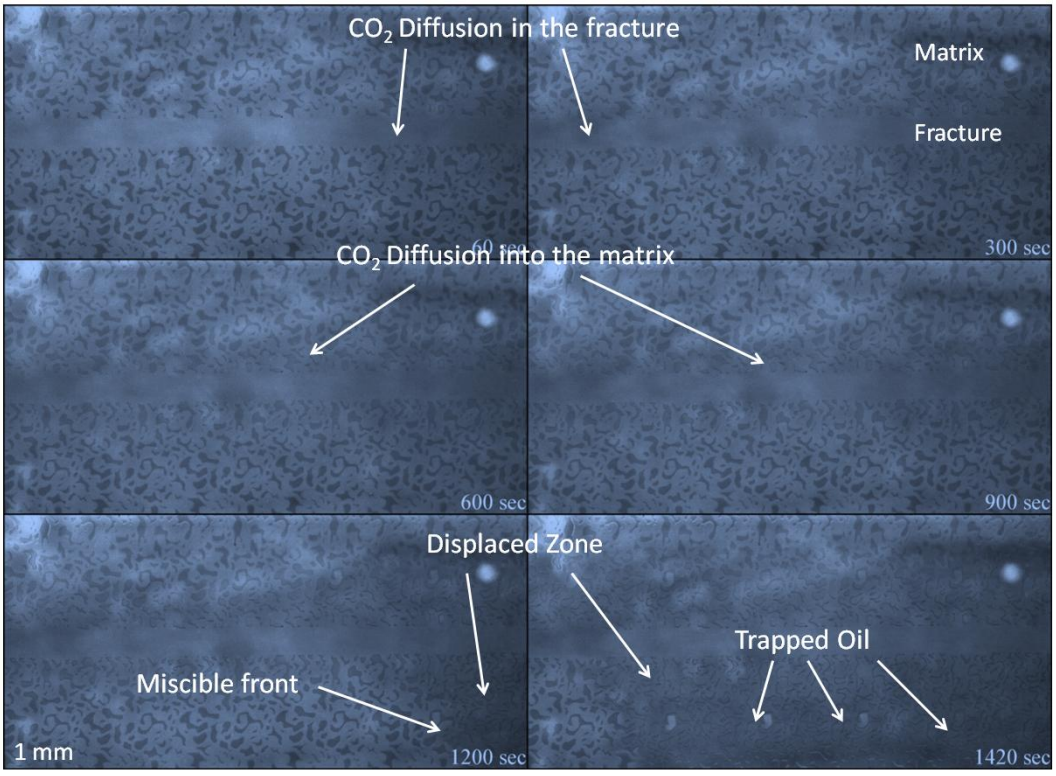

Figure 5.13 Displacement of n-decane by CO_2 in the model with heterogeneous pattern at 1500 psi and 50 ml/hr. Supercritical state CO_2 initially diffuses into the oil in the fracture then into the oil in the matrix. CO_2 diffusion into oil, miscible front and the trapped oil are indicated with arrows. Fuzzy areas represent the mixing zone (or oil displacement). See also image processed version in the Appendix.

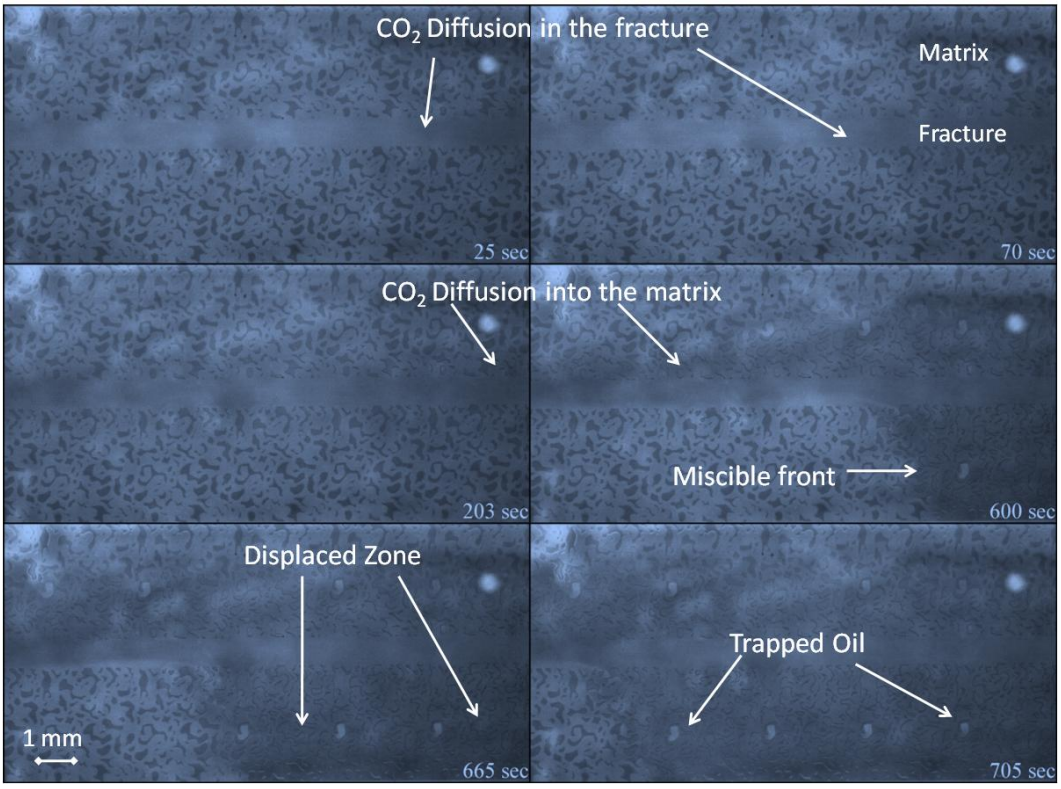

Figure 5.14 Displacement of n-decane by CO_2 in the model with heterogeneous pattern at 1500 psi and 150 ml/hr. Supercritical state CO_2 initially diffuses into the oil in the fracture then into the oil in the matrix. CO_2 diffusion into oil, miscible front and the trapped oil are indicated with arrows. Fuzzy areas represent the mixing zone (or oil displacement). See also image processed version in the Appendix.

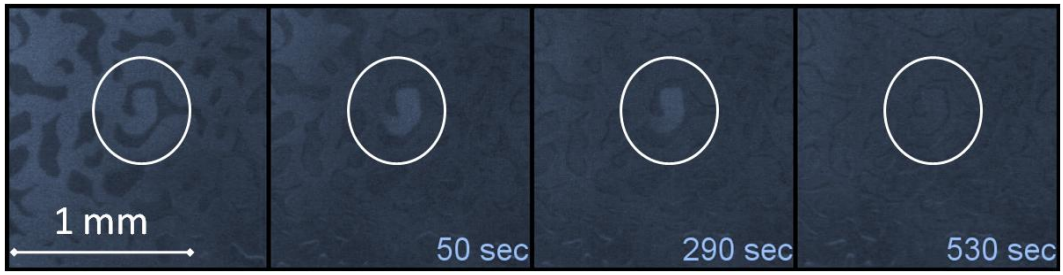

Figure 5.15 Diffusion of CO_2 into trapped oil at 1200 psi and 50 ml/hr. Lighter color represents the oil phase and the darker color represents the miscible CO_2 phase.

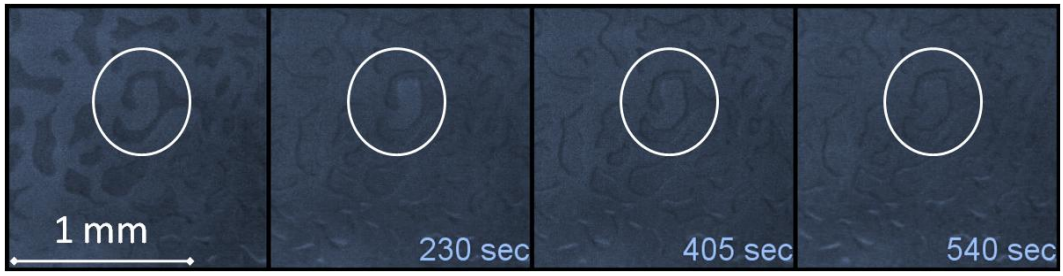

Figure 5.16 Diffusion of CO_2 into trapped oil in the oil wet model with heterogeneous pattern at 1200 psi and 50 ml/hr. Lighter color represents the oil phase and the darker color represents the miscible CO_2 phase.

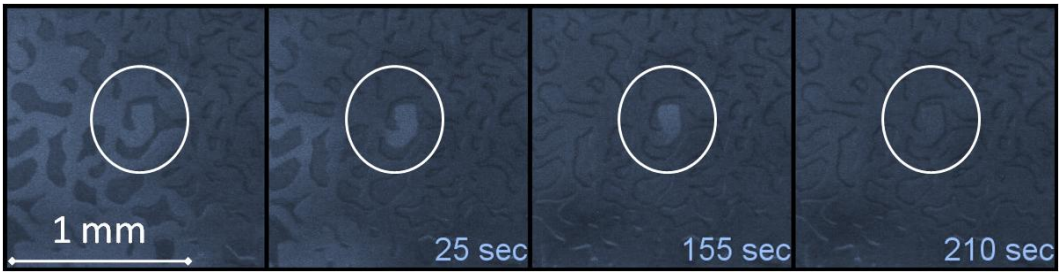

Figure 5.17 Diffusion of CO_2 into trapped oil in the model with heterogeneous pattern at 1500 psi and 50 ml/hr. Lighter color represents the oil phase and the darker color represents the miscible CO_2 phase.

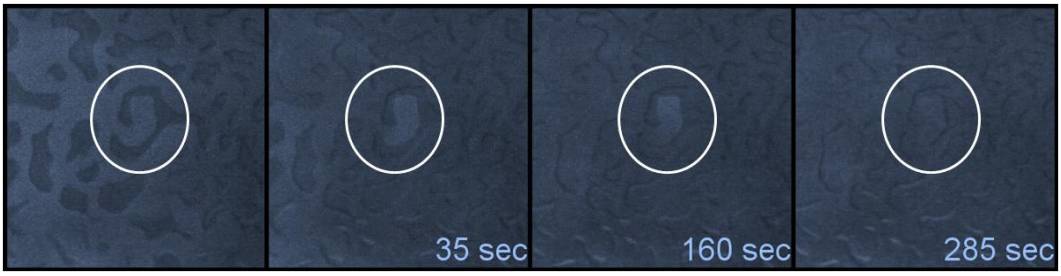

Figure 5.18 Diffusion of CO_2 into trapped oil in the oil wet model with heterogeneous pattern at 1500 psi and 50 ml/hr. Lighter color represents the oil phase and the darker color represents the miscible CO_2 phase.

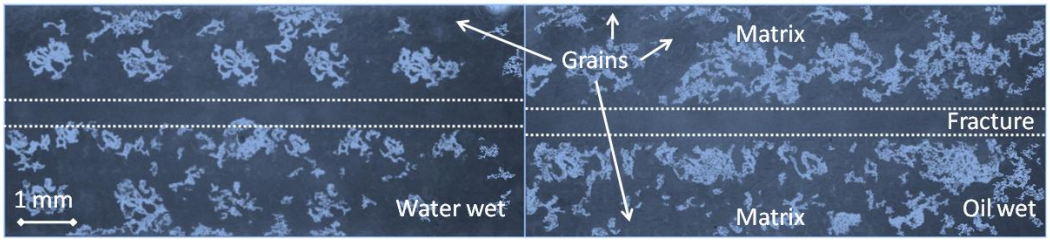

Figure 5.19 Residual oil (represented by the light color) after immiscible displacement at 600 psi and 50ml/hr in the model with heterogeneous pattern. Lighter color represents the trapped oil in the matrix.

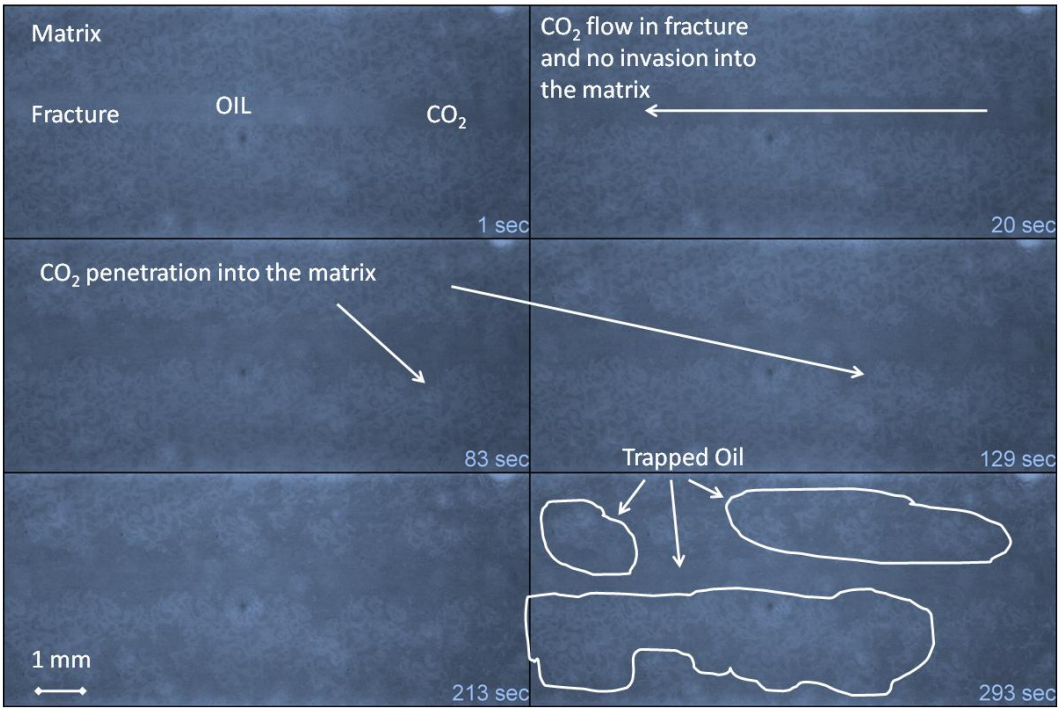

Figure 5.20 Displacement of n-decane by CO_2 in the oil wet model with heterogeneous pattern at 600 psi and 50 ml/hr. Displacement of oil in the fracture, CO_2 invasion into the matrix and trapped oil are indicated with arrows. The lighter color represents the oil phase and the darker color represents the immiscible CO_2 phase. See also image processed version in the Appendix.

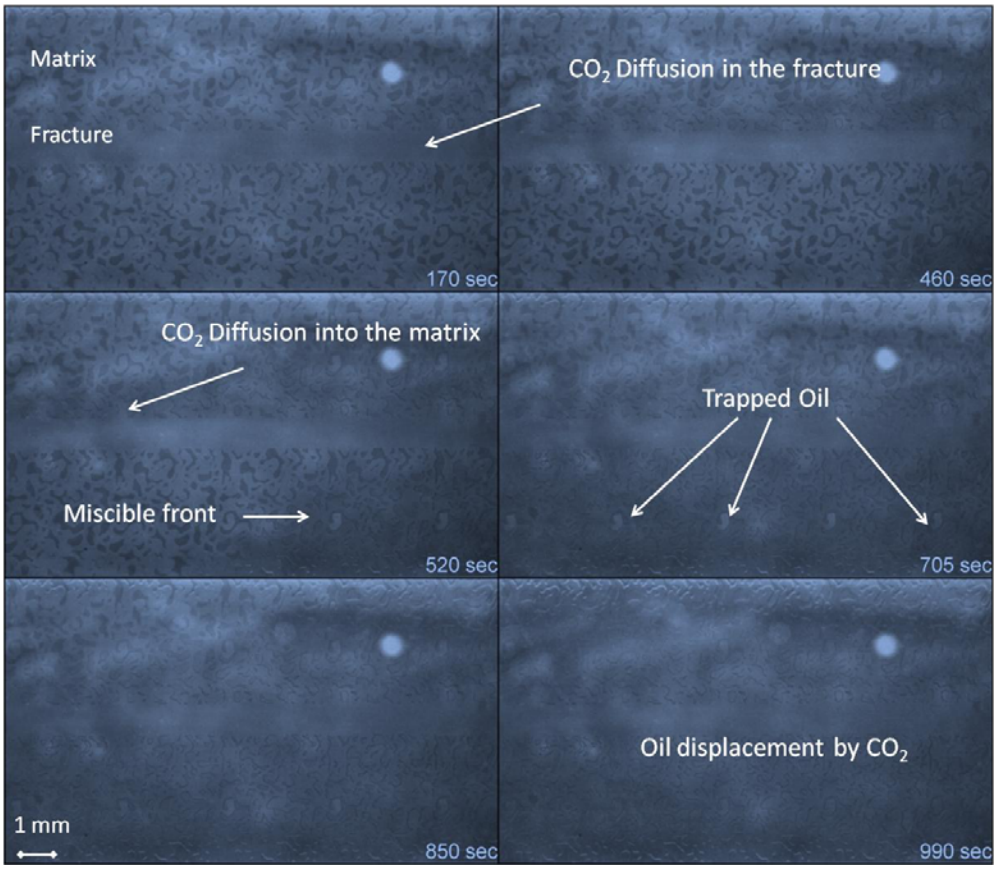

Figure 5.21 Displacement of n-decane by CO_2 in the oil wet model with heterogeneous pattern at 1200 psi and 50 ml/hr. CO_2 diffusion into oil, miscible front and the trapped oil are indicated by arrows. Fuzzy areas represent the mixing zone (or oil displacement). See also image processed version in the Appendix.

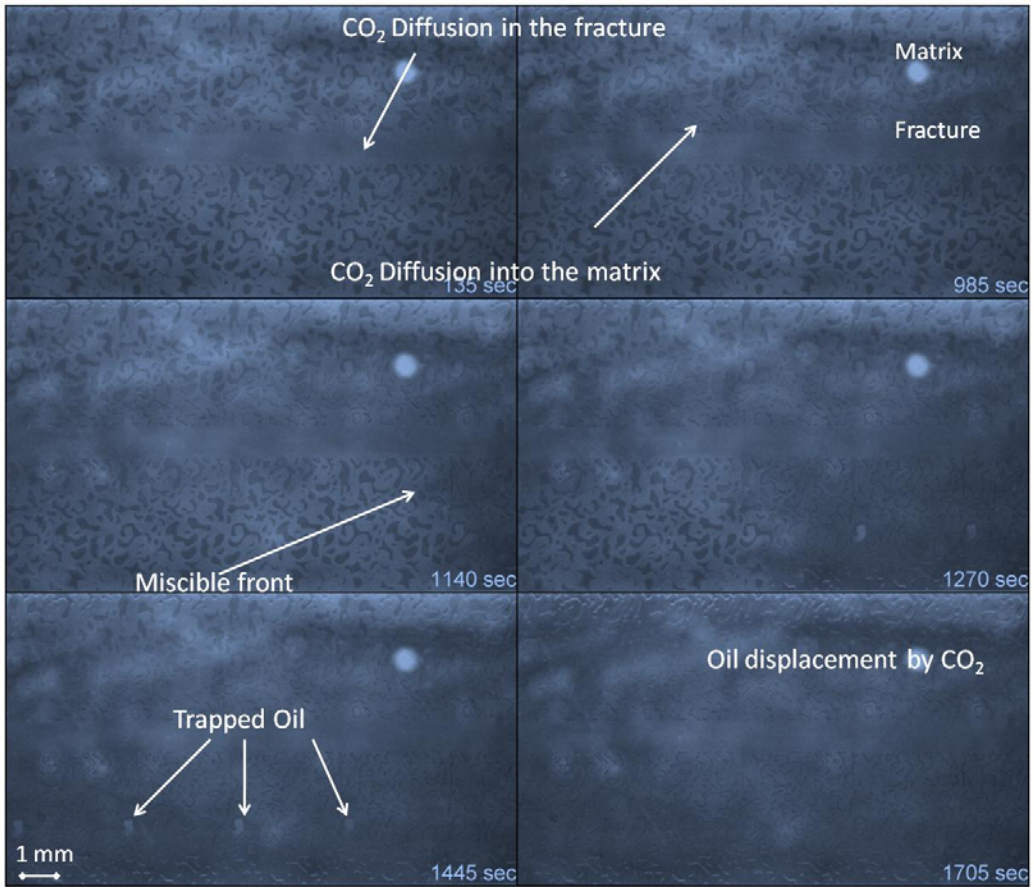

Figure 5.22 Displacement of n-decane by CO_2 in the oil wet model with heterogeneous pattern at 1500 psi and 50 ml/hr. CO_2 diffusion into oil, miscible front and the trapped oil are indicated with arrows. Fuzzy areas represent the mixing zone (or oil displacement). See also image processed version in the Appendix.

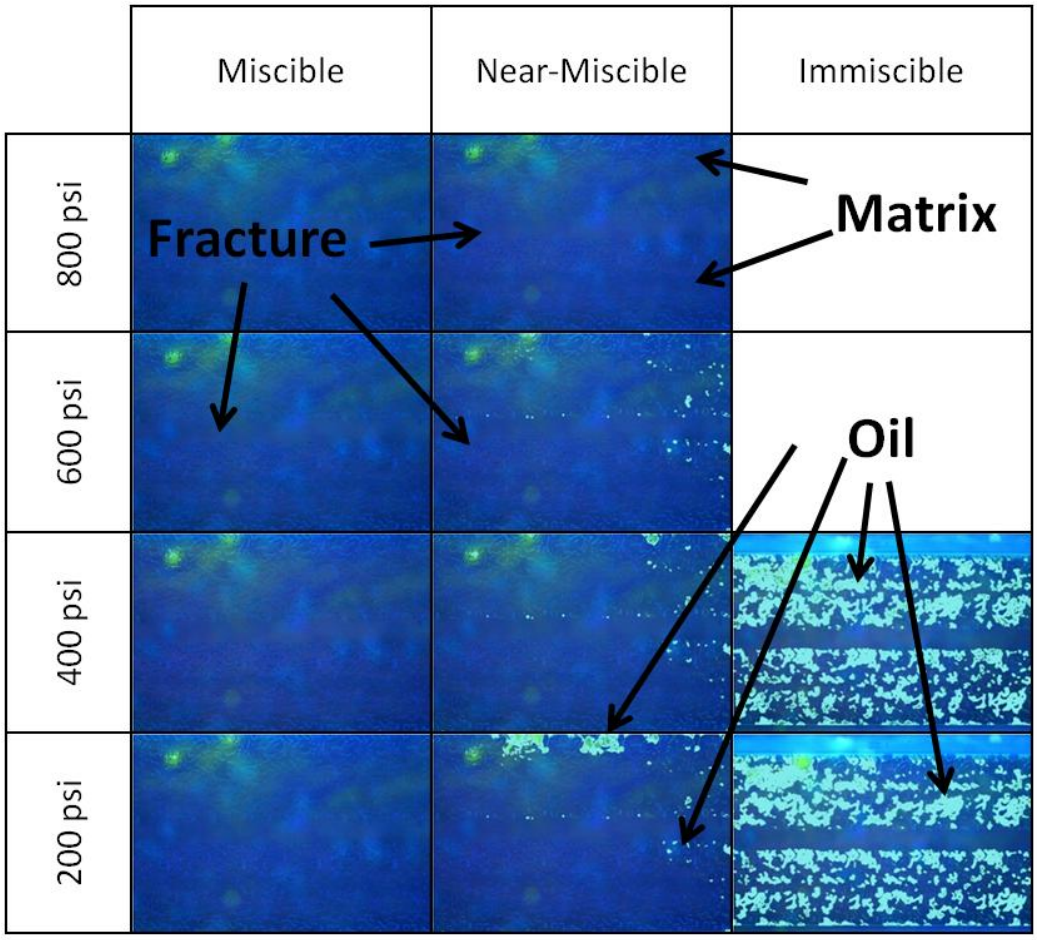

Figure 5.23 Blow-down after miscible, near-miscible and immiscible displacement experiments for water wet case. Light color (greenish) represents the oil phase and dark color (dark blue) is CO_2. No oil appeared and got trapped in the miscible case, a little amount was observed in the near-miscible experiment at the end of experiment (abandonment pressure of 200 psi).

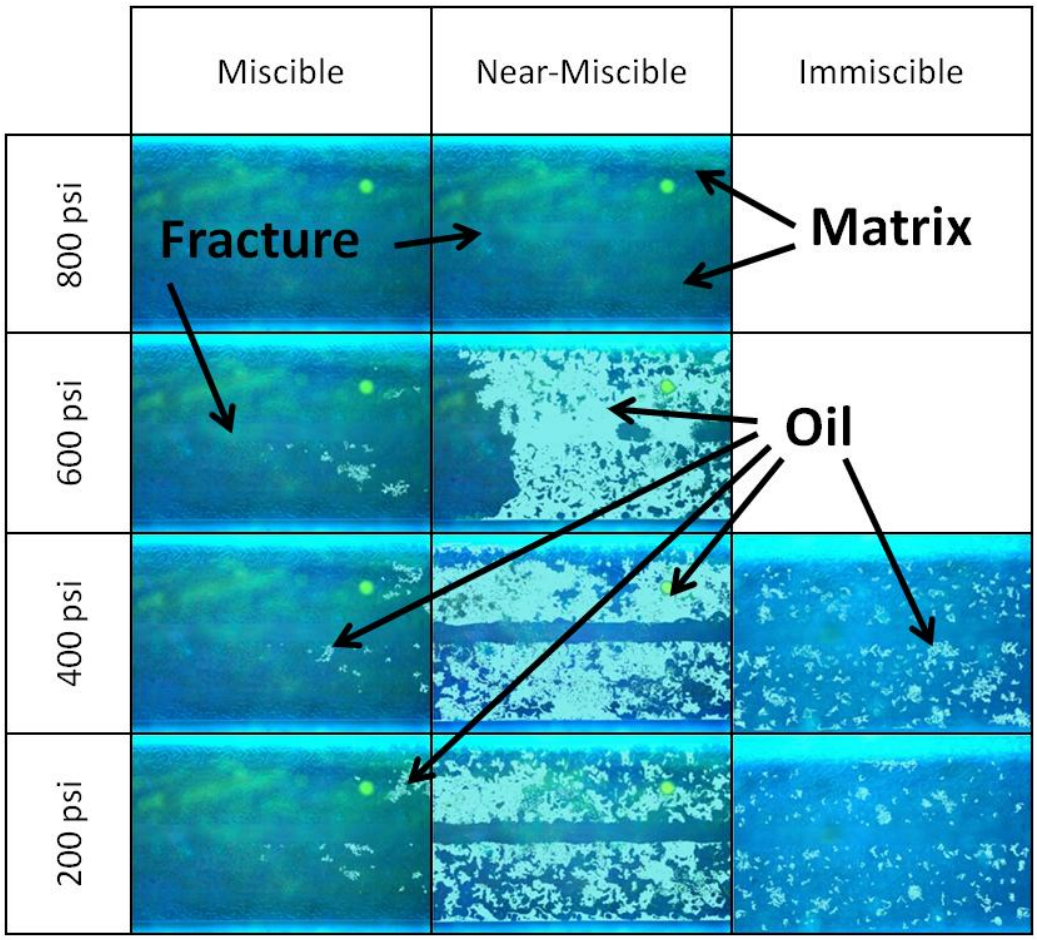

Figure 5.24 Blow-down after miscible, near-miscible and immiscible displacement experiments for oil wet case. Light color (greenish) represents the oil phase and dark color (dark blue) is CO_2. A little amount of oil appeared and got trapped in the miscible case at the end of experiment (abandonment pressure of 200 psi). The oil entrapped in the near-miscible cases is remarkably higher than the water-wet counterpart. Interestingly, oil entrapped at the end of the immiscible experiment is lower than the water-wet case yielding more CO_2 storage.

Chapter 6

Conclusions

6.1 First Contact Miscible Displacement Experiments

1. At lower injection rates, the efficiency in terms of injected solvent amount and the ultimate recovery is higher compared to high rates. Although faster recoveries are obtained at high rates, low rates are more effective in terms of CO_2 storage and ultimate oil recovery.
2. At low viscosities, solvent diffusion into the matrix is much higher compared to high viscosities. Increasing viscosity difference between displacing and displaced fluids results in viscous fingerings, hence, decreases the efficiency.
3. At lower injection rates, the gravity force overcomes the viscous forces and increases the sweep efficiency of displacement creating a stable front during vertical displacement (from top to bottom).

6.2 Numerical Modeling of First Contact Miscible Displacements

1. In fractured systems, the dominant recovery mechanism is the diffusion, which is effective in the matrix compared to the dispersion, which is effective only in the fracture.

2. Higher injection rates reduce the diffusion of solvent into the matrix and increase the amount of solvent to be used. Lower injection rates make diffusion more effective. This, however, delays the ultimate recovery. Hence, determination of the critical rate is essential.
3. Increasing viscosity difference between solute and solvents yields to decrease the efficiency of displacement due to a negative effect on diffusion coefficients.
4. The diffusion coefficient was observed to be the most critical parameter on the process of matrix-fracture interaction. Dispersivities were adjusted to do fine tuning on displacement patterns. Although small changes in the diffusion coefficient affected the displacement pattern significantly, it required high adjustments, in the order of hundreds for dispersivities to see the same effect.
5. The results imply that an "effective matrix-fracture interaction coefficient" could be developed as a function of the injection rate, flow direction, and oil viscosities. The solute (oil) diffusion coefficient could be used as the "effective diffusion term" in the dimensionless groups

6.3 Pore Scale Investigation of Matrix-Fracture Interaction during CO_2 Injection

1. Immiscible displacement of CO_2 in fractured reservoirs leaves a high amount of trapped oil in the matrix especially in heterogeneous patterns.
2. Increased rate during the immiscible injection of CO_2 reduces the amount of oil trapped in the matrix.

3. Increased rate during the miscible displacement of CO_2 results in faster recovery however it requires more amount CO_2 to be cycled to reach the same amount of production.
4. Increasing pressure above the MMP increases the diffusion coefficient between CO_2 and n-decane.
5. Altering matrix wettability from water wet to oil wet increases the amount of oil trapped in the matrix after immiscible displacement of CO_2 and delays the diffusion of CO_2 in miscible displacement.

6.4 Future Work

1. Both, micromodel and glass model, experiments can be conducted with initial water saturation. Such experiments can help to observe trapped oil and water as well as CO_2 under different matrix, fluid, fracture and injection conditions
2. Heavy oil or crude oil can be used as the oleic phase in the experiments to be more representative of the interactions taking place in real reservoir matrix-fracture systems.
3. Additional vertical injection experiments can be conducted for wider range of injection rate and oil viscosity. An analytical model can be developed with obtained results and such model can be integrated into the available numerical reservoir simulators.
4. Micromodels can be utilized for vertical injection experiments to visualize fluid dynamics in immiscible and miscible displacements at pore scale

Chapter 7

Contributions

It is believed that the following items are the major contributions to the literature out of this dissertation.

- Quantitative and qualitative data are provided from visualization experiments for a wide variety of matrix, fracture, fluid (solvent and oil), and injection (mainly rate and direction, i.e., horizontal and vertical directions) parameters.
- The importance of the injection rate was shown visually and quantitatively. Optimum injection rate is also defined for practical purposes.
- It is revealed that gravity facilitates the forming of a stable front during first contact miscible displacements in the case of vertical fractures and the vertical injection.
- 2-D experiments are successfully modeled and visually matched. Unlike in the non-fractured cases, dominance of diffusion over dispersion in fractured systems is shown.
- Visual support for previous speculations based on core scale experiments and numerical model studies on matrix-fracture interaction during miscible and immiscible CO_2 injection was provided at pore scale with glass etched microfluidic devices for a

wide variety of matrix (heterogeneity, wettability), fracture (flow rate), and miscibility (immiscible, near-miscible, fully miscible) cases.

- To our knowledge, miscible CO_2 injection at high pressure level in micromodels has not been done before in fractured systems.

Bibliography

Al-Wahaibi, Y.M., Muggeridge, A.H. and Grattoni, C.A., 2006, "Gas/Oil Nonequilibrium in Multicontact Miscible Displacements within Homogeneous Porous Media", SPE 9972, 15th SPE-DOE Improved Oil Recovery Sym., April 22-26.

Al-Wahaibi, Y.M., Muggeridge, A.H., Grattoni, C.A., 2007, "Experimental and Numerical Studies of Gas/Oil Multicontact Miscible Displacements in Homogeneous Porous Media". Society of Petroleum Engineers Journal, Vol. 12, No. 1, March, p.62-76.

Asghari, K. and Torabi, F., 2008, "Effect of Miscible And Immiscible CO_2 Flooding on Gravity Drainage: Experimental and Simulation Results", SPE-110587, SPE/DOE Improved Oil Recovery Symposium, Tulsa, Oklahoma, April 19-23.

Bahralolom, I. M. and Orr, F. M., 1988-a, "Solubility and Extraction in multiple-Contact Miscible Displacements: Comparison of N_2 and CO_2 Flow Visualization Experiments", SPE Reservoir Engineering Journal, Vol. 3, No. 1, February, p. 213-219.

Bahralolom, I., Bretz, R.E. and Orr, F.M., 1988-b, "Experimental Investigation of the Interaction of Phase Behavior with Microscopic Heterogeneity in a CO_2 Flood", SPE Reservoir Engineering, Vol. 3, No. 2, May, p. 662-672.

Campbell, B.T. and Orr, F.M., 1985,"Flow Visualization for CO_2/Crude-Oil Displacements;, Society of Petroleum Engineers Journal, Vol. 25, No. 5, Oct, 665-678.

Chatzis, I., Morrow, R.N., and Lim, H.T., 1983, Magnitude and Detailed Structure of Residual Oil Saturation", Society of Petroleum Engineers Journal, April, P. 311-326.

Darvish, G.R., Lindeberg, E., Holt, T., Utne, S.A. and Kleppe, J., 2006, "Reservoir-Conditions Laboratory Experiments of CO_2 Injection into Fractured Cores", SPE-99650, SPE Europec/EAGE Annual Conference and Exhibition, Vienna, Austria, June 12-15.

Dastayari, A., Bashukooh, B., Shariatpanahi, S.F., and Haghighi, M., 2005, "Visualization of Gravity Drainage in a Fractured System during Gas Injection Using Glass Micromodel", SPE-93673, 14th SPE Middle East Oil & Gas Show and Conference, Bahrain, March 12-15.

Dijke, M. I. J., Sorbie K.S. and Danesh, A., 2004, "Simulation of WAG Floods in an Oil-Wet Micromodel Using a 2-D Pore-Scale Network Model", Journal of Petroleum Science and Engineering, 52, p. 71-86.

Er, V. and Babadagli, T., 2007, "Visual Investigations on the Oil Recovery and Sequestration Potential of CO_2 in Naturally Fractured Reservoir", CIPC 2007-33, Canadian International Petroleum Conference, Calgary, Alberta, June 12-14.

Er, V. and Babadagli T., 2008, "Miscible Interaction between Matrix and Fracture: A Visualization and Simulation Study", SPE-117579, SPE Regional/AAPG Eastern Section Joint Meeting, Pittsburgh, Pennsylvania, October 11-15., Accepted for publication in SPE Reservoir Evaluation and Engineering Journal.

Feng, Q., Di, L., Tang, G., Chen, Z., Wang, X. and Zou, J., 2004, "A Visual Micro-Model Study: The Mechanism of Water Alternative Gas Displacement

in Porous Media", SPE-89362, SPE/DOE 14th Symposium on Improved Oil Recovery, Tulsa, Oklahoma, April 17-21.

Firoozabadi, A. and Markeset, T.I., 1997, "Miscible Displacement in Fractured Porous Media: Part I – Experiments", SPE 27743, SPE/DOE 9th Improved Oil Recovery Symposium, Tulsa, OK, 17-20 April.

Garder, A.O., Peaceman, D.W. and Pozzi, A.L. 1963, "Numerical Calculation of Multidimensional Miscible Displacement by the Method of Characterization", SPE-683, SPE Annual Fall Meeting, New Orleans, Oct. 6-9.

Goss, M.J. 1971, "Determination of Dispersion and Diffusion of Miscible Liquids in Porous Media by a Frequency Response Method",SPE-3525, Annual Fall Meeting of SPE of AIME, New Orleans, LA., Oct. 3-6.

Haghighi, M., Xu, B. and Yortsos, Y.C., 1994, "Visualization and Simulation of Immiscible Displacement in Fractured Systems Using Micromodels: I. Drainage" Journal of Colloid and Interface Science, Vol. 166, No. 1, August, p.168-179.

Hatiboglu, C.U. and Babadagli, T., 2005, 'Experimental and Stochastic Modelling of Diffusion Controlled Matrix-Fracture Transfer in Naturally Fractured Oil Reservoirs" SPE 95474, SPE Annual Technical Conference and Exhibition, Dallas, TX, October 9-12.

Hatiboglu, C.U., 2007, "Miscible and Immiscible Transfer of Liquid-Liquid and Gas-Liquid Pairs between Matrix and Fracture under Static Conditions", Ph.D. Thesis, University of Alberta, Edmonton, AB, Canada.

Huang, E.T.S. and Tracht, J.H., 1974, "The Displacement of Residual Oil by Carbon Dioxide", SPE 4735, Society of Petroleum Engineers of AIME, Tulsa, OK, 22-24 April.

Islaz-Juarez, R., Smanego-V, F., Luna, E., Perez-Rosalez, C. and Cruz, J., 2004, "Experimental Study of Effective Diffusion Coefficient in Porous Media", SPE-92196, SPE International Conference, Pebla, Mexico, November 8-9.

Javadpour, F. and Fisher, D., 2008, "Nanotechnology-Based Micromodel and New Image Analysis to Study Transport in Porous Media", Journal of Canadian Petroleum Technology, Vol. 47, No. 2, p. 31-37.

Leahy-Dios, A. and Firoozabadi, A. 2007, "A Unified Model for Diffusion Coefficient Prediction in Non-Ideal Petroleum Fluids", SPE-113021, SPE Annual Technical Conference and Exhibition, Anaheim, California, November 11-14.

Lenormand, R., Le Romancer, J.F., Le Gallo, Y. and Bourbiaux, B., 1998, "Modeling the Diffusion Flux between Matrix and Fissure in a Fissured Reservoir", SPE-49007, SPE Annual Conference and Exhibition, New Orleans, LA, Sept. 27-30.

Morin, N., 2001, "Hands-on Demonstration of Basic Processing", NanoFab, University of Alberta, Edmonton, AB, Canada.

Paidin, W. R., 2006, "Physical Model Study of the Effects of Wettability and Fractures on Gas-Assisted Gravity Drainage (GAGD) Performance", M. Sc. Thesis, Louisiana State University, Baton Rouge, LA, United States.

Perez-Cardenas, F., Cruz-Hernandez, J. and Perez-Rosalez, C., 1990, "Miscible Displacement in Fractured Porous Media", SPE-20798

Perkins, T.K. and Johnston, O.C., 1963, "A Review of Diffusion and Dispersion in Porous Media", Society of Petroleum Engineers Journal, Vol. 9, No.2, March, p.70-84.

Rangel-German, E.R. and Kovscek, A. R., 2004-a, "A Micromodel Investigation of Two-Phase Matrix-Fracture Transfer Mechanisms", Water Resources Research, Vol.42, W03401, doi: 10.1029/2004WR003918.

Rangel-German, E.R. and Kovscek, A. R., 2004-b, "Microvisual Analysis of Matrix-Fracture Interaction, SPE-92133, International Petroleum Conference, Puebla, Mexico, November 8-9.

Romero-Zeron, L. and Kantzas, A., 2006, "Evolution of Foamed Gel Confined in Pore Network Models", Journal of Canadian Petroleum and Technology, Vol. 45, No.11, November, p. 51-62.

Schramm, L. L., Isaacs, E., Singhal, A.K, Hawkins, B., Schulmiser, B. Wassmuth F., Randall, L., Turta, A., Zhou, J., Tremblay, B., Lillico, D., and Wagg, B., 2000, "Technology Development for Conventional Petroleum Reservoirs", Journal of Canadian Petroleum and Technolgy, Canadian Advantage, p. 31-46.

Shariatpanahi, S.F., Dastyari, A., Haghighi, M., Sahimi, M., and Ayatollahi, S.S., 2005, "Visualization Experiments on Immiscible Gas and Water Injection by Using 2D-Fractured Glass Micromodels", SPE-93537, 14th SPE Middle East Oil & Gas Show and Conference, Bahrain, March 12-15.

Silvia, F.V. and Belery, P., 1989, "Molecular Diffusion in Naturally Fractured Reservoirs: A Decisive Recovery Mechanism", SPE-19672 Annual Technical Conference and Exhibition, San Antonio, TX, Oct. 8-11.

Sincock, K.J. and Black, C.J.J. 1988, "Validation of Water/Oil Displacement Scaling Criteria Using Microvisualization Techniques", SPE-18294, 63rd Annual Technical Conference and Exhibition of the Society of Petroleum Engineers, Houston, Texas, October 2-5.

Smith, D., Ahmadi, G., Ji, C., Bromhal, G. and Ferer, M.V., 2002, "Experimental and Numerical Study of Gas-Liquid Displacements in Flow Cells, with

Application to Carbon Dioxide Sequestration in Brine Fields" FEDSM2002-31296, Asme 2002 Fluid Engineering Division Summer Meeting, July 14-18.

Sohrabi, M., Henderson, G.D. Tehrani, D.H. and Danesh, A. and, 2000, "Visualization of Oil Recovery by Water Alternating Gas (WAG) Injection Using High Pressure Micromodels – Water-Wet Systems", SPE-63000, SPE Annual Technical Conference and Exhibition, Dallas, Texas, October 1-4.

Sohrabi, M., Tehrani, D.H., Danesh, A. and Henderson, G.D., 2001, "Visualisation of Oil Recovery by Water Alternating Gas (WAG) Injection Using High Pressure Micromodels – Oil-Wet & Mixed-Wet Systems", SPE-71494, SPE Annual Technical Conference and Exhibition, New Orleans, Louisiana, September 30-October 3.

Sohrabi, M., Danesh, A. and Jamiolahmady, M., 2007-a, "Visualisation of Residual Oil Recovery by Near Miscible Gas and SWAG Injection Using High-Pressure Micromodels", Transport in Porous Media, Vol. 74, No. 2, p. 239-257.

Sohrabi, M., Danesh, A. and Jamiolahmady, M., 2007-b, "Microscopic Mechanisms of Oil Recovery By Near-Miscible Gas Injection", Transport in Porous Media, Vol.72, No.3/April, p. 351-367.

Sun, W. and Tang, G.-Q., 2006, "Visual Study of Water Injection in Low Permeable Sandstone", Journal of Petroleum Science and Technology, Vol. 45, No. 11, p. 21-26.

Tai, K., 2005, "NanoFab Glass Microfluidic Device Fabrication Manual", NanoFab, University of Alberta, Edmonton, AB, Canada.

Thompson, J.L. and Mungan, N., 1969, "A Laboratory Study of Gravity Drainage in Fractured Systems Under Miscible Conditions", Society of Petroleum Engineers Journal, Vol. 9, No. 2, June, p.247-254.

Trivedi, J.J. and Babadagli, T., 2006, "Efficiency of Miscible Displacement in Fractured Porous Media", SPE-100411, SPE Western Regional AAPG Pacific Section/GSA Cordilleran Section Joint Meeting, Anchorage, Alaska, May 8-10.

Trivedi, J.J. and Babadagli, T., 2008-a, "Experimental Analysis of CO_2 Sequestration Efficiency during Oil Recovery in Naturally Fractured Reservoirs", SPE-117607, SPE Regional/AAPG Eastern Section Joint Meeting, Pittsburgh, Pennsylvania, October 11-15.

Trivedi, J.J. and Babadagli, T., 2008-b, "Scaling Miscible Displacement in Fractured Porous Media Using Dimensionless Numbers", Journal of Petroleum Science and Engineering, Vol. 61, p.58-66.

Wan, J., Tokunaga, T.K., Tsang, C. and Bodvarsson, G.S., 1996, "Improved Glass Micromodel Methods for Studies of Flow and Transport in Fractured Porous Media", Water Resources Research, Vol.32, No. 7, P. 1955-1964.

Wang, G.C., 1982, "Microscopic Investigation of CO_2 Flooding Process", Journal of Petroleum Technology, Vol. 34, No. 8, Aug, p.1789-1797.

Appendix

Processed version of the images for micromodel experiments

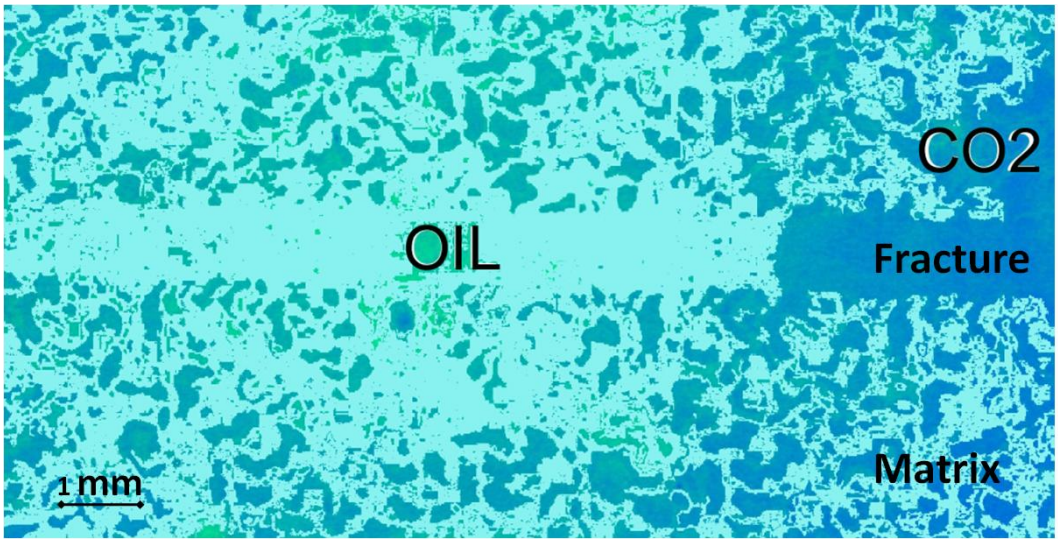

Image processed version of Figure 5.6. Immiscible oil-CO_2 interface during the displacement at 600 psi and 50 ml/hr after 1 second. Gaseous CO_2 displaces oil in the fracture initially. Heterogeneous matrix model.

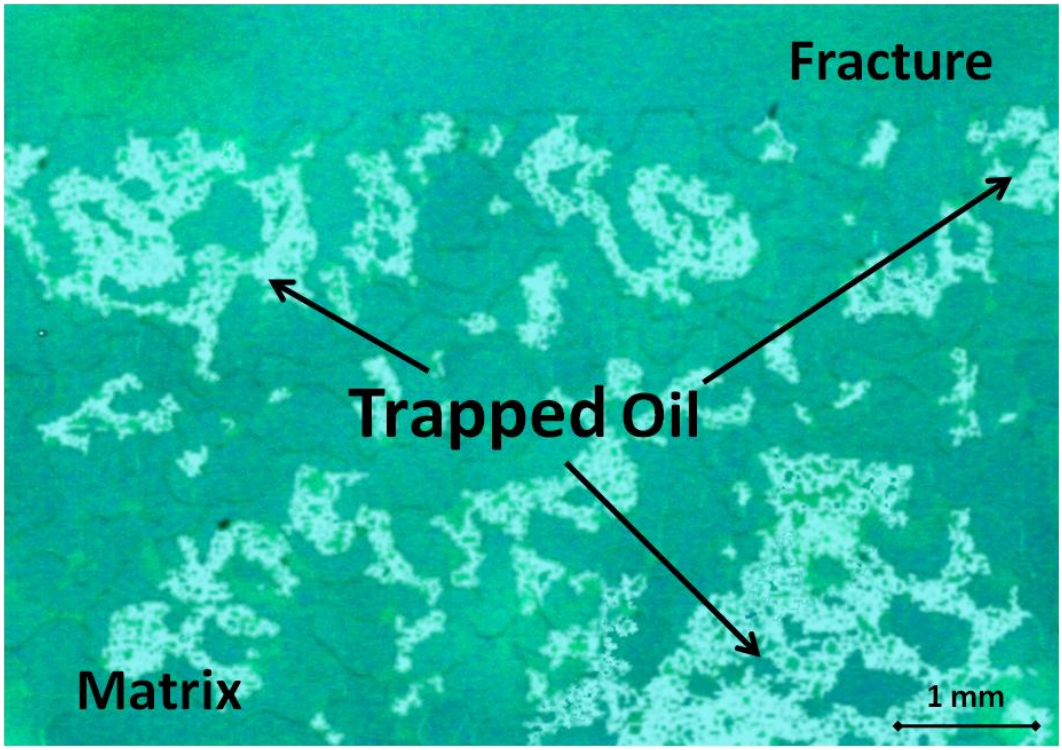

Image processed version of Figure 5.8. Trapped oil in the model with heterogeneous pattern after the displacement at 600 psi and 50 ml/hr. Dark color areas shows CO_2 phase and light color area shows oil phase. Some of the trapped oil is indicated by arrows.

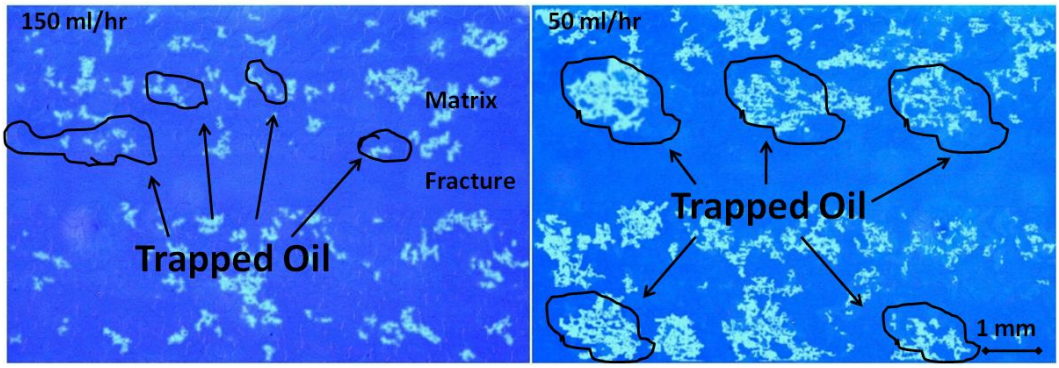

Image processed version of Figure 5.9. Comparison of residual oil patterns in the matrix after CO_2 injection at 150 ml/hr and 50 ml/hr in the model with heterogeneous pattern at 600 psi. The darker color (dark blue) represents CO_2 phase and the lighter color (greenish) represents the oil phase. To differentiate it better, some of the trapped oil is indicated by arrows.

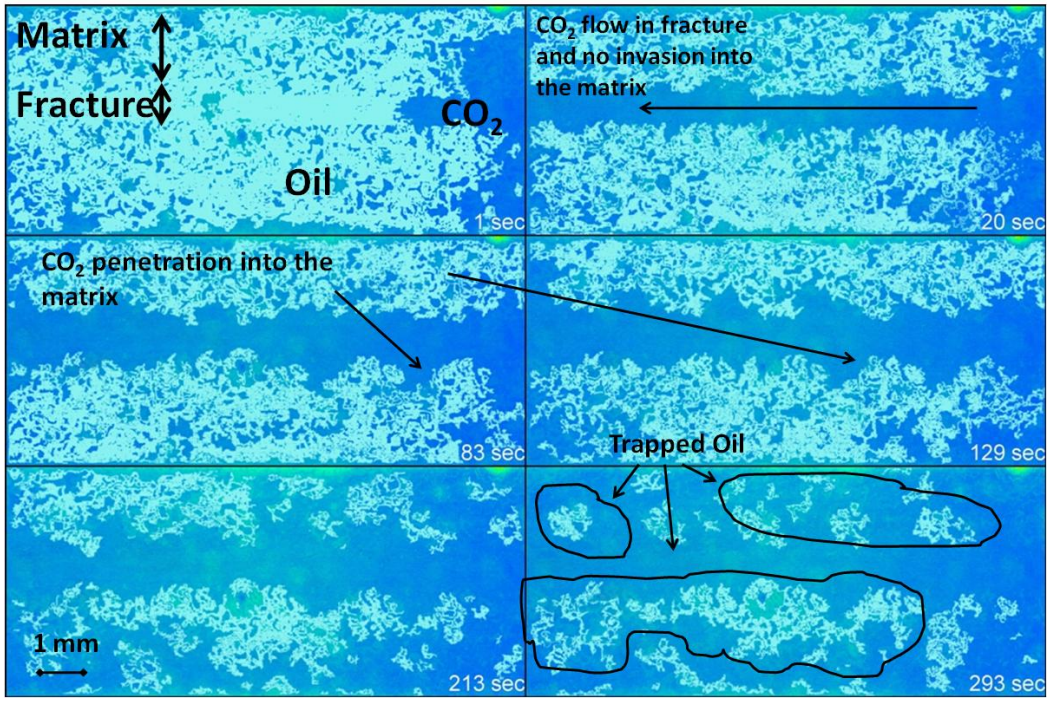

Image processed version of Figure 5.10. Displacement of n-decane by CO_2 in the model with heterogeneous pattern at 600 psi and 50 ml/hr. Lighter color (greenish) shows the oil phase and darker color (dark blue) shows CO_2 phase. Some of the trapped oil in the pores is indicated by arrows.

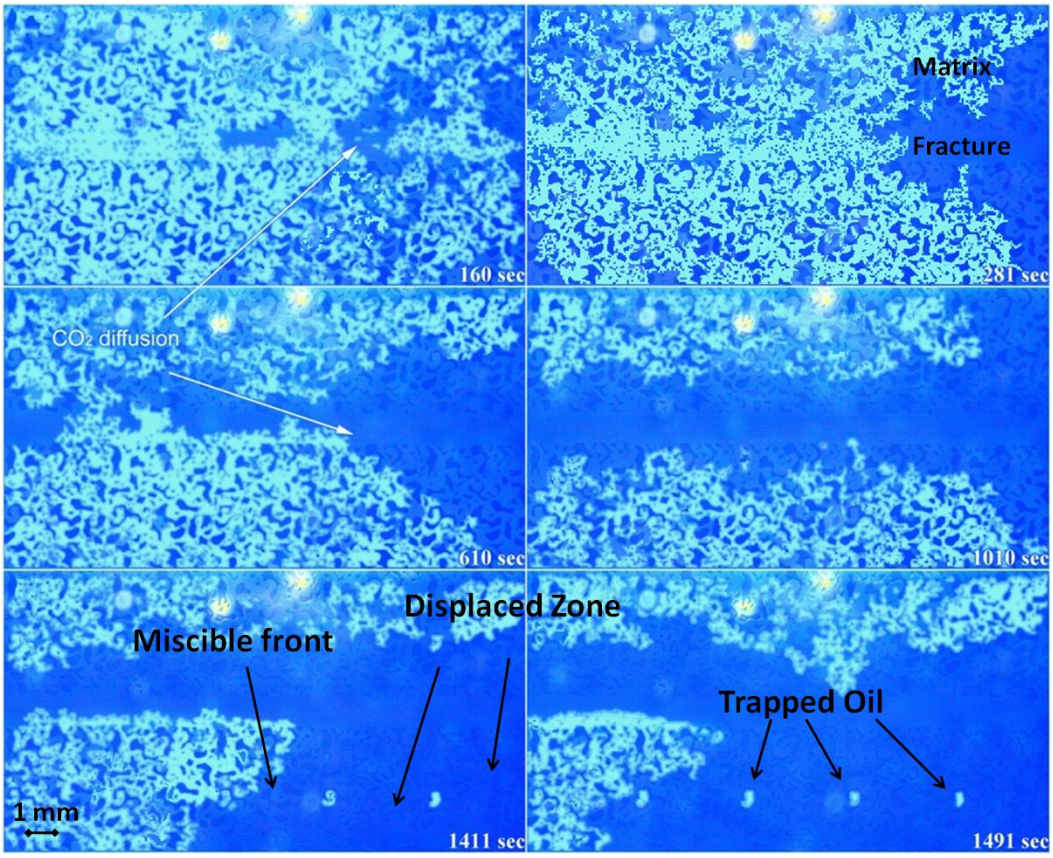

Image processed version of Figure 5.11. Displacement of n-decane by CO_2 in the model with heterogeneous pattern at 1200 psi and 50ml/hr. Lighter color (greenish) shows oil phase and darker color (dark blue) shows CO_2 phase. Supercritical state CO_2 initially diffuses into the oil in the fracture then into the oil in the matrix. CO_2 diffusion into oil, miscible front and the trapped oil are indicated by arrows.

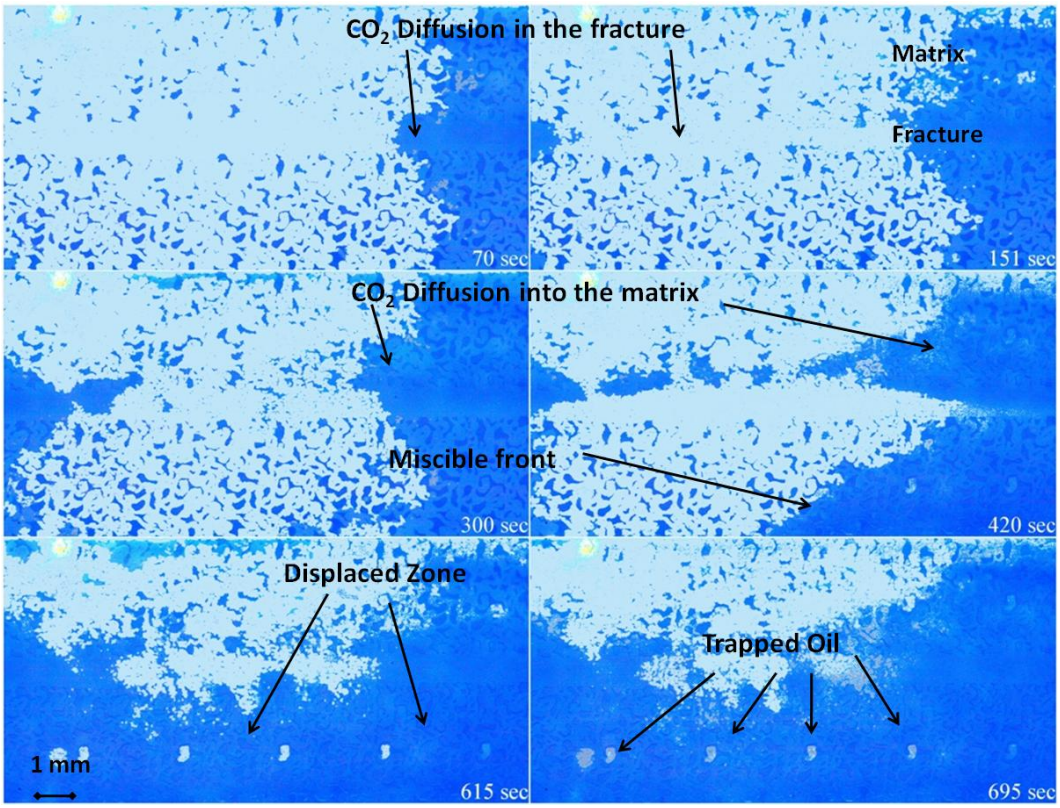

Image processed version of Figure 5.12. Displacement of n-decane by CO_2 in the model with heterogeneous pattern at 1200 psi and 150 ml/hr. Supercritical state CO_2 initially diffuses into the oil in the fracture then into the oil in the matrix. CO_2 diffusion into oil, miscible front and the trapped oil are indicated by arrows. Lighter color (greenish) shows oil phase and darker color (dark blue) shows CO_2 phase.

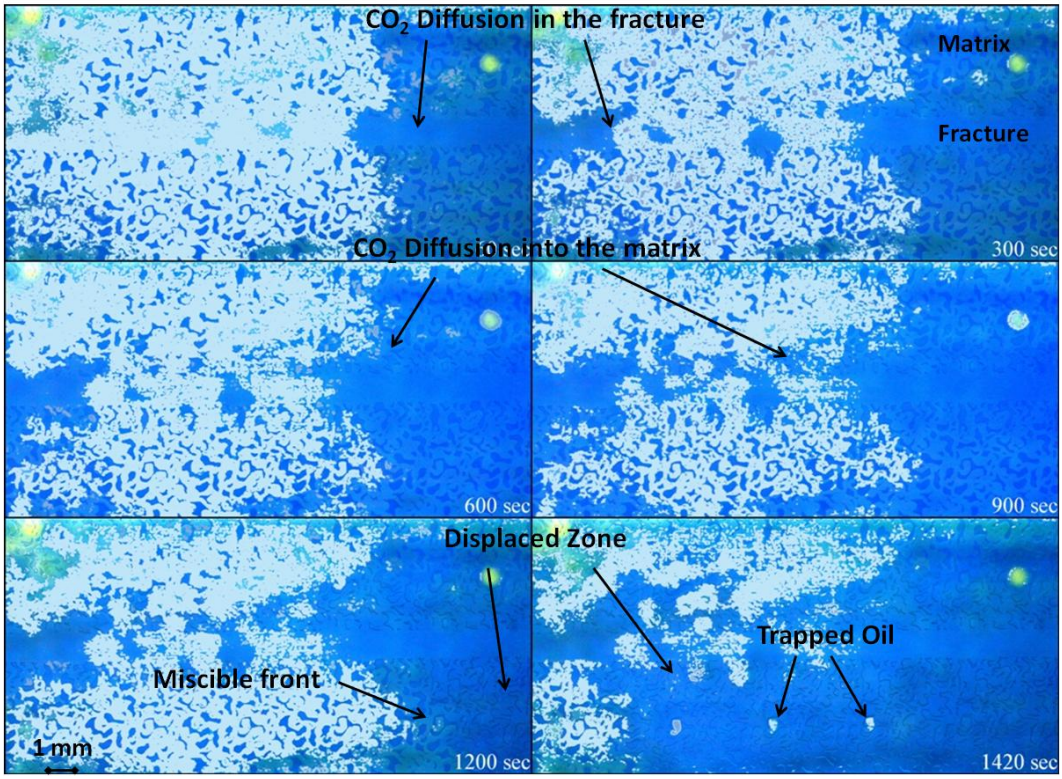

Image processed version of Figure 5.13. Displacement of n-decane by CO_2 in the model with heterogeneous pattern at 1500 psi and 50 ml/hr. Supercritical state CO_2 initially diffuses into the oil in the fracture then into the oil in the matrix. CO_2 diffusion into oil, miscible front and the trapped oil are indicated with arrows. Fuzzy areas represent the mixing zone (or oil displacement). Lighter color (greenish) shows oil phase and darker color (dark blue) shows CO_2 phase.

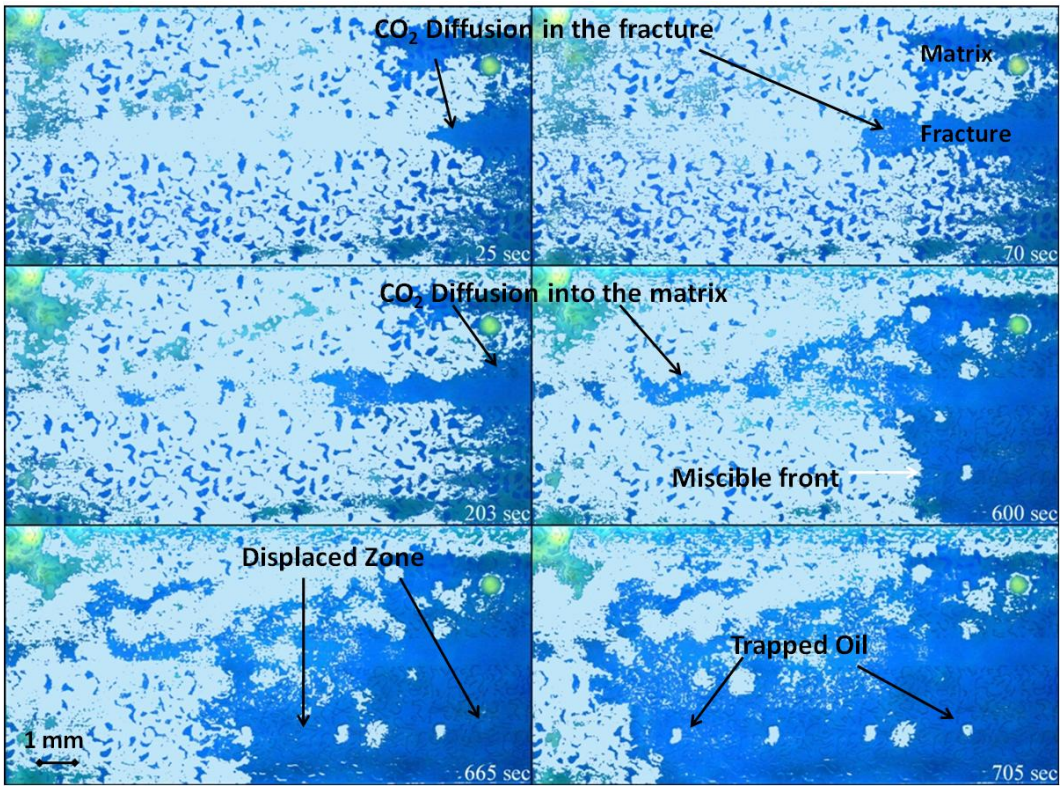

Image processed version of Figure 5.14. Displacement of n-decane by CO_2 in the model with heterogeneous pattern at 1500 psi and 150 ml/hr. Supercritical state CO_2 initially diffuses into the oil in the fracture then into the oil in the matrix. CO_2 diffusion into oil, miscible front and the trapped oil are indicated with arrows. Fuzzy areas represent the mixing zone (or oil displacement). Lighter color (greenish) shows oil phase and darker color (dark blue) shows CO_2 phase.

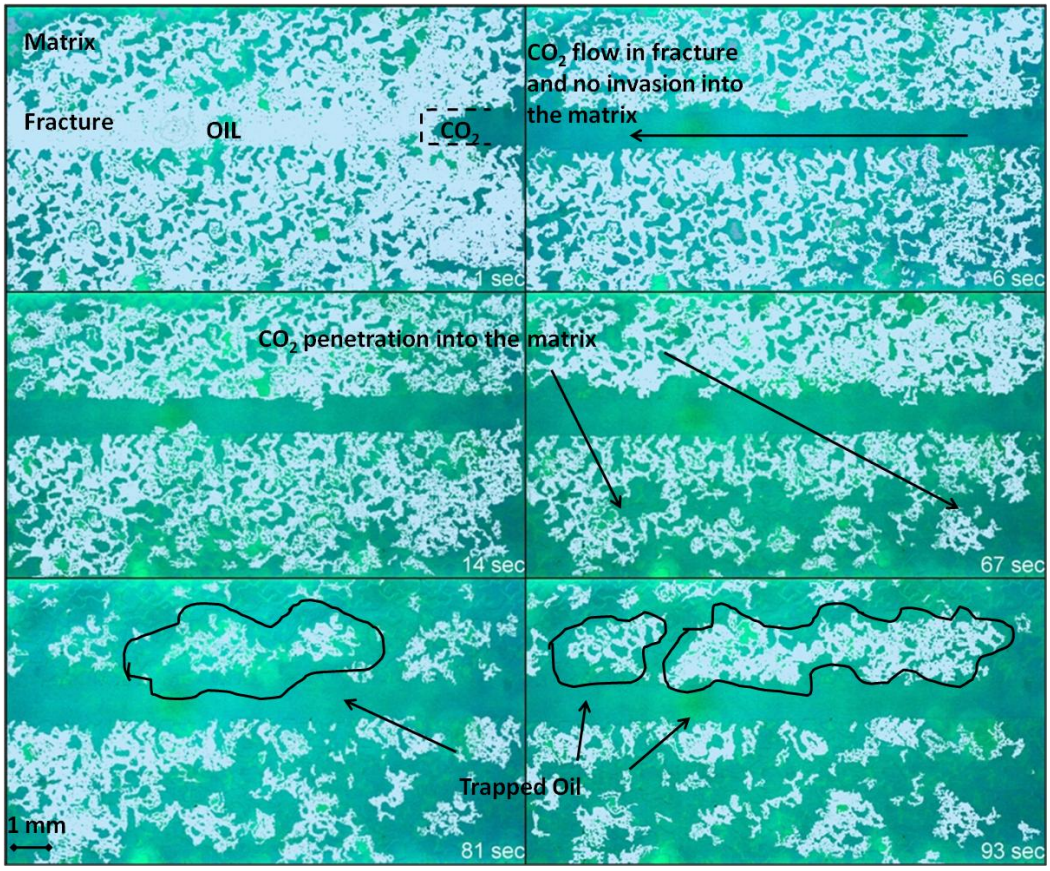

Image processed version of Figure 5.20. Displacement of n-decane by CO_2 in the oil wet model with heterogeneous pattern at 600 psi and 50 ml/hr. Displacement of oil in the fracture, CO_2 invasion into the matrix and trapped oil are indicated with arrows. Lighter color shows oil phase and darker color shows CO_2 phase.

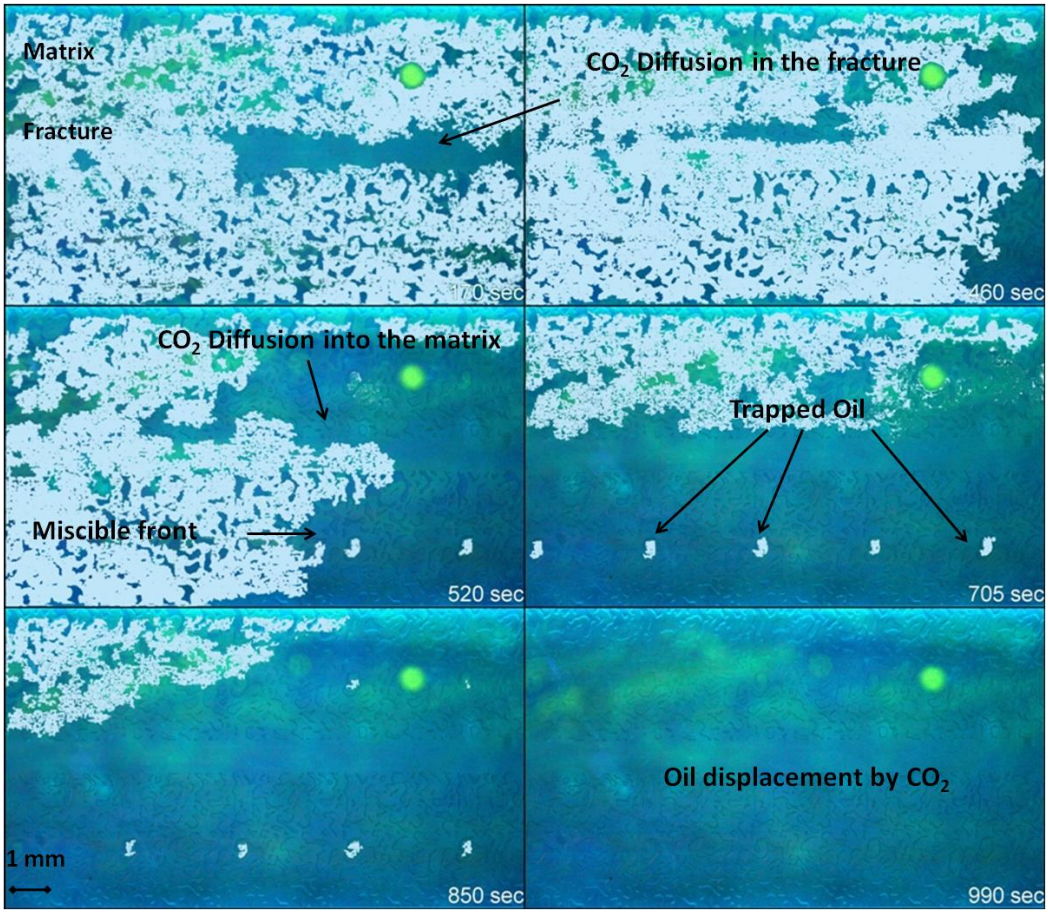

Image processed version of Figure 5.21. Displacement of n-decane by CO_2 in the oil wet model with heterogeneous pattern at 1200 psi and 50 ml/hr. CO_2 diffusion into oil, miscible front and the trapped oil are indicated by arrows. Fuzzy areas represent the mixing zone (or oil displacement). Lighter color (greenish) shows oil phase and darker color (dark blue) shows CO_2 phase.

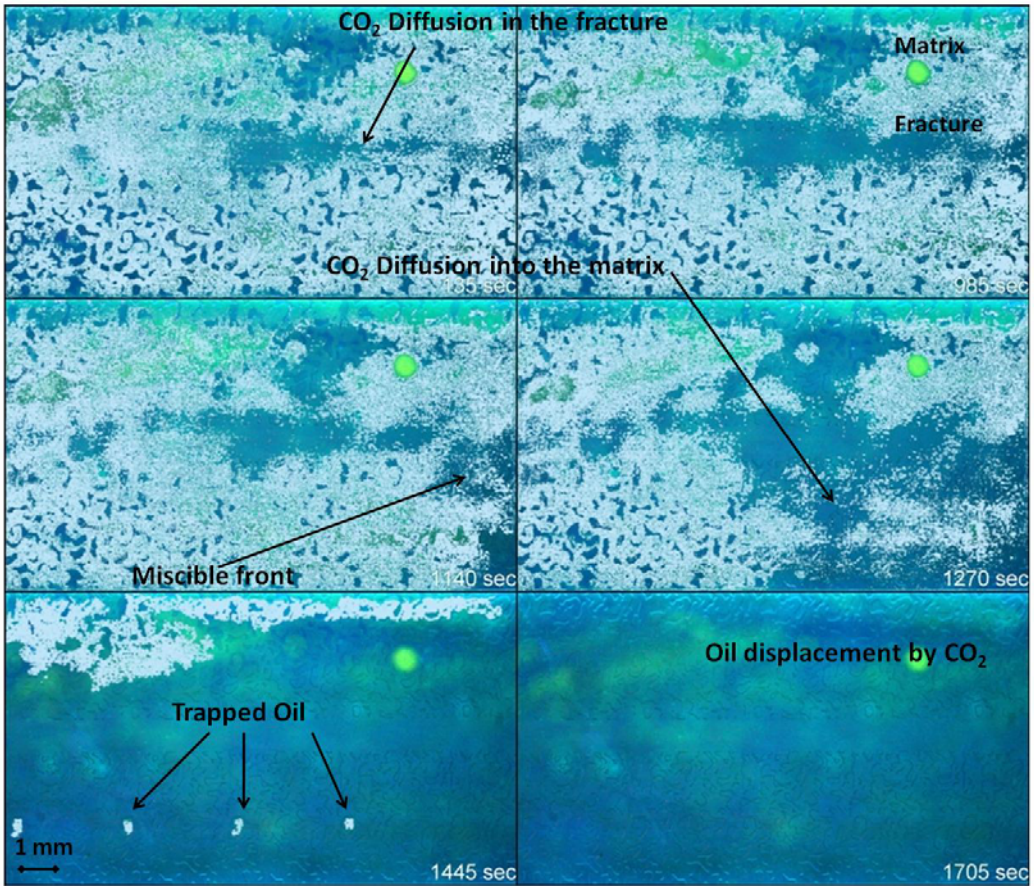

Image processed version of Figure 5.22. Displacement of n-decane by CO_2 in the oil wet model with heterogeneous pattern at 1500 psi and 50 ml/hr. CO_2 diffusion into oil, miscible front and the trapped oil are indicated with arrows. Fuzzy areas represent the mixing zone (or oil displacement). Lighter color (greenish) shows oil phase and darker color (dark blue) shows CO_2 phase.